UNIVERSITA' DELLA CALABRIA

Dottorato di Ricerca in

"Scienze e Tecnologie delle Mesofasi e dei Materiali Molecolari"
(STM^3)-XX° Ciclo

Ph.D. Thesis

Dense Hyflon® AD membranes for gas separation: influence of the solvent and determination of local free volume

Settore Disciplinare: CHIM07

Supervisore
Prof. Marcello Longeri

Coordinatore
Prof. Carlo Versace

Supervisore esterno
Prof. Yuri Yampolskii

Direttore ITM-CNR
Prof. Enrico Drioli

Candidato
Dr. Marialuigia Macchione

ANNO ACCADEMICO 2007/2008

To my angel:
my son Mario with all my love

Introduction

Membrane technology, important for nonthermal separation devices, will be the focus of this thesis. The separation of gases by membranes is a dynamic and rapidly growing field. Membranes are being used to separate gases from their mixtures by the differential permeation of the components through them. The membrane separation processes offer a number of advantages in terms of low energy consumption and capital investments. The process requires simple, easy to operate and compact equipment. As a result, the process has acquired a significant role in the industrial scenario in terms of economical considerations, as gases occupy a central position in the chemical feed stock industry.

The main objective of the present thesis is the preparation and characterization of gas separation membranes of innovative and very interesting perfluorinated polymers.

Perfluoropolymers are known as highly insoluble polymers due to their resistance to organic solvents. In this framework, the first goal was the preparation, by the solution casting and solvent evaporation method, of perfluorinated membranes of Hyflon® AD60X and Hyflon® AD80X and to study how some of the membrane properties depend on the preparation conditions. Because of the extraordinary properties of Hyflon the first aim of my thesis gains importance on the applicative point of view. In several aspects, Hyflon has superior properties, for instance chemical stability and solvent resistance, compared to most of the currently available commercial gas separation membranes. Nevertheless the successful practical application requires still a significant research effort. The main part of this thesis will be devoted to illustrate the characterization of Hyflon® AD membranes in terms of mechanical, thermal, structural as well as transport properties. In particular the entire thesis will be divided as follows:

Part I: General Introduction

Chapter 1: *Membranes for gas separation*. This chapter is a general overview about the different type of polymer membranes, with particular attention for the gas separation membranes and processes. The main equations related to the gas transport properties and their measurements are also shown and described.

Chapter 2: *Perfluoropolymer membranes and free volume in polymers.* In this chapter perfluoropolymers properties will be described, focusing the attention on their potentiality as membrane materials. The concept of free volume will be also introduced and the main technique commonly used to measure it will be described.

Chapter 3: *Photochromism.* In this chapter fundamentals of photochromism and photochromic molecules will be introduced, paying particular attention to azobenzene and stilbene derivatives. The importance of trans-cis photoisomerization of this class of dye molecules will be described and their possible use in different fields of application.

Part II: Results

Chapter 4: *Influence of the residual solvent in Hyflon® AD membranes.* The tendency of Hyflon® AD membranes to retain casting solvent will be described in this chapter. The influence of such a solvent retention on the main properties of Hyflon® AD membranes will be reported.

Chapter 5: *Analysis of the distribution of local free volume in Hyflon®AD membranes by photochromic probes.* In this chapter a quite common photochromic probe technique will be shown to be useful for the determination of the distribution of local free volume in Hyflon®AD membranes. For the first time photochromic Hyflon®AD membranes were obtained and the preparation method will be described in detail.

Chapter 6: *Smart light-switchable Hyflon®AD membranes.* The unusual effect of the photoisomerization of photochromic compounds on transport properties of Hyflon®AD membranes will be discussed in this chapter. Particular attention will be devoted to azobenzene containing Hyflon®AD60X membranes which show the more interesting behaviour.

Summary: In this final chapter the most important conclusions of the previous chapters will be summarized and the perspectives of practical application of Hyflon membranes will be briefly discussed.

Acknowledgements

I would like to thank all people who contributed to the good outcome of this thesis and who helped me in carrying out the research work. First of all I want to thank John: my tutor, my coworker, my referee but most of all my friend. He was always kind and present when necessary: in planning together the research work as well as in interpreting obtained results. Thanks to Elena Tocci, who gave a substantial contribute to the theoretical part of my work. Of course thank to Prof. Drioli: he gave me the possibility to work in his lab and, most important, the financial support to carry out the research. I want to thank Pina De Luca who helped me both to perform NMR characterization of the membranes and when I needed a friend and confidant. A very special thank to Prof. Longeri. I already knew his great talent and capability as scientist, but now I have found out a very special person as well. In other words he is "simply" a BIG MAN. Thanks to Prof. Yampolskii, I appreciated very much his contribution to my thesis and I have been positively struck by his liking and kindness. I want to thank also all my friends: Isabella, Sameh, Luigia, Cesare; my parents, my sisters: Ilaria and Francesca and my dear grandmother Luciana. *"Dulcis in fundo"* a warm thank to my husband Gianni to have been (and to be!!) always close to me!

Thanks to who there is not more here, I miss you!

List of papers

1. J. C. Jansen, M. Macchione, and E. Drioli, "High flux asymmetric gas separation membranes of modified poly(ether ether ketone) prepared by the dry phase inversion technique" *J. Memb. Science*, 255, 167-180, (**2005**).

2. J. C. Jansen, M. Macchione, C. Oliviero, R. Mendichi, G. A. Ranieri, and E. Drioli "Rheological evaluation of the influence of polymer concentration and molar mass distribution on the formation and performance of asymmetric gas separation membranes by dry phase inversion" *Polymer*, 46, 11366-11379, (**2005**).

3. M. Macchione, J. C. Jansen, E. Tocci, E. Drioli "Influence of residual solvent on the gas transport properties of dense Hyflon® AD60X gas separation membranes" *Desalination*, 200, 49-51, (**2006**).

4. J. C. Jansen, M. Macchione, E. Drioli "On the unusual solvent retention and the effect on the gas transport in perfluorinated Hyflon AD® membranes" *J. Memb. Sci*., 287, 132-137, (**2007**).

5. M. Macchione, J. C. Jansen, G. De Luca, E. Tocci, M. Longeri and E. Drioli "Experimental and theoretical analysis of the gas transport in dense Hyflon® AD60X gas separation membranes. Influence of residual solvent" *Polymer*, 48, 2619-2635, (**2007**).

6. M. Macchione, J. C. Jansen, and E. Drioli "Analysis of the distribution of local free volume in Hyflon® AD membranes by photochromic probes" in preparation, not reported.

Patent:

1. J. C. Jansen, M. Macchione, E. Drioli "Smart light-switchable Hyflon® AD membranes" submitted for patenting, not reported.

Contents

Introduction.....V

Acknowledgements.....VII

List of papers.....VIII

PART I: General introduction

Chapter 1

Membranes for gas separation 1

1.1. Types of membranes 1
1.1.1. Porous membranes 2
1.1.2. Non-porous membranes 2
1.1.3. Asymmetric Membranes 3
1.2. Transport through polymeric membrane 5
1.2.1. Robeson plot 5
1.2.2. Driving forces 7
1.2.3. Transport through porous membranes 8
1.2.4. Transport through non-porous membranes 11
1.2.5. Solubility and sorption models 13
1.2.6. Diffusion and time lag 15
References 18

Chapter 2

Perfluoropolymer membranes and free volume in polymers 20

2.1. Introduction 20
2.1.1. Chemical structure of perfluoropolymers 20
2.1.2. Chemical-physical properties of perfluoropolymers 22
2.2. Perfluoropolymers (PFPs) as membrane materials 23
2.2.1. PTFE 24
2.2.2. Amorphous glassy PFPs for dense membranes 25
2.3. Gas and vapor transport in amorphous PFPs 27
2.4. Free Volume in polymers 29
2.4.1. Definition of free volume 29

2.5. Methods to determine FV 30
2.5.1. Positron Annihilation Lifetime Spectroscopy (PALS) 31
2.5.2. ^{129}Xe Nuclear Magnetic Resonance (^{129}Xe NMR) 32
2.5.3. Inverse Gas Chromatography (IGC) 33
2.5.4. Photochromic probe technique 35
2.5.5. Spin probe technique 35
2.5.6. The electrochromic probe technique 36
References 37

Chapter 3

Photochromism 40
3.1. Introduction and a brief historical survey 40
3.1.1. Mechanisms of photoreactions 41
3.1.2. Photochromic compounds 42
3.2. Photochemistry of Azobenzene 44
3.3. Azobenzene in polymer films 47
3.3.1. Non-Linear Optics (NLO) 48
3.3.2. Photobiological experiments 49
3.3.3. Photochromic probes to measure the distribution of local free volume in films. 50
3.4. Photo-induced switching of macroscopic properties with azobenzene 51
3.4.1. Change of gas permeation by photoinduced switching of zeolite-azobenzene membranes 52
3.4.2. Change of gas permeation by photoinduced switching of polymer-azobenzene membranes 53
References 54

PART II: Results

Chapter 4

Influence of the residual solvent in Hyflon AD membranes 59
4.1. Introduction 59
4.1.1. Objectives of the work 61
4.2. Experimental 61
4.2.1. Materials 61
4.2.2. Membrane preparation 62
4.2.3. Gravimetric measurements 63
4.2.4. Differential Scanning Calorimetry 63
4.2.5. ^{1}H High Resolution Magic Angle Spinning Nuclear Magnetic Resonance (^{1}H HRMAS NMR) 63
4.2.6. Mechanical testing 64
4.2.7. Density measurement 64

4.2.8. Gas permeation measurements ... 65
4.2.9. Solubility and diffusion coefficient ... 68
4.2.10. Modeling of transport properties. ... 69
4.2.10.1. Generation and equilibration of polymer structures. ... 69
4.2.10.2. Generation and equilibration of polymer structures. ... 71
4.2.10.3. Theoretical calculation of diffusion and solubility coefficients with the TST ... 72
4.3. Results and discussion ... 73
4.3.1. Quantitative analysis of the residual solvent. ... 73
4.3.2. Density. ... 75
4.3.3. Influence of the residual solvent on the thermal properties. ... 75
4.3.4. Influence of the solvent on the mechanical properties. ... 79
4.3.5. Influence of residual solvent on gas permeation. ... 80
4.3.6. Gas diffusion - experimental. ... 83
4.3.7. Gas diffusion - simulations. ... 85
4.3.8. Gas solubility - experimental. ... 86
4.3.9. Gas solubility - simulations. ... 87
4.3.10. Solid-state NMR spectroscopy. ... 88
References ... 90

Chapter 5

Analysis of the distribution of local free volume in Hyflon®AD membranes by photochromic probes. ... 95
5.1. Introduction ... 95
5.1.1. Theoretical background of the photochromic probe method ... 96
5.1.2. Perfluorinated polymers and free volume ... 96
5.2. Experimental section ... 97
5.2.1. Materials ... 97
5.2.2. Membrane preparation ... 98
5.2.3. UV-Visible characterization ... 100
5.3. Results and discussion ... 101
5.3.1. Fractional Free Volume (FFV) by the group contribution method ... 101
5.3.2. Membrane preparation and phase diagram ... 103
5.3.3. Progress of the photoisomerization reaction ... 104
5.3.4. Determination of molar absorption coefficients ... 105
5.3.5. Determination of the total volume of photochromic molecules ... 106
5.3.6. Determination of local free volume distribution ... 107
5.4. Conclusions ... 108
References ... 110

Chapter 6

Smart light-switchable Hyflon®AD membranes ... 112
6.1. Introduction ... 112
6.2. Experimental ... 113
6.2.1 Photochromic membrane preparation ... 113

6.2.1.1 Phase diagram 113
6.2.1.2 Preparation of reference membranes 113
6.2.2 Photoisomerization and spectroscopic analysis 114
6.2.3 Permeation measurements 114
6.3. Results and discussion 115
6.3.1 Photochromic membrane preparation 115
6.3.2 Photoisomerization and spectroscopic analysis 115
6.3.3 Permeation measurements 117
6.3.3.1 Photochromic membranes of Hyflon® AD60X 117
6.3.3.2 Effect of photoisomerization on gas transport 118
6.3.3.3 Diffusion and solubility of AZB containing Hyflon® AD60X membrane 121
6.3.3.4 Influence of the solvent 125
6.3.3.5 Influence of the polymer 127
References 128

Summary 131

Symbols and abbreviations 134

Appendix: enclosed papers 139

PART I

General introduction

1.

Membranes for gas separation

1.1. Types of membranes

A membrane may be defined as a permselective barrier between two homogeneous phases. Based on structure and materials, membranes can be classified in several categories: porous or dense, symmetric or asymmetric, integral or composite and almost any combination of these.

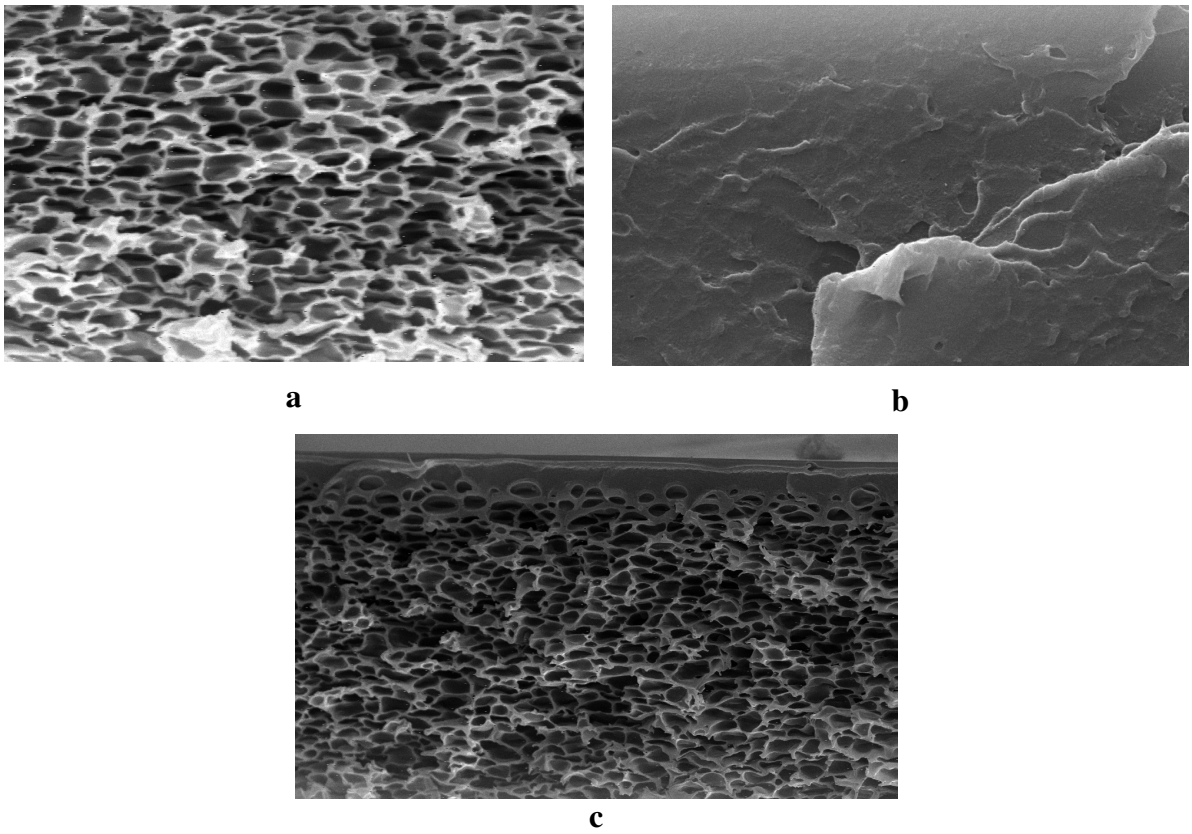

Figure 1.1. *Schematic representation of the structure of a) an asymmetric porous membrane with interconnected pores, b) a dense membrane with closed pores and c) an asymmetric membrane with a dense skin layer and a porous support.*

1.1.1. Porous membranes

A porous membrane is a rigid, highly voided structure with randomly distributed inter-connected pores, see Figure 1.1a.

The separation of molecules by porous membranes is mainly a function of the permeate character and the membrane properties like the pore size and pore size distribution. A porous membrane is very similar in its structure and function to a conventional filter.

In general, only those molecules or particles that differ considerably in size can be separated effectively by microporous membranes. Porous membranes for gas separation can exhibit very high levels of flux but provide for low separation and selectivity. Microporous membranes are characterized by the average pore diameter d, the membrane porosity ε (the void fraction of the total membrane), and the tortuosity of the membrane τ.

There are several ways to prepare porous polymeric membranes, such as, sintering, stretching, track etching and phase separation. In the latter case, the final morphology of the obtained membrane will vary greatly, depending on the properties of materials and the process conditions utilized.

1.1.2. Non-porous membranes

Non-porous or dense membranes provide high selectivity or separation of gases but the rates of the transport of gases are usually low. An important property of dense membranes is that even permeants of similar size may be separated if their solubility in the membrane differs significantly. Dense membranes usually can be prepared by melt-processing of the polymer powder at an opportune pressure and at a temperature above the glassy transition temperature, Tg, of the polymer. An easier alternative procedure to produce dense membranes is the solvent evaporation from a casting solution containing the solvent and the polymer, as shown in Figure 1.2.

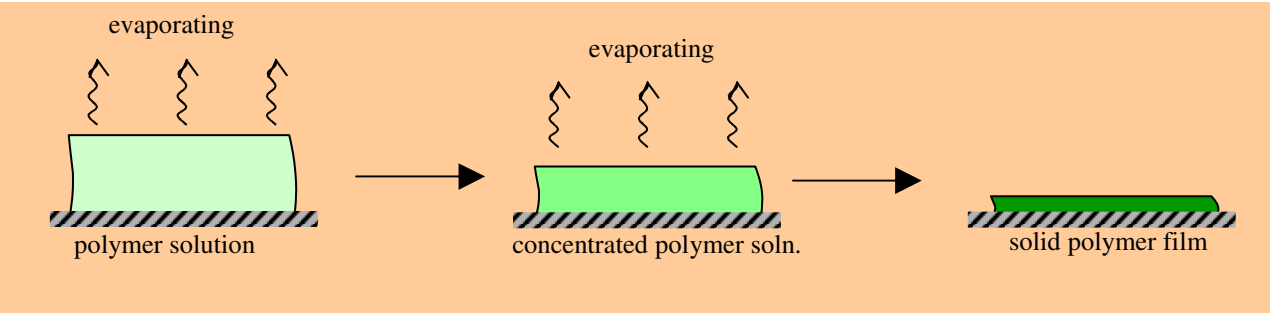

Figure 1.2. *Schematic representation of the preparation of a dense membrane by solvent evaporation.*

1.1.3. Asymmetric Membranes

Asymmetric membranes, Figure 1.1c, consist of two structurally distinct layers, one of which is a thin, dense (or nearly dense!!), selective skin or barrier layer and the other a thick, porous matrix whose main function is to provide a physical support for the thin skin.

Two general classes of asymmetric membranes are universally recognized: integrally skinned and thin film composite types.

Since the first integrally skinned cellulose acetate membranes prepared by Loeb and Sourirajan's method [1], dry-wet casting is the most widely used preparation method for asymmetric membranes of nearly any kind of (soluble) polymer, having either a dense or a porous top layer. Since Loeb and Sourirajan's discovery an endless number of papers and books has been published, covering nearly every aspect of the dry-wet phase inversion process, the thermodynamic and kinetic factors involved and the morphologies that can be obtained, both by experimental and by theoretical studies [2-6].

An interesting alternative is the dry phase inversion process. Although the literature reports the formation of isotropic porous structures by this process [7,8], under the right conditions it is possible to obtain skinned asymmetric membranes.

This method offers several advantages compared to the traditional 'wet' immersion precipitation process, such as the simplicity of the method and the absence of a coagulation bath. Instead of using a coagulation bath, the polymer is dissolved in a mixture of volatile solvent and less volatile nonsolvent. Upon evaporation of the solvent from the cast film the increasing nonsolvent concentration induces phase inversion of the polymer solution into a polymer-rich and a polymer-poor phase.

Further evaporation of the solvent will lead to an increase of the concentration and to vitrification of the polymer. A vitrified but still plasticized polymer cannot be separated into a polymer-rich and a polymer-poor phase [9-11], so if the evaporation is sufficiently fast and the time scale of polymer vitrification at the air-cast film interface is shorter than that of pore nucleation, then a dense skin will result. Further drying of the film occurs by relatively slow diffusion of solvent through the vitrified skin.

Therefore nucleation and pore growth can still occur in the underlying film and finally a porous substructure and a dense skin will be formed. The evaporation process for a typical ternary-casting system, consisting of polymer/solvent/nonsolvent used for the preparation of membrane made by dry/wet phase inversion, is described by the phase diagram, (Figure 1.3.). The binodal curve delimitates the two-phase region, namely the polymer-rich and the polymer-lean phases. Their composition is given by the tie lines. The spinodal curve represents the line where all possible fluctuations in terms of phase separation can occur and that lead to instability within the system. The region between the binodal and spinodal corresponds to a metastable composition where phase separation by nucleation and growth takes place. Therefore, the membrane morphology and transport properties can be controlled by the choice and concentration of the nonsolvent in the casting solution [11] and by the temperature and air circulation during the casting process [12].

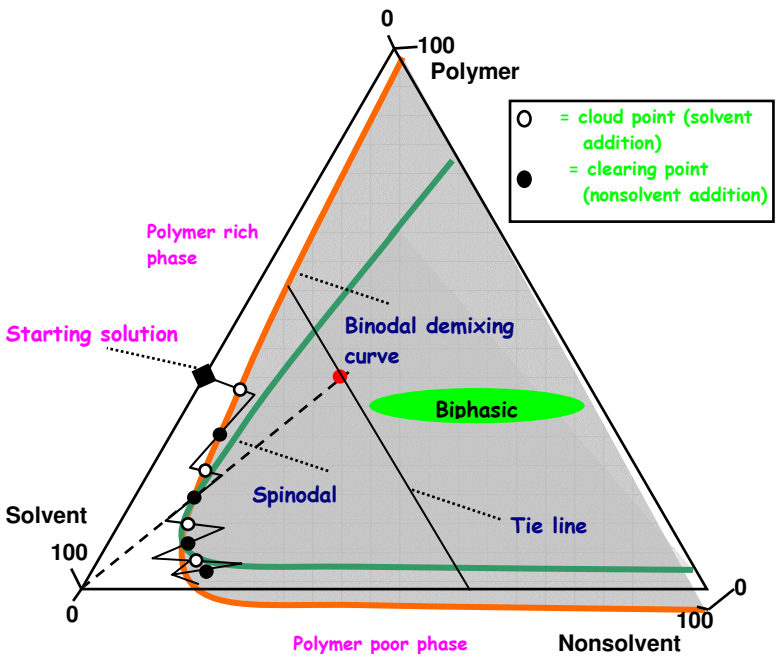

Figure 1.3. *Schematic representation of the ternary phase diagram and the determination of the binodal demixing curve by alternating addition of nonsolvent (cloud point, ○) and solvent (clearing point, ●) to the polymer solution.*

1.2. Transport through polymeric membranes

In many processes, including those in nature, transport proceeds via diffusion rather than convection. Substances diffuse spontaneously from places with a high chemical potential to those where the chemical potential is lower. The permeability of a gas through an elastomeric and a glassy material may differ by more than five orders of magnitude, despite both materials being non-porous. This difference arises from large differences in segmental motion which is very restricted in the glassy state. The presence of crystallites can further reduce the mobility. A factor that enhances segmental mobility, or chain mobility in general, is the presence of low molecular weight penetrants. Increasing concentrations of penetrants inside the polymeric membrane generally leads to an increase in the chain mobility and consequently to an increase in permeability. The concentration of penetrant inside the polymeric membrane is determined mainly by the affinity between the penetrant and the polymer. In gas separation there is usually hardly any interaction between the gas molecules and the membrane material and the gas concentration in the membrane is very low. The gas molecules must diffuse through a rigid membrane structure with the state of the polymer being hardly affected by their presence. Only CO_2 at high pressure is often a strong plasticizer. Gas separation is possible even with two extreme types of membrane: porous and non-porous. The transport mechanisms through these two types of membranes, however, are completely different.

1.2.1. Robeson plot

A well-known empirical rule is that more permeable polymers are, statistically, less permselective and vice versa. Unfortunately, this “tradeoff” behavior of the transport parameters has not received a comprehensive theoretical explanation. This observation was made by many authors as a result of the examination of numerous permeation parameters of different gas/polymer systems in the form of tables or plots of permeability versus permselectivity for various gas pairs M_i and M_j [14,15]. However, the most detailed and comprehensive analysis of this regularity was given by Robeson [16], who presented plots of log Pi versus log α_{ij} for six simple gases and several hundred polymers. A potential attractiveness of a polymer as the membrane material is determined by the position of the point (i.e. the combination of α_{ij} and Pi values) on such a graph. It was shown that the

transport parameters α_{ij} and Pi form a cloud on this diagram which is located below a so-called upper bound, which is a line drawn through the points corresponding to the best achieved combination of α_{ij} and Pi values. According to Robeson, above the upper bound, virtually no values exist. The closeness of a point to the upper bound line is regarded as a measure of how attractive the polymer is for application as a membrane material. From a practical point of view, it is quite desirable to find polymers that would exhibit both high permeability Pi and permselectivity α_{ij} , that is to go above and to the right of the upper bound line. In fact, the efforts of synthetic chemists and physical chemists in membrane material science of the last decade are directed towards achieving this objective.

Figure 1.4 illustrates the permeability-permselectivity diagram for the O_2/N_2 pair showing the dynamics of data accumulation for different glassy and rubbery polymers. Since the first demonstration of the existence of the upper bound line in 1980 the synthesis and investigation of novel polymers has continuously moved this line upward in later years.

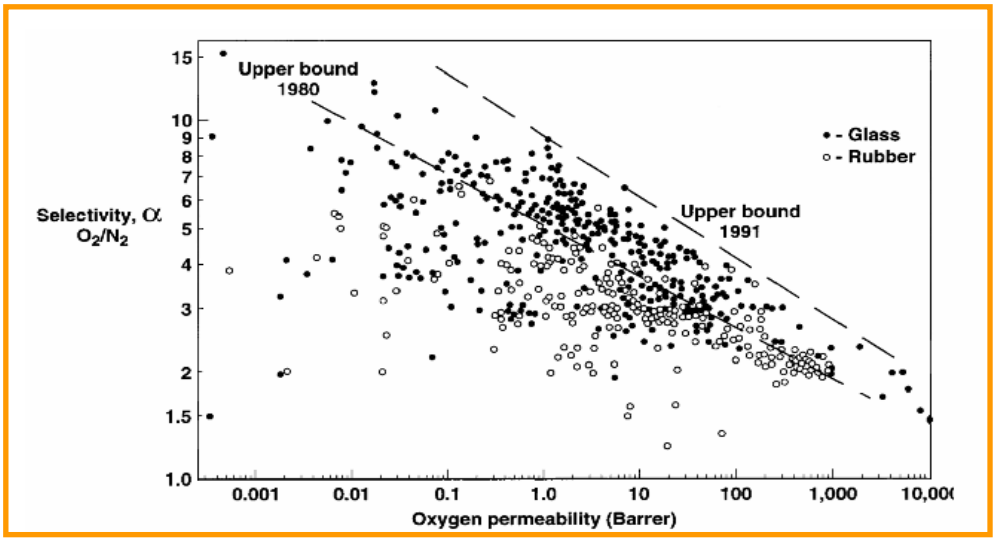

Figure 1.4. *The dynamics of accumulation of the transport parameters for permeability of glassy polymers with respect to oxygen and nitrogen.*

However, there is no rational basis to believe that it will be the same in the future due to the possible appearance of novel polymers with improved transport properties. On the other hand, there is no doubt that the position of the clouds in permeability/permselectivity diagrams for every gas pair M_i and M_j is unique and related to parameters of the gas molecules.

1.2.2. Driving forces

The starting point for the mathematical description of permeation in all membranes is the proposition, solidly based in thermodynamics, that the driving forces of pressure, temperature concentration and electromotive force are interrelated and that the overall driving force producing movement of a permeant, i, is the gradient in its chemical potential, μ_i. Thus the flux J_i (g/cm^{2}s) across the membrane is described by the simple equation:

$$J_i = c_i\, v_i = c_i\, U_i\, \frac{d\mu_i}{dx} \qquad (1.1)$$

where $d\mu_i/dx$ is the gradient in chemical potential of component i and U_i is a coefficient of proportionality linking the chemical potential driving force $d\mu_i/dx$ with the velocity of component i, v_i. When this velocity is multiplied by the concentration of component i molecules, c_i, the result is the flux of component i. All the common driving forces, such as gradients of concentration, pressure, temperature and electromotive force, can be reduced to a chemical potential gradient, and their effect on flux expressed by this equation. This approach is extremely useful, because many processes involve more than one driving force.

If we consider driving forces generated by concentration and pressure gradients, the chemical potential is written as:

$$d\mu_i = RT\, d\ln(\gamma_i n_i) + v_i\, dp \qquad (1.2)$$

where n_i is the mole fraction (mol/mol) of component i, γ_i is the activity coefficient linking concentration with activity, p is the pressure and v_i is the partial molar volume of component i. In incompressible phases, such as a liquid or a solid membrane, volume does not change appreciably with pressure. Integrating equation (1.2) with respect to concentration and pressure then gives:

$$\mu_i = \mu_i^\circ + RT \ln(\gamma_i n_i) + v_i\,(p - p_i^\circ) \qquad (1.3)$$

where μ_i° is the chemical potential of pure i at a reference pressure p_i°.

In compressible gases, the molar volume changes with pressure; using the ideal gas laws and integrating equation (1.2) then gives:

$$\mu_I = \mu_I^\circ + RT\ ln\ (\gamma_i n_i) + RT\ ln \left(\frac{p}{p_i^0} \right) \qquad (1.4)$$

A number of assumptions must be made to define any model of permeation. Usually, the first assumption is that the fluids on either side of the membrane are in equilibrium with the membrane material at the interface. This means that there is a continuous gradient in chemical potential from one side of the membrane to the other. It is implicit in this assumption that the rates of absorption and desorption at the membrane interface are much higher than the rate of diffusion through the membrane. This appears to be the case in almost all membrane processes. The second assumption concerns the way this chemical potential across the membrane is expressed within the membrane.

The mostly widely used solution-diffusion model assumes that the pressure within a membrane is uniform and that the chemical potential gradient of a permeant across the membrane is represented only as a concentration gradient.

On the contrary the pore-flow model assumes that the permeant concentration within a membrane is uniform and that the chemical potential gradient across the membrane is represented only as a pressure gradient.

1.2.3. Transport through porous membranes

Porous membranes consist of a polymeric matrix in which pores within the range of 2 nm to 10 μm are present. Different mechanisms may be involved in the transport of gases across a porous membrane. Figure 1.5 gives a schematic representation of the mechanisms for the permeation of gases through porous membranes.

For light gases, the permeation of gas through porous membranes consists of Knudsen diffusion and Poiseuille flow. The proportions of Knudsen to Poiseuille flow are governed by the ratio of the pore radius (r) to the mean free path (λ) of the gas molecules.

The mean free path (λ) is given by:

$$\lambda = \frac{3\eta}{2P}\frac{\sqrt{(\pi RT)}}{2M} \tag{1.5}$$

where η is the viscosity of the gas, R the universal gas constant, T the temperature, M the molecular weight of the gas molecule and P the permeate pressure.

If $\lambda/r \ll 1$, viscous or Poiseuille flow (G_{vis}) predominates and the gas flux trough the pore is described by the following equation:

$$G_{vis} = \frac{r_2(P_1 - P_2)}{16L\eta RT} \tag{1.6}$$

where r is the pore radius, P_1 the partial pressure of the gas on the feed side, P_2 the partial pressure on the permeate side, and L the pore length.

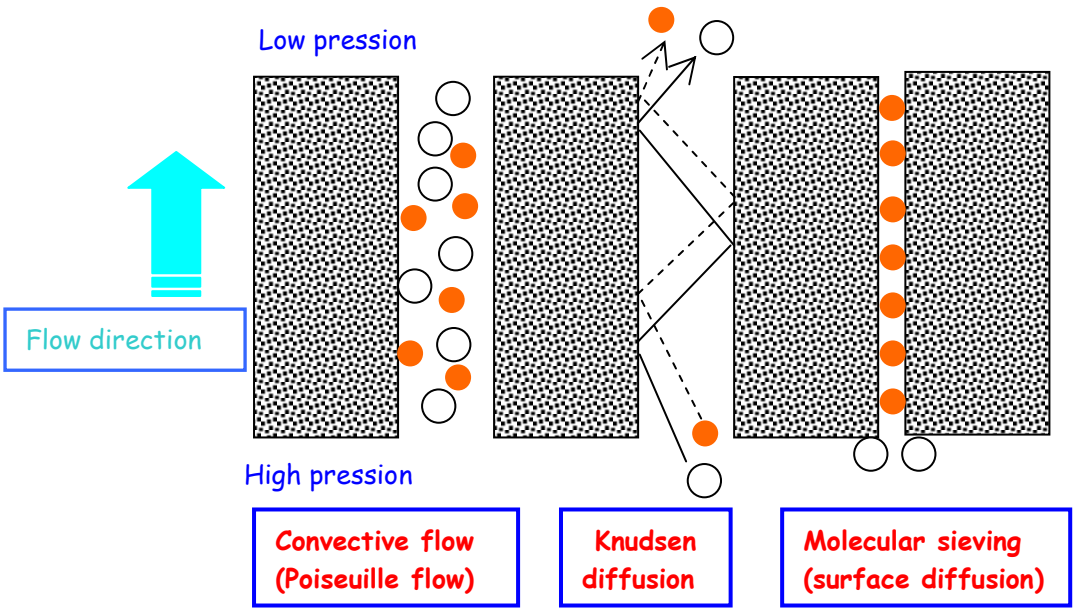

Figure 1.5 *Schematic representation of possible transport mechanisms of light gases in porous membranes.*

In Knudsen flow r/λ is much less than one, then there are more collisions with the pore walls than with other molecules. At every collisions with the pore walls the gas molecules are momentarily absorbed and then reflected in a random direction. As there are less collisions among molecules than with the pore walls, each molecule will move independent from the others. Hence, the separation of a gas mixture is achieved because different gas

species move at different velocities. The molecular flow of the gas (G_{mol}) in such a case is described by the expression:

$$G_{mol} = \frac{8r\,(P_1 - P_2)}{3L\sqrt{(2\pi MRT)}} \tag{1.7}$$

where M is the molecular weight of the gas. For Knudsen flow, the selectivity ratio, a_{ij}, or the separation factor for binary gas mixtures is determined exclusively by the square root of the ratio of the molecular weights:

$$a_{ij} = \frac{G_i}{G_j} = \frac{\sqrt{(RT/3M_i)}}{\sqrt{(RT/3M_j)}} = \sqrt{\frac{M_j}{M_i}} \tag{1.8}$$

Knudsen separation can be achieved with membranes having pores sizes smaller than about 50 nm. Based on Knudsen flow, separation factors for several gas pairs have been calculated and they represent ideal separation factors. Table 1.1 presents the ideal separation factors for various pairs of gases. The actual separation factor, however, is found to be smaller due to the back diffusion, to non-separative diffusion, concentration polarization on the feed or on the permeate side and the occurrence of viscous flow in larger pores.

Table 1.1. Calculated separation factors based on Knudsen flow for selected binary gas mixtures.

Gas pair	Separation factor
H_2/N_2	3.73
H_2/CO	3.73
H_2/H_2S	4.11
H_2/CO_2	4.67
H_2/SO_2	5.64
N_2/O_2	1.07
O_2/CO_2	1.17

In order to function as a molecular sieve, membranes must have pore diameters that are in between those of the gas molecules to be separated. Separation factors greater than 10 should be achievable as the pores become smaller than about 0.5 nm. If the membrane has pore sizes between the diameter of the smaller and the larger gas molecules, then only the

smaller molecule can permeate and a very high separation would be achieved [13]. However the pore size in polymeric membranes is usually larger and molecular sieving mechanism generally occurs only in zeolite and carbon membranes. In practical situations, there will be a distribution of pore sizes in polymeric membrane, and thus the gas permeability is actually influenced by a combination of transport mechanisms.

1.2.4. Transport through non-porous membranes

When the sizes of molecules are in the same order of magnitude, as with oxygen and nitrogen or hexane and heptane, porous membranes cannot effect a separation. In this case nonporous membranes must be used. However, the term nonporous is rather ambiguous because pores are present on a molecular level in order to allow transport even in such membranes. The existence of these dynamic molecular pores can be adequately described in terms of free volume. Fick's law is the simplest description of gas diffusion through a non-porous structure:

$$J = -D\frac{\delta c}{\delta x} \tag{1.9}$$

where J is the flow rate through the membrane, D is the diffusion coefficient and the driving force $\delta c/\delta x$ is the concentration gradient across the membrane. Under steady state conditions this equation can be integrated to give:

$$J = \frac{D(c_0 - c_l)}{l} \tag{1.10}$$

where c_0 and c_l are the concentrations in the membrane on the upstream side and downstream side, respectively. The quantity l is the thickness of the membrane.

The concentrations are related to the partial pressure by Henry's law which states that a linear relationship exists between the concentration inside the membrane and the pressure of gas outside the membrane:

$$c = S\,p \tag{1.11}$$

where S is the solubility coefficient. Combining the previous two equations gives:

$$J = \frac{DS(p_0 - p_l)}{l} \tag{1.12}$$

An equation which is generally used for the description of gas permeation trough membranes. The product of the diffusion coefficient D (cm^2/sec) and the solubility coefficient S ($cm^3_{STP}/cm^3 bar$) is called the permability coefficient P:

$$P = DS \tag{1.13}$$

Solubility is a thermodynamic parameter and involves both an enthalpic aspect (interaction between permeant and matrix) and an entropic aspect (maximum degree of freedom and optimal distribution of the space), in other words it gives a measure of the amount of penetrant sorbed by the membrane under equilibrium conditions. In contrast, the diffusivity is a kinetic parameter which indicates how fast a penetrant is transported through the membrane. The pure or ideal gas selectivity, α, is a measure of the potential separation characteristics of the membrane material. It is defined as the ratio of the permeability coefficients of pure gases A and B:

$$\alpha_{A/B} = P_A/P_B \tag{1.14}$$

Considering Eq. (1.13), the selectivity can be also expressed by:

$$\alpha_{A/B} = (D_A/D_B)\,(S_A/S_B) \tag{1.15}$$

The selectivity is clearly the product of two contributions. The first is the ratio of the diffusion coefficients and is often called the mobility or diffusivity selectivity; the second contribution is the sorption selectivity or solubility selectivity and reflects the relative sorption of the gases in the polymer matrix. Equations (1.13)-(1.15) define the three fundamental transport parameters in a dense polymeric membrane: permeability, solubility and diffusivity. If the gas solubility is determined independently, for instance by sorption measurements, then Eq. (1.13) allows the calculation of the diffusion coefficient from

permeation data. Alternatively, measurement of P and D allows the calculation of the solubility of the gas in the polymer matrix

1.2.5. Solubility and sorption models

Solubility of gases in polymers has been of continuous experimental and theoretical interest because gas and vapor separation membranes are based on the so-called solution–diffusion mechanism, according to which thermodynamic parameters of gas sorption determine the mass transfer driving force. The transport of penetrant through a polymer film is commonly described by a three-step solution-diffusion process, characterized by absorption of the gas at the polymer-gas interface at the feed side, followed by diffusion of the dissolved species across the membrane and desorption of the gas species from the polymer-gas interface at the low pressure side. The first important factor is thus the sorption of the gas at the feed side, which depends on the solubility of the specific gas in the polymer matrix. The solubility of light gases in polymers is generally low (< 0.2 % by volume) and it is assumed that the gas diffusion coefficient is constant.

Such cases can be considered as ideal systems where Fick's law is obeyed. On the other hand, the solubility of organic liquids (and vapours) can be relatively high and the diffusion coefficient is now assumed to be concentration-dependent.

For ideal systems, where the solubility is independent of the concentration (S = constant), the sorption isotherm is linear (Henry's law), i.e. the concentration, c, inside the polymer is proportional to the applied pressure, P ($c = Sp$), see Figure 1.6. This behaviour is normally observed with gases in elastomers. In materials with a limited sorption capacity, for example in zeolites, the sorption isotherm is generally curved (Langmuir sorption). This process dominates when a permanent gas is absorbed in specific sites at high pressure. The concentration of the gas reaches a saturation level (S has an asymptotic maximum). On the contrary, in the case of non-ideal system, the solubility increases continuously with the pressure (Flory-Huggins model, Figure 1.7). Such a behaviour represents the tendency of the penetrant to form clusters, i.e. the penetrant becomes a plasticizer for the polymer.

The dual mode sorption model is the most common for the glassy polymers and exists only in the glassy phase. According to this model, it is assumed that two sorption mechanisms occur simultaneously, i.e. sorption according to Henry's law and sorption via

Langmuir type, Figure 1.6. At low pressure, the dual mode curve sorption approaches linearity and the solubility can be considered constant as in the case of Henry sorption.

From a physical point of view, however, it is difficult to understand the existence of two different types of sorbed gas molecules.

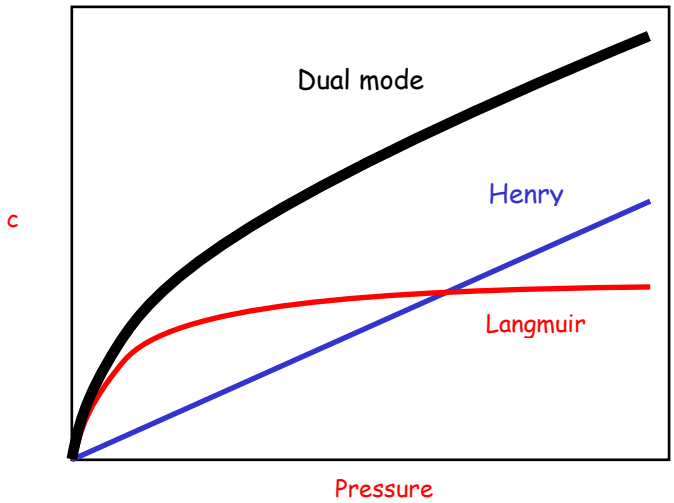

Figure 1.6 *Typical isotherm plots of gas concentration versus pressure.*

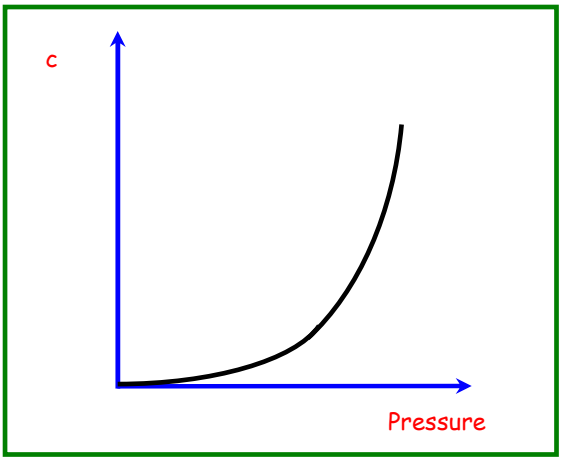

Figure 1.7 *Flory-Huggins isotherm.*

Usually, in the case of dual mode sorption, the concentration of the penetrant in the membrane is given by the following equation:

$$C = K_d P + \frac{c_h^{'} bP}{1 + bP} \tag{1.16}$$

where K_d (cm^3 (STP) cm^{-3} bar^{-1}) is the Henry coefficient, c'_h (cm^3 (STP) cm^{-3}) is the capacity of saturation in the cavities of the Langmuir isotherm and b (bar^{-1}) is the hole affinity constant.

1.2.6. Diffusion and time lag

The overall transport across the membrane depends on the penetrant solubility but also on its diffusion coefficient, as already illustrated with Eq. 1.13. A common procedure to determine the diffusion coefficient by permeation experiments is the time lag method, based on the penetration theory. If a penetrant-free membrane is exposed to the penetrant at the feed side at t=0 and the penetrant concentration is kept very low at the permeate side, then the total amount of penetrant, Q_t, passing through the membrane in time t is given by [17]:

$$\frac{Q_t}{l \cdot c_i} = \frac{D \cdot t}{l^2} - \frac{1}{6} - \frac{2}{\pi} \sum_{l}^{\infty} \frac{(-1)^n}{n^2} \exp\left(- \frac{D \cdot n^2 \cdot \pi^2 \cdot t}{l^2} \right) \tag{1.17}$$

in which c_i is the penetrant concentration at the membrane interface at the feed side and l is the membrane thickness. Physically this equation represents the following process, which is schematically displayed in Figure 1.8 and Figure 1.9. In the absence of any significant transport resistance at the feed side the gas reaches nearly instantaneously an equilibrium concentration in the membrane just at the interface (c_1). If the membrane has been carefully evacuated before, the penetrant concentration at that stage is still zero in the rest of the membrane cross section. This is schematically displayed in Figure 1.8. In the subsequent penetration phase the gas gradually diffuses into the membrane and a concave concentration profile is established (red curves). In this phase no permeation occurs because the penetrant concentration at the permeate side is still zero and the permeate pressure remains constant, see Figure 1.9. In the transition stage, as soon as the fastest molecules reach the permeate side, they desorb at the membrane-permeate interface and the permeate pressure gradually starts rising (blue curves in Figure 1.8 and transient zone in Figure 1.9) until a linear concentration profile is established. In the final stage, the steady state situation, a linear concentration profile is present in the membrane and the pressure increase rate in the permeate volume is constant (green curves in Figure 1.8). The penetrant concentration in the

membrane at the interface at the permeate side is in equilibrium with the gas pressure in the permeate volume. In practical experiments this pressure is usually very low and negligible compared to the feed pressure. This model, which assumes a pressure-independent solubility and a concentration independent diffusivity, is generally valid for light gases in both glassy and rubbery polymers up to moderately high pressures.

At long times the exponential term in Eq. (1.17) approaches to zero and Eq. (1.17) reduces to:

$$Q_t = \frac{D \cdot c_i}{l}\left(t - \frac{l^2}{6D}\right) \tag{1.18}$$

A plot of Q_t versus time describes a straight line which intersects the time axis at $t = l^2/6D$, defined as the time lag, Θ.

$$\Theta = \frac{l^2}{6D} \tag{1.19}$$

In a constant volume setup the amount Q is directly proportional to the permeate pressure.

The time lag can be obtained by linear extrapolation of the steady state pressure increase curve to the time axis or to the starting pressure (Figure 1.9). Knowing the membrane thickness, the diffusion coefficient can then be obtained from Eq. (1.19) and subsequently the solubility can be obtained from the steady state permeation and Eq. (1.13): $S = P/D$.

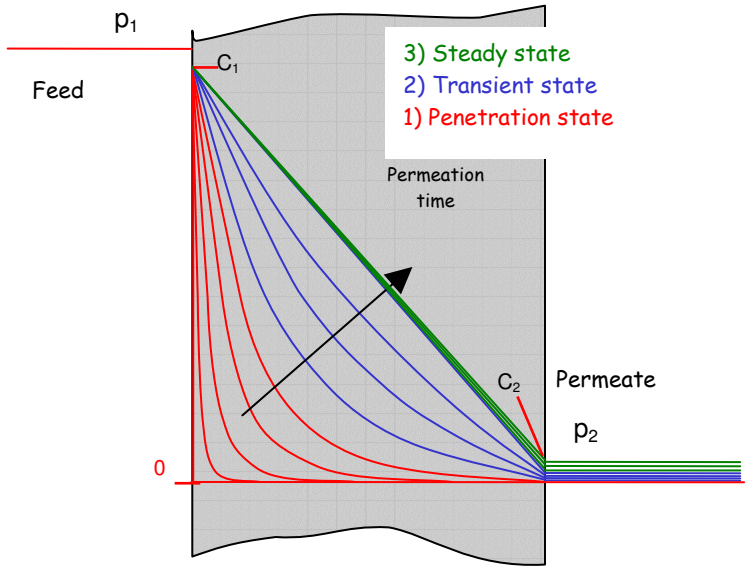

Figure 1.8 *Scheme of the concentration profile of the gas in a non-porous membrane after the first exposure. Difference between P_1 and P_2 is usually larger but is underestimated here for clarity.*

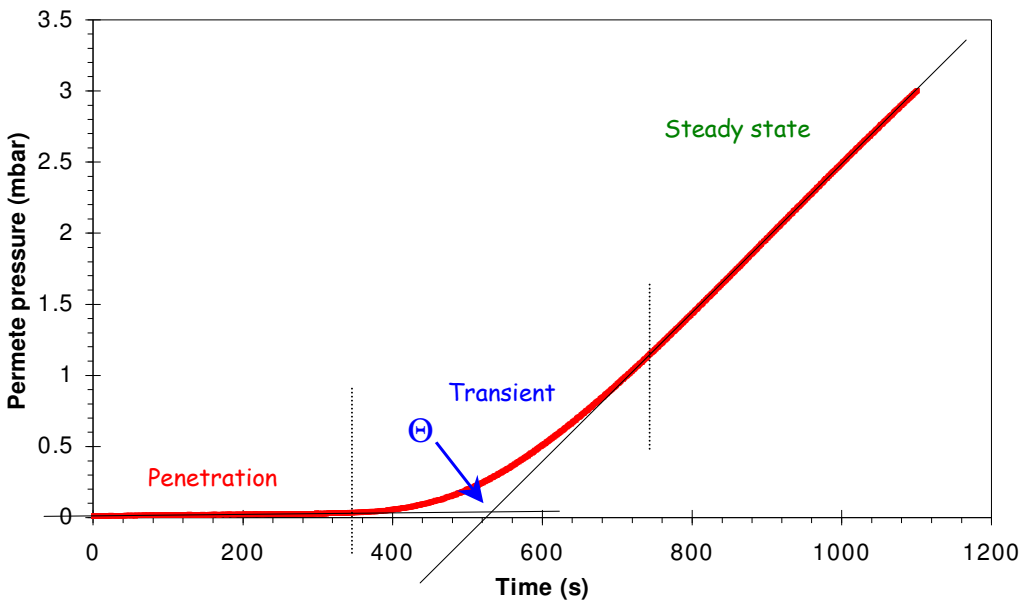

Figure 1.9 *Typical time lag experiment in which the pressure of a fixed permeate volume is measured as a function of time from the first exposure of the membrane to the gas.*

References

1. S. Loeb, and S. Sourirajan, Sea water demineralization by means of an osmotic membrane, Saline Water Conversion-II, *Adv. Chem.*, **1963**, 28, 117.
2. A.J. Reuvers, J.W.A. van den Berg and C.A. Smolders, Formation of membranes by means of immersion precipitation. Part. I. A model to describe mass transfer during immersion precipitation, *J. Membrane Sci.*, **1987**, 34, 45.
3. A.J. Reuvers and C.A. Smolders, Formation of membranes by means of immersion precipitation. Part. II. The mechanism of formation of membranes prepared from the system cellulose acetate-acetone-water, *J. Membrane Sci.*, **1987**, 34, 67.
4. M. Mulder, Basic Principles of Membrane Technology; Kluwer, Dordrecht, The Netherlands, **1991**.
5. R.E. Kesting,; A.K. Frietzsche, Polymeric Gas Separation Membranes, Wiley, New York, **1993**.
6. R.E. Kesting, Synthetic Polymeric Membranes. A structural perspective, 2nd Ed., Wiley, New York, **1985**.
7. H. Matsuyama, M. Tachibana, T. Maki, M. Teramoto, Light scattering study on porous membrane formation by dry-cast process., *J. Appl. Polym. Sci.*, **2002**, 86, 3205-3209.
8. T.-H. Young, J.-H. Huang, W.-Y. Chuang, Effect of evaporation temperature on the formation of particulate membranes from crystalline polymers by dry-cast process, *Eur. Polym. J.*, **2002,** 38, 63-72.
9. M. Wessling, M. Lidon Lopez, H. Strathmann, Accelerated plasticization of thin-film composite membranes used in gas separation, *Sep. Purif. Technol.*, **2001**, 24, 223-233.
10. H. Matsuyama, M. Teramoto and T. Uesaka, Membrane formation and structure development by dry-cast process, *J. Membrane Sci.*, **1997**, 135, 271.
11. J.C. Jansen, M. Macchione, and E. Drioli, High flux asymmetric gas separation membranes of modified poly(ether ether ketone) prepared by the dry phase inversion technique, *J. Membrane Sci.*, **2005**, 255, 167-180.
12. M. Macchione, J.C. Jansen, and E. Drioli, The dry phase inversion technique as a tool to produce highly efficient asymmetric gas separation membranes of modified PEEK. Influence of temperature and air circulation, *Desalination*, **2006**, 192, 132-141.
13. R. M. Barrer, E. Strachan, Proc. R. Soc. Lond., Ser **1955**, A231, 52.

14. S. A. Stern, Gas separation processes, in: S. Loeb, P.E. Lacey (Eds.), Industrial Processing with Membranes, Elsevier, NY, **1972**, p.279.
15. W. J Koros, R. T. Chern, Separation of gaseous mixtures, in: R. Y. Rousseau (Ed.), Handbook of Separation Progress Technology, Wiley, **1987**.
16. L. M. Robeson, Correlation of separation factor versus permeability for polymeric membranes, *J. Membr. Sci*., **1991**, 62, 165.
17. J. Crank, G.S. Park, Diffusion in Polymers, Academic Press, London, **1986**

2.

Perfluoropolymer membranes and free volume in polymers

2.1. Introduction

Membrane processes are receiving increasing attention in the scientific community and in industry because in many cases they offer a favorable alternative to processes that are not easy to achieve by conventional routes. In this context, membranes made with perfluorinated polymers are of particular interest because of the unique features demonstrated by these materials. In many applications fluoropolymers offer the highest protection afforded by any polymer available today, to a huge variety of chemicals, such as acids and alkalis, fuels and oils, low molecular weight esters, ethers and ketones, aliphatic and aromatic amines, and strong oxidizing substances.

Both highly hydrophobic and hydrophilic membranes have been developed from appropriate perfluoropolymers that were, in turn, obtained by copolymerizing TFE with special monomers available on an industrial scale. Highly hydrophobic films obtained from the glassy copolymers of TFE and 2,2,4-trifluoro-5 trifluoromethoxy-1,3 dioxole (Hyflon AD) exhibit properties that make them particularly well suited for use in optical applications, in the field of gas separation, and in gas-liquid contactors. Hydrophylic highly conductive proton exchange membranes obtained from the copolymer of TFE and a short-side-chain (SSC) perfluoro-sulfonylfluoride-vinylether (Hyflon Ion) find interesting application in the field of fuel cells, especially in view of the current tendency to move to high temperature operation.

2.1.1. Chemical structure of perfluoropolymers

The discovery of polytetrafluorothylene (PTFE, Figure 2.1) in 1938 by Roy Plunkett [1] at DuPont spurred the development of a wide variety of rubbery and glassy perfluoropolymers (PFPs) such as Teflon® AF by DuPont [2,3], Cytop™ by Asahi Glass [4] and Hyflon® AD

by Ausimont (now Solvay Solexis) [5]. The chemical structures and selected properties of these polymers are shown in Table 2.1. For comparison, semicrystalline polytetrafluoroethylene is included in this table as well.

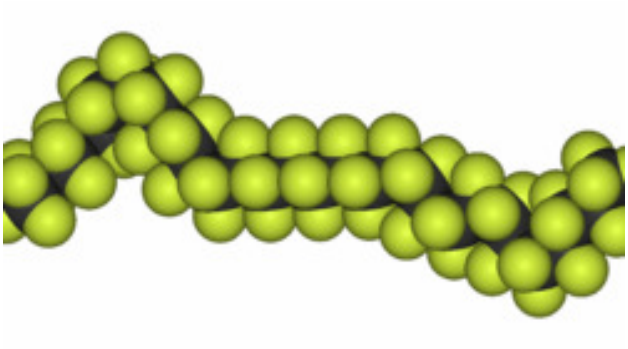

Figure 2.1. *Modeling of the structure of polytetrafluoroethylene (PTFE).*

Glassy polymers, based on copolymers of tetrafluoroethylene and 2,2-bis(trifluoromethyl)-4,5-difluoro-1,3-dioxole, can be readily dissolved in and cast from perfluorinated solvents. The large, bulky dioxole monomer hinders efficient polymer chain packing, thereby preventing crystal formation and yielding a completely amorphous polymer. Monomers used for the synthesis of fluorinated polymers can be briefly classified into two categories, 1) base monomers and 2) special monomers. The former are represented by those monomers that constitute the basic structure of modern fluoropolymers and the latter by those other monomers that add specially desired characteristics to match specialty application requirements, see Figure 2.2.

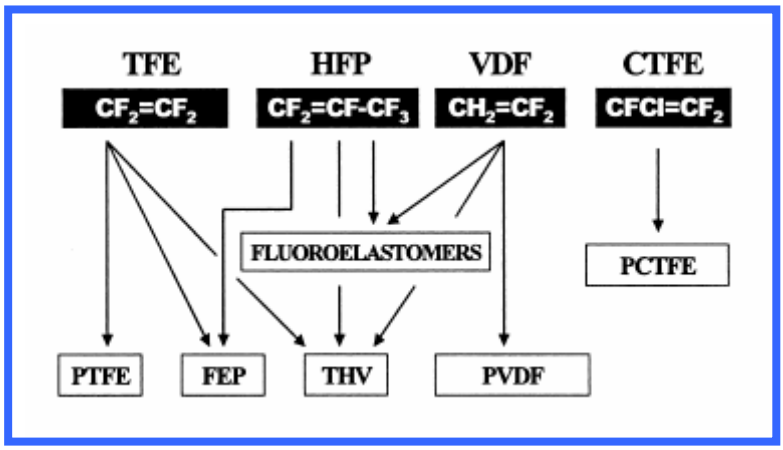

Figure 2.2*. Schematic representation of the constitution of base fluorinated homo- and copolymers.*

Within the scheme above, base fluoromonomers are tetrafluoroethylene (TFE), hexafluoropropylene (HFP), vinylidenefluoride (VDF), and chlorotrifluoroethylene (CTFE).

Proper combination of these monomers yields homo- or copolymers with the most diverse characteristics: PTFE, FEP, fluoroelastomers, PVDF, PCTFE, and THV. In the field of films and membranes the base polymers mentioned above find wide application: just to mention some examples, films for anticorrosion (PTFE and FEP), films for protective packagings (PCTFE), microfiltration and ultrafiltration membranes (PVDF and PTFE), vapor permeable clothes and shoes (PTFE), and separators for lithium ion batteries (PVDF).

2.1.2. Chemical-physical properties of perfluoropolymers

Fluoropolymer materials are capturing greater and greater interest in industrial applications because of the remarkable combination of properties that they exhibit when compared to other polymeric materials. The most well-known property for which fluoropolymers are employed in high-demanding applications is their outstanding thermal and chemical resistance. However, the peculiar nature of the carbon–fluorine bond confers on these materials other unique physical properties (e.g., electrical, optical, and superficial) that can be valuably exploited in the most variegated fields. Perfluoropolymers represent the ultimate in resistance to hostile chemical environments and high service temperature because of the high bond energy of C–F and C–C bonds of fluorocarbons, equal to 485kJ/mol and 360kJ/mol, respectively [6].

Fluoropolymers also possess exceptional optical, electrical and surface properties [6,7] that have resulted in the commercial use of fluoropolymers in numerous areas, including the automotive, electronic, aerospace, chemical, specialty packaging and medical industries [6-8].

Table 2.1. : Structures and properties of selected perfluoropolymers, [9]

Polymer	Chemical structure	Density (g/cm^3)	Tg [9] (°C)	N_2 Permeability (barrer)
PTFE	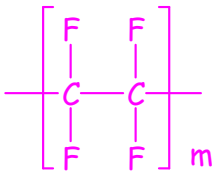	2.1	30	1.3 [10]
Teflon® AF	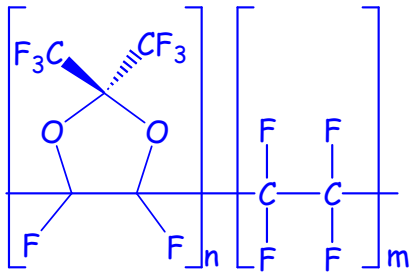	1.74	240	480 [11]
Cytop®	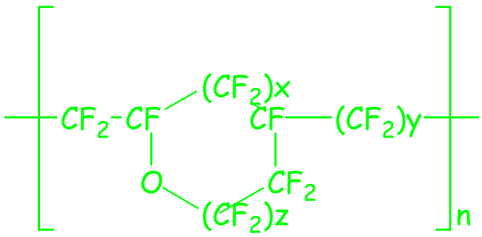	2.03	108	5.0[11]
Hyflon® AD	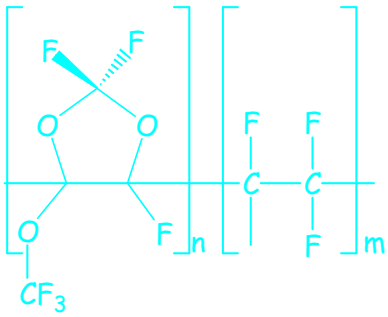	1.92	130	24[12]

2.2. Perfluoropolymers (PFPs) as membrane materials

The discovery in the past 20 years of amorphous, solvent-processable perfluoropolymers, such as Teflon®AF, Cytop®TM and Hyflon®AD, has created new opportunities for perfluorinated materials in membrane separations. Indeed, the high gas permeability of these polymers [2,3,12], due to the great amount of free volume, combined with the usual perfluoropolymer chemical and thermal stability, makes them intriguing membrane materials for gas and vapor separations. These amorphous perfluoropolymers can be

fabricated into thin, high-flux, composite membranes while retaining the excellent chemical stability typical of fluorinated materials.

Relative to PTFE, Teflon AF is significantly less dense due to the large, rigid dioxole monomer, which obstacles efficient chain packing. The resultant open polymer structure causes Teflon AF2400 to be more than two orders of magnitude more permeable to nitrogen than PTFE. Similarly, the other amorphous perfluoropolymers are also substantially more permeable than PTFE. In addition, and perhaps most important from an applications standpoint, all three amorphous perfluoropolymer types are soluble in selected perfluorinated solvents, which renders them amenable to composite membrane fabrication via solution casting.

2.2.1. PTFE

The common statement that PTFE is a spin-off from the United States space program is an urban legend. PTFE, was discovered accidentally by Roy Plunkett of DuPont in 1938 [1].

Legend has it that, while he attempted to make a new chlorofluorocarbon (CFC) refrigerant, the perfluorethylene polymerized in its pressurized storage container (in this original chemical reaction, iron from the inside of the container acted as a catalyst.) DuPont patented it in 1941 and registered the Teflon trademark in 1944.

It was first sold commercially in 1946. By 1950, DuPont was producing over a million pounds (450 t) per year in Parkersburg, West Virginia. In 1954, french engineer Marc Grégoire created the first pan coated with Teflon non-stick resin.

PTFE is a white solid at room temperature, with a density of about 2.2 g/cm³. According to DuPont its melting point is 327 °C [6], but its properties degrade above 260 °C. PTFE is insoluble in all common solvents and not melt-processable by conventional means because of its high melting point, making it difficult to use as selective materials in commercial asymmetric hollow fibers or composite membranes where solution-casting fabrication techniques are generally used.

Since PTFE presents excellent dielectric properties, especially at high radio frequencies, it is suitable for use as an insulator in cables and connector assemblies and as a material for printed circuit boards used at microwave frequencies. Combined with its high melting temperature, this makes it the material of choice as a high-performance substitute for the

weaker and lower melting point polyethylene that is commonly used in low-cost applications. Due to its semi-crystalline structure, PTFE is mainly used for porous membrane (e.g. Gore®Tex). Indeed, Xing and co-workers used porous PTFE to reinforce SPEEK [13] and Yamaguchi used porous PTFE as a porous substrate and filled the pores with poly (vinylsulfonic acid/acrylic acid) crosslinked gel. Porous PTFE membrane were also used to reinforce Nafion membranes[14]. Indeed, the good tensile strength made it possible for a thinner composite membrane to be used in the fuel cell which improves the cell performance.

2.2.2. Amorphous glassy PFPs for dense membranes

Amorphous perfluoropolymers show glass transition temperatures (Tg) greater than room temperature [10], a thermal decomposition temperature exceeding 400°C and are highly transparent to light from far UV to near infrared. TFE–TTD copolymers, commercially known as Hyflon®AD polymers, are synthesized by free radical polymerization. Amorphous polymers of Hyflon®AD are obtained when m/n is less than about 4 (see Table 1.1); that is, when the TTD molar content is higher than about 20%.

Due to the cyclic structure and the effective steric hindrance of the side group, chain motion is severely hindered and high Tg glassy polymers result. When $m = 0$, as is the case with TTD homopolymer, Tg = 170°C. At increasing m/n values (decreasing TTD content), Tg decreases, see Figure 2.3, [15].

Polymer	TFE	TTD	PDD	BVE	T_g
	(% mol)				(°C)
TTD homopolymer	—	100	—	—	170
Hyflon AD 80	15	85	—	—	135
Hyflon AD 60	40	60	—	—	110
PDD homopolymer	—	—	100	—	335
Teflon AF 2400	13	—	87	—	240
Teflon AF 1600	35	—	65	—	160
Cytop	—	—	—	100	108

***Figure 2.3**. Glass transition temperature (Tg) for amorphous perfluoropolymers at various compositions*

Teflon®AF is obtained by the copolymerization of perfluoro- 2,2 dimethyldioxole (PDD) with TFE. Cytop is obtained by the cyclopolymerization of perfluoro-butenylvinylether (BVE), which offers a controlled alternate structure but fixes the content of the cyclic portion of the chain to 50%, thus limiting the Tg of the polymer to 108° C.

TFE–TTD copolymers exhibit very high thermal stabilities, as shown by the weight loss at increasing temperatures obtained by TGA. One-percent weight losses are measured at temperatures as high as 400°C, demonstrating thermal stabilities typical of perfluoropolymers [15]. Two characteristics of TFE–TTD copolymers that make them very attractive for membrane preparation are their high solubilities in perfluorinated solvents and their low solution viscosities [5]. Both features allow great flexibility in the selection of proper conditions for the preparation of membranes with various structures. Moreover, low solution viscosities imply greater ease of purification. This aspect is very important, since it is often crucial in the polymer and polymeric solutions to avoid the presence of both suspended and dissolved contaminants, such as dust or dissolved organic molecules. In fact contaminants can substantially affect properties, such as light transmittance and signal attenuation of optical devices. Various procedures have been tuned to prepare membrane typologies to match application requirements. Examples of solvents used to dissolve amorphous PFPs are Galden®HT110 and Galden®HT55: perfluopolyether oils with the following structure

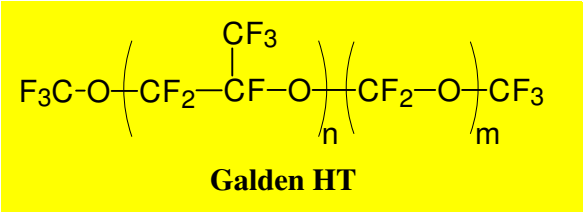

Galden HT

Normal boiling points are equal to 110°C and 55°C, respectively.

Flat sheet porous and non porous symmetric membranes can be obtained by following the evaporation method [16]. Hyflon membranes can be prepared by using a Braive Instruments knife to cast a polymeric solution on glass plates with various initial thicknesses and evaporation temperatures. Flat sheet asymmetric membranes can be prepared by following the dry–wet phase inversion method [16,17].

Symmetric dense films of Hyflon AD find application as UV resistant protective films for the semiconductor industry because of their high transparency at the far-UV wavelength, where conventional nitrocellulose pellicles are degraded due to high energy absorption. In this application, transparent pellicles are used in microlithography to cover the photomask and avoid dust depositing on it and disturbing the preparation of the photoresist. The protective film puts the dust particles out of focus.

2.3. Gas and vapor transport in amorphous PFPs

Prior to the mid-1980s, there were relatively few studies of gas or vapor transport through dense fluoropolymer membranes. This was due in part to the low permeability of the existing semicrystalline fluoropolymer (PTFE), but perhaps primarily due to processing difficulties that limited their potential use as gas separation membranes [18]. Nevertheless, the first systematic report on transport in dense fluorocarbon-based polymer films was an examination of gas diffusion in PTFE, tetrafluoroethylene-hexafluoropropylene copolymer (FEP) and poly-chlorotrifluoroethyelene (PCTFE) by Brandt and Anysas [19]. These authors found anomalously low activation energies of diffusion in the fluoropolymers compared to results in hydrocarbon polymers.

They suggested this unexpected behavior might be related to pre-existing holes or microchannels frozen into the fluoropolymer films during fabrication. Pasternak *et al.* reported permeability, diffusion and solubility data for several gases and vapors in PTFE [20] and FEP [21]. They found that activation energies of diffusion were lower in PTFE than in polyethylene (PE), consistent with results of Brandt and Anysas. Pasternak *et al.* also reported that light-gas solubilities were higher in FEP than in PE, whereas the reverse was true for hydrocarbon gas and vapor. The authors recognized that compared to PE the fluoropolymers were more permeable to light gases, but much less permeable to higher-boiling hydrocarbons [21].

These results were consistent with a growing body of patent data, which indicated that fluoropolymers were excellent permeation barriers to hydrocarbon liquids and vapors and thus useful as gas tank and flexible hose liners [22-24]. In the early 1980s, Koros and coworkers [25,26] examined hydrocarbon gas and vapor transport in PTFE and FEP. The results were similar to those of Pasternak *et al.*, but also included mixed-gas experiments

and the effects of polymer annealing. These authors found that annealing the fluoropolymers reduced both gas solubility and diffusivity, presumably due to polymer recrystallization at the annealing temperature.

Since the mid-1980s, a significant amount of research has been conducted on polymer gas separation membranes containing fluorinated functional groups.

Some of the materials investigated have included fluorinated polysulfones [27] polycarbonates [28] and polyimides [29]. In general, bulky fluorine-containing groups were added to these size-sieving, glassy polymers to inhibit chain packing and increase polymer permeability. However, it is in PFPs that the unique nature of the carbon-fluorine bond has its greatest impact on transport properties

Hyflon AD membranes show values of permeability and selectivity to gases that make them interesting for gas separation applications.

In Table 2.2, permeability values for Teflon AF are reported for comparison with those one of Hyflon AD [18] together with the Tg values of the various polymers. Examination of these data shows that, independently of the fluoropolymer type and gas, a linear correlation exists between permeability and Tg.

Table 2.2.: Gas permeability data (expressed in Barrer) of amorphous perfluoropolymers with various glass transition temperatures

Polymer	*Tg (°C)*	*P(NO_2)*	*P(CO_2)*	*P(O_2)*	*P(H_2)*	*P(CH_4)*
Hyflon AD80	135	77	473	194	563	49
Hyflon AD60	110	17	124	51	202	8
Hyflon AD40	91	8	64	26	_	_
Teflon AF2400	240	490	2800	990	2200	340
Teflon AF1600	160	_	_	340	_	_

In this respect, gas permeation is often attributed to the presence of voids at the molecular scale and to their size distribution. Amorphous perfluoropolymers show an experimental density that is lower than that expected theoretically. Considering the chemical structure of amorphous perfluoropolymers, the low values of the experimental density can be ascribed, at least qualitatively, to differences in chain packing resulting from the low chain mobility and steric hindrance offered by the large dioxole groups. In other words, the high chain stiffness leads to difficulties in the close packing of chain segments and thus to “nanovoids”.

Since, in amorphous perfluoropolymers, Tg is mainly related to the macromolecular chain stiffness, which controls the dimension of nanosize holes, it follows that the higher the Tg value, the higher is gas permeation.

2.4. Free Volume in polymers

Free volume (FV) is an extremely important characteristic of polymer materials which influences their properties, such as viscosity, diffusivity and permeability and, to some extent, the parameters of sorption thermodynamics and mechanical behavior. Because of its influence on transport properties, the concept of FV is extremely important for membrane science and technology. Some excellent reviews have been written by Yampolskii [30-32].

However, in contrast to other properties of polymers, free volume can be regarded as a complex physical object within polymers that can be characterized by size and size distribution of microcavities or free volume elements (FVEs) that form it, by topology and architecture of its nanostructure. Being initially formulated for the liquid state [33], it was extended to amorphous polymers that are either above or below the glass transition temperature (Tg) [34-36]. At temperatures above Tg one can distinguish in the free volume the "hole" component, characterized by zero energy expenditure for redistribution of FVE, and the interstitial component that becomes accessible to transport owing to energy fluctuations greater than kT. At temperatures below Tg, yet another component of the free volume appears corresponding to the nonequilibrium thermodynamic state of glassy polymers [35,36].

Elaboration of additive incremental (group contribution) methods for inclusion of the effect of the chemical structure of the polymers on their properties became an important step towards establishment of relations between the free volume using the van der Waals atomic radii and particular concepts of chain packing in polymers [37].

2.4.1. Definition of free volume

The thermal movement of molecules in the liquid phase is impossible without random fluctuation of the local density. Molecules in liquids perform irregular oscillations around their equilibrium positions. The average "local" lifetime, τ, of a molecule coincides with the

mean fluctuation time of the potential field in its closest neighborhood. In liquids with low viscosities this lifetime has the order of 10^{-11} sec. The lifetime τ increases with the viscosity of the liquid. The same concept holds for rubbery polymers; however, here kinetic segments play the role of individual molecules in low-molecular-mass liquid compounds. As the size of the kinetic segments is relatively large, the lifetimes τ in rubbers should be much longer.

In glassy polymers, where all of the segmental mobility is frozen, the lifetimes τ become infinitely long, and so FVEs should be viewed as areas with reduced local density imbedded in the frozen matrix.

The simplest assumption that can be made regarding free volume is based on its representation as the difference between the total or specific volumes of polymers (V_{sp}), which can be defined as the reciprocal density, and the occupied volume, V_{occ}:

$$V_f = V_{sp} - V_{occ} \tag{2.1}$$

For application of this equation, there should be ways to calculate V_{occ}. An approach to find the occupied volume of polymers was proposed by Bondi [37], who suggested calculation of the van der Waals volume (V_w) of repeat units of polymers by using the tabulated increments in V_w for smaller groups. He postulated that $V_{occ} = 1.3\ V_w$.. This method is very simple and so became popular for finding the Bondi free volume or fractional free volume *(FFV)* = V_f/V_{sp} and for drawing various correlations between the transport parameters (D and P values) with V_f and FFV.

2.5. Methods to determine FV

For several reasons, the previous approach to determine the FFV in the polymers seems to be unsatisfactory and can serve only for very rough estimates. Much attention was thus drawn to the problem of experimental evaluation of free volume in polymers. Attempts to characterize free volume resulted in development of various methods that are often united by the term “probe methods”. A common feature of these methods is that probes of different nature and size (atoms or molecules) are introduced into a polymer and observation of their

behavior, which is sensitive to free volume, makes it possible to deduce some information on nano-structure of free volume.

2.5.1. Positron Annihilation Lifetime Spectroscopy (PALS)

Positron annihilation lifetime spectroscopy is probably the most powerful and most widely used method for FV determination. It allows one to obtain information on the size distribution and concentration of free volume elements as well as on the effect of temperature, pressure, mechanical deformations and phase compositions of polymers on the free volume [38,39]. Parameters of PAL spectra strongly depend on the polymer structure but only slightly on for instance the molecular mass [40], which facilitates comparison of different polymers. The PALS method is based on measuring the positron lifetimes in matter. In polymers, positrons can exist in both free (e^+) and bound state, the latter being represented by H-like positronium atom, i.e. an electron-positron pair (Ps or e^-e^+). The singlet state of this species, *p*-Ps, has antiparallel spins and a short lifetime (0.125 nsec in vacuum), whereas the triplet state, *o*-Ps, with parallel spins has a much longer lifetime (142 nsec in vacuum). It is believed that long-lived species, *o*-Ps, appear in the regions with reduced electron density (i.e. in the FVE) [41-43]. The observed lifetimes depend on the FVE size: the larger the FVE the longer the positron lifetime in the polymer. An experimental setup for measuring positron annihilation lifetimes consists of a source of positrons, usually ^{22}Na isotope with a half-life time of 2.6 years, placed between two samples of the polymer under study. The lifetimes are measured using an electronic system (time-amplitude converter). The semiempirical expression relating the lifetime of *o*-Ps (τ_3) to the average radius (R_3) of a spherical FVE in a polymer (the Tao-Eldrup relationship) [42,43] is the following:

$$\tau_3 = \frac{1}{2}\left[1-\left(\frac{R_3}{R_0}\right)+\frac{1}{2\pi}\sin\left(\frac{2\pi R_3}{R_0}\right)\right]^{-1} \qquad (2.2)$$

where $R_0 = R_3 + \Delta R$ (the fitting parameter $\Delta R = 1.66$ Å was determined from analysis of the data for media with the known "hole" size including zeolites). The FVE radii increase almost linearly as τ_3 increases.

2.5.2. *^{129}Xe Nuclear Magnetic Resonance (^{129}Xe NMR)*

Chemical shifts in the ^{129}Xe NMR spectra are highly sensitive to the free volume in the medium where gaseous xenon is sorbed. Qualitatively, the larger the FVE size the smaller the ^{129}Xe chemical shift relative to the chemical shift characteristic of the gas phase. In this respect, polymers do not differ significantly from other condensed media, namely, large chemical shifts are observed in the media with high refractive indices. In this light, the xenon atom placed inside the FVE is in a local low-refraction medium and characterized by a smaller chemical shift [44]. According to Fraissard and co-workers [45,46], who studied the sorption of xenon in various zeolites, the chemical shift in the NMR spectrum of a ^{129}Xe atom sorbed in a nanoporous medium in the absence of paramagnetic species or admixtures producing a strong local electric field, can be written as follows:

$$\delta_{\Sigma} = \delta_0 + \delta + \delta_{Xe/Xe}\rho \qquad (2.3)$$

where δ_0 is a constant, δ is the chemical shift due to collisions with the FVE walls, $\delta_{Xe/Xe}$ is the chemical shift due to collisions with other xenon atoms in the gas phase and ρ is the density of the gas phase. Therefore, after extrapolation to zero pressure of gaseous xenon the difference

$$\delta = \delta_{\Sigma} - \delta_0 \qquad (2.4)$$

should characterize only the collisions with the walls within the FVE. Based on analysis of the data for zeolites, an empirical relation for the experimentally measured chemical shift was proposed [46]:

$$\delta = \frac{499.1}{2.054 + \lambda} \qquad (2.5)$$

where λ (in Å) is the mean free path of a xenon atom within the FVE. It is important to note that this method is only applicable to studies of those FVEs of which the size exceeds that of the xenon atom. Assuming different FVE geometries, one can estimate the diameter of

either a spherical cavity (D_{sp}) or a cylindrical FVE (D_c) with a large length-to-diameter ratio from the λ value by the following relations:

$$\lambda = \frac{D_{sp}}{2} - 2.2 \tag{2.6}$$

$$\lambda = D_c - 4.4 \tag{2.7}$$

The free terms in relations (3.6) and (3.7) are the radius and diameter of the xenon atom, respectively. By extending relationships (3.5)-(3.7) to other nanoporous systems, in particular polymers, it is possible to estimate their FVE sizes.

2.5.3. Inverse Gas Chromatography (IGC)

Inverse gas chromatography is used to study the thermodynamics of sorption of gases and vapours in polymers and to determine their physicochemical parameters [47]. To this aim, a polymer is applied on the surface of a solid porous substrate and the sorbate is introduced in the carrier gas flow. The principle is based on the differences in the sorption of different penetrants in the polymer while transported by the carrier gas. Under particular conditions, by measuring the retention times t_r one can calculate various thermodynamic parameters of the polymer-gas system. From the known t_r values, it is possible to calculate the net retention volume V_n of a sorbate:

$$V_n = (t_r - t_a) J_n^m F_c \frac{273}{T} \tag{2.8}$$

where t_a is the retention time of the "non-sorbable" component (e.g. air), which takes into account the dead volume of the chromatograph; J_n^m is the correction for pressure drop in the column, F_c is the rate of the carrier gas; and T is the temperature at which the experiment is carried out. The main thermodynamic characteristic of bulk sorption is the specific retention volume V_g defined as follows:

$$V_g = \frac{V_n}{\omega_L} \tag{2.9}$$

where ω_L is the mass of the polymer in the column. With this parameter known, one can calculate [48] the solubility factors (S) at infinite dilution:

$$S = V_g \frac{\rho}{p_0} \exp\left[(2B_{11} - V_1) J_n^m \frac{p_0}{RT} \right] \tag{2.10}$$

where ρ is the density of the polymer at temperature T; p_0 is the standard pressure (1 atm); the exponential term, which includes the second virial coefficient B_{11} and the molar volume of the sorbate V_1, takes into account the non-ideal state of vapours; R is the universal gas constant. The partial molar enthalpy of mixing, ΔH_m, characterizes the sorbate-polymer interaction and can be calculated from the temperature dependence of the activity coefficient (a_1/w_1):

$$\Delta H_m = R \frac{\partial \ln(a_1 / w_1)_\infty}{\partial (1/T)} \tag{2.11}$$

Studies of several glassy polymers showed that the ΔH_m values strongly depend in the size of the sorbate molecule. It was assumed [49] that the critical size of the sorbate molecule, which corresponds to the minimum in the enthalpy curve and the highest exothermicity of mixing, is also related to the average size of FVE. This hypothesis is substantiated by establishment of correlations between the minimum ΔH_m values and the diffusion coefficients and gas permeabilities of glassy polymers. Probably, this behavior is due to the ability of FVE to absorb molecules with sizes smaller than the FVE size. Sorption within FVE requires no energy expenditure to overcome the intermolecular interaction forces; therefore, the observed ΔH_m values are negative. The smaller the size difference between the sorbate molecule and FVE size the softer the restrictions imposed on the internal degrees of freedom of the sorbed molecule.

Thus the IGC technique permits estimation of the FVE size. Quantitative determination of the FVE size from IGC data requires a strategic choice of the probe size that are usually n-alkanes sorbed in polymers.

2.5.4. Photochromic probe technique

This method involves measurements of the degree of trans-cis photoisomerization of a probe in a glassy polymer and in a dilute solution in a non-viscous model solvent where the free volume imposes no restrictions on the isomerizations. Having determined the ratio of these parameters as a function of the probe size, more exactly as a function of the volume necessary for isomerization to occur, one can estimate the average size of FVE. The technique is thus based on the hypothesis [50] that the implementation of monomolecular chemical reactions, in particular photoisomerization, in glassy matrices requires a minimum FFV in the immediate vicinity of the dissolved probe molecule. Victor and Torkelson [51] studied the fee volume in glassy polystyrene using various stilbene and azobenzene derivatives with the van der Waals volumes in the range of 127-571 $Å^3$ as probes. The cis isomer fraction Y was determined from spectrophotometric absorbance by:

$$Y = \frac{1 - A / A_{dark}}{1 - \varepsilon_{cis} / \varepsilon_{trans}} \tag{2.12}$$

where A_{dark} is the absorbance with only trans isomer present, A is the absorbance at wavelength λ and ε_{cis} and ε_{trans} are the molar absorption coefficients of the cis and trans isomers respectively.

2.5.5. Spin probe technique

The spin probe technique was one of the first method used for estimating the free volume in polymers. It is based on the concept that the mobility of the spin probe, generally, stable nitroxyl radicals, and especially 2,2,6,6,-tetramethylpiperidine-1-oxyl (TEMPO), is sensitive to the dynamic or structural features of the polymers in which the probes are dissolved [52].

Depending on the ν_{cor} (rotational frequency of the spin probe), slow and fast motions of probes in polymers are distinguished. At room temperature, the rotational frequencies of probes in rubbers decrease as the glass transition temperature increases. Thus, even assuming that the parameter ν_{cor} does not reflect the actual dynamics of spin probe motions

in FVE, it can be considered as an indicator of the probe-to-FVE ratio in polymers, which shows the relative differences in the FVE values in different polymers.

2.5.6. The electrochromic probe technique

The electrochromic effect, i.e. a change in colour under the action of an electric field, is due to the effect of the electric field on the light-absorption of organic compounds.

Orientation of light-absorbing molecules in an electric field changes their extinction coefficients. This can be used for estimating the molecular mobility or the free volume in polymers [53]. To this end, the light-absorbing molecules acting as probes are dissolved in polymers. Experiments involve detection of changes in the extinction coefficients upon switching the electric field on and then off when random reorientation of the dissolved probe molecules occurs. To make the effect more pronounced, the probe molecules should have large dipole moments. To estimate the average FVE size, one has to analyse the kinetic curves of changes in the optical density upon orientation of dipoles by the electric field and after switching this field off. Experiments are carried out with probes of different sizes. The FVE size is determined using the Cohen-Turnbull model [33,34].

References

1. R. J. Plunkett, Tetrafluoroethylene polymers, *US Patent 2 230 654*, **1941.**
2. E. N. Squire, Amorphous copolymers of perfluoro-2,2-dimethyl-1,3-dioxole, *US Patent 4 754 009*, **1988.**
3. E. N. Squire, Optical fibers comprising cores clad with amorphous copolymers of perfluoro-2,2-dimethyl-1,3-dioxole, *US Patent 4 530 569*, **1985.**
4. M. Nakamura, I. Kaneko, K. Oharu, G. Kojima, M. Matsuo, S. Samejima and M. Kamba, Cyclic polymerization, *US Patent 4 910 276*, **1990.**
5. P. Colaianna, G. Brinati, and V. Arcella, Amorphous perfluoropolymers, *US Patent 5 883 177*, **1999.**
6. J. G. Drobny, Technology of Fluoropolymers, CRC Press, Boca Raton, FL, USA pp 172 **2001**.
7. V. Arcella, A. Ghielmi and G. Tommasi, High performance perfluoropolymer films and membranes, *Ann. NY Acad. Sci.,* **2003**, 984, 226-244.
8. H. Schroeder, Fluorocarbon elastomers, in *Rubber thechnology*, M. Morton (Ed.), New York, USA, pp. 631 **1987**.
9. Y. Yampolskii, I. Pinnau, B. D. Freeman, *Material Science of Membrane*, **2006**, Wiley.
10. S. Pauly, "Permeability and diffusion data", in *Polymer, Handbook* J. Brandrup and E. H. Immergut (Eds.), John Wiley & Sons, Inc., New York, NY, USA, **1989**.
11. T. C. Merkel, V. I. Bondar, K. Nagai, B. D. Freeman and Y. Yampolskii, Gas sorption, diffusion and permeation in poly(2,2-bistrifluoro-methyl-4,4-difluoro-1,3-dioxole-*co*-tetrafluoro-ethylene, *Macromolecules*, **1999**, 32, 8427-8440.
12. M. Macchione, J. C. Jansen, G. De Luca, E. Tocci, M. Longeri, and E. Drioli, Experimental analysis and simulation of the gas transport in dense Hyflon® AD60X membranes: Influence of residual solvent, *Polymer*, **2007**, 48, 2619-2635.
13. L. Wang, D.M. Xing, Y.H. Liu, Y.H. Cai, Z.-G. Shao, Y.F. Zhai, H.X. Zhong, B.L. Yi, H.M. Zhang, *J. Power Sources,* **2006,** 161, 61–67.
14. T. Yamaguchi, F. Miyata, S. Nakao, *J. Membr. Sci*., **2003,** 214, 283–292.
15. V. Arcella, A. Ghielmi, and G. Tommasi, High Performance Perfluoropolymer Films and Membranes, *Ann. N.Y. Acad. Sci*., **2003**, 984, 226–244.
16. A. Gordano et al.. Hydrophobic membranes of tetrafluoroethylene and 2,2,4 trifluoro 5 trifluorometoxy 1,3 dioxole. *Korean Membr. J*., **1999**, 1, 50–58.

17. V. Arcella et al., A study on a perfluoropolymer purification and its application to membrane formation. *J. Membr. Sci.*, **1999**, 163, 203–209.
18. P. R. Resnick and W. H. Buck, Teflon AF amorphous fluoropolymers, in *Modern Fluoropolymers: High Performance Polymers for Diverse Application*, J. Scheirs (Ed.), Wiley & Sons, Ltd, UK, pp. 397-419 **1997**.
19. W. W. Brandt and G. A. Anysas, Diffusion of gases in fluorocarbon polymers, *J. Appl. Polym. Sci.,* **1963**, 7, 1919-1931.
20. R. A. Pasternak, M. V. Christensen and J. Heller, Diffusion and Permeation of oxygen, nitrogen, carbon dioxide, and nitrogen dioxide through Polytetrafluoroethylene, *Macromolecules*, **1970**, 3, 366-371.
21. R. A. Pasternak, G. L. Burns and J. Heller, Diffusion and Solubility of simple gases through a copolymer of hexafluoropropylene and tetrafluoroethylene, *Macromolecules*, **1971**, 4, 470-475.
22. D. R. Rexford, Copolymer Elastomer of vinylidene-fluoride and hexafluoropropene, *US Patent 3 051 677*, **1962**.
23. S. Satoh and T. Suzuki, Rubber hose for automotive fuel line *US Patent 4 330 017*, **1982.**
24. D. Stivers, Fluoroelastomer/polyepichlorohydrin elastomer articles, *US Patent 4 343 861*, **1982.**
25. N. Yi-Yan, R. M. Felder and W. J. Koros, Selective permeation of hydrocarbon gases in polytetrafluoroethylene and poly(fluoroethylene-propilene) copolymer, *J. Appl. Polym. Sci.,* **1980**, 25, 1755-1774
26. T. Duncan, W. J. Koros and R. M. Felder, Permeation of methyl chloride and benzene through FEP Teflon, *J. Appl. Polym. Sci.,* **1983**, 28, 209-218.
27. J. S. MacHattie, W. J. Koros and D. R. Paul, Gas transport properties of polysulphones:2. Effect of bisphenol connector group, *Polymer*, **1991**, 32, 2618-2625.
28. M. W. Hellums, W. J. Koros, G. R. Husk and D. R. Paul, Fluorinated polycarbonates for gas separation, *J. Memb. Sci.*, **1989**, 46, 93-112.
29. K. Tanaka, H. Kita, M. Okano, and K. Okamoto, Permeability and permselectivity of gases in fluorinated and non-fluorinated polyimides, *Polymer*, **1992**, 33, 585-592.
30. Y. Yampolskii, *Russian Chemical Reviews*, **2007**, 76, 59-78

31. A. Y. Alentiev, Y. Yampolskii, V. P. Shantarovich, S. M. Nemser, N. A. Platè, *J. Memb. Sci.*, **1997**, 126, 123-132.
32. A. Y. Alentiev, Y. Yampolskii, *J. Memb. Sci.*, **2000**, 165, 201-216.
33. M. H. Cohen, D. Turnbull, *J.Chem. Phys,* **1959**, 31, 1164.
34. D. Turnbull, .M. H. Cohen, *J.Chem. Phys,* **1961**, 34, 120.
35. J. S. Vrentas, J. L. Duda, in *Encyclopedia of Polymer Science and Engineering*, New York, Wiley **1986**.
36. J. L. Duda, J. M. Zelinsky, *Free-Volume Theory in Diffusion in Polymers*, New York, Marcel Decker, **1996**.
37. A. Bondi, *Physical prop. of Molecular Crystals, Liquids and Gases*, N.Y., Wiley, **1968.**
38. D. M. Shrader, Y. C. Jean, *Positron and Positronium Chem.*, Amsterdam, Elsevier, **1988**.
39. R. A. Pethrick, *Prog. Polym. Sci.*, **1997**, 22, 1.
40. M. Ban, M. Kyoto, A. Uedono, T. Kawano, S. Tanigawa, *J. Polym. Sci., Part B: Polym. Phys.*, **1996**, 34, 1189.
41. W. Brandt, J. Spirn, *Phys. Rev.*, **1966**, 142, 231.
42. J. Tao, J. *Chem. Phys.*, **1972**, 56, 5499.
43. M. Eldrup, D. Lightbody, J. N. Sherwood, *Chem. Phys.,* **1981**, 63, 51.
44. Y. Wang, P. T. Inglefield, A. J. Jones, *Polymer*, **2002**, 43, 1867.
45. J. Demarquay, J Fraissard, *J. Chem. Phys. Lett.*, **1987**, 136, 314.
46. J. Fraissard, T. Ito, *Zeolites*, **1988**, 8, 350.
47. J. M. Braun, J. E. Guillet, *Adv. Polym. Sci.*, **1976**, 21, 107-145.
48. M. Kawakami, S. Kagawa, *Bull. Chem. Soc. Jpn.*, **1978**, 51, 75.
49. Y. Yampolskii, S. Durgaryan, in *Chromat. and thermod. determ. of phys.-chem. Param*, **1986**, Warsaw, Inst. of Phys. Chem., Polish Academy of Sciences.
50. C. S. Paik, H. Morawetz, *Macromolecules*, **1972**, 5, 171.
51. J. G. Victor, J. M. Torkelson, *Macromolecules*, **1987**, 20, 2241.
52. A. M. Vasserman, A. L. Kovarskii, *Spin porbes and labels in physical the chemistry of polymers*, **1986**, Moscow.
53. F. P. Chernayakovskii, *Electrochromism as method for study of slow movements in macromolecules*, Usp. Khim., **1979**, 47, 563.

3.

Photochromism

3.1. Introduction and a brief historical survey

Photochromism is a reversible transformation of a chemical species between two forms, **A** and **B**, having different absorption spectra induced in one or both directions by absorption of electromagnetic radiation, see Figure 3.1 below.

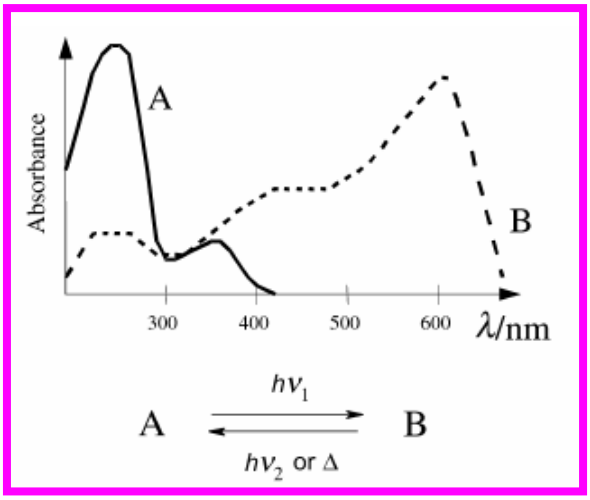

Figure 3.1. *UV-Visible spectra of two forms, A and B, of a chemical species irradiated at proper wavelengths to induce isomerization from A to B or vice versa. The back reaction from B to A may also be induced thermally.*

The thermodynamically stable form **A** is transformed by irradiation into form **B**. The back reaction can occur thermally (*Photochromism of type T*) or photochemically (*Photochromism of type P*). The most common photochromic molecules have a colorless or pale yellow form **A** and a colored form **B** (e.g., red or blue). This phenomenon is referred to as ***positive photochromism***. Otherwise, when λ_{max}(**A**) > λ_{max}(**B**), ***photochromism*** is ***negative*** or ***inverse***. The first observation of photochromism of organic molecules was made by Fritzsche in 1867 [1] who reported the bleaching of an orange-colored solution of tetracene in the daylight and the regeneration of the color in the dark. Later, ter Meer [2] observed a change of color of the potassium salt of dinitroethane in the solid state (yellow in the dark;

red in the daylight). Early examples were published by Phipson and Orr [3], who noted that a painted gate post appeared black all day and white all night due to a zinc pigment, probably lithopone. In 1899, Markwald studied the reversible color change of 2,3,4,4-tetrachloronaphthalen-1(4H)-one β-TCDHN in the solid state [4]. He believed it was a purely physical phenomenon, naming it "phototropy". Although used in that period, that term is not proper and should be avoided because it is akin to phototropism, which denotes biological phenomena. Interest in photochromism was continuous but limited until the 1940–1960 period, which saw an increase of mechanistic and synthetic studies, particularly in the research groups of Hirshberg and Fischer in Israel. In 1950, Hirshberg [5] suggested the term "photochromism", from the Greek words: ***phos*** (light) and ***chroma*** (color), to describe the phenomenon. This is the name used today. However, it is not limited to colored compounds; it applies to systems absorbing from the far UV to the IR, and to very rapid or very slow reactions. Photochromism expanded during the 1960s in parallel with the development of physical methods such as IR, NMR, X-ray, UV, time-resolved and flash spectroscopy and organic synthesis. Photochromic glasses became available at that period and further stimulated research. Applications, such as the PhotoChromic Micro Image (PCMI) process, which showed the possibility of reducing the 1245 pages of a Bible to about 6 cm^2, attracted considerable interest. An important text book on photochromism was published in 1971 [6]. However, it appeared that the photodegradation of the known families of organic photochromes limited their potential for applications [7].

3.1.1. Mechanisms of photoreactions

In general, the photochromic processes involve a ***one-photon mechanism:*** B is formed by absorption of one photon. Occasionally B may also be formed from a populated upper excited state by ***absorption*** of ***two photons***. In the latter case, the probability to populate the final state and hence to obtain the photoproduct depends on the product of the photon irradiances $Ep_{(1)}$ and $Ep_{(2)}$ of the two exciting beams.

It is, therefore, advantageous to utilize lasers emitting high photon irradiance, such as those generating picosecond or subpicosecond pulses. Figure 3.2 shows two mechanisms of two-photon absorption. In particular they may be distinguished in:

a) simultaneous absorption of two photons via a virtual level.

b) stepwise (or sequential) two-photon absorption where the second photon absorption takes place from a real level.

The simultaneous process (a) has been successfully used for exciting photochromic molecules from a ground state S_0 to an excited state S_n by a simultaneous absorption of two photons, $h\nu_1$ and $h\nu_2$, inside a volume for 3D memory systems (writing process).

A stepwise two-photon absorption process was also used to excite the written molecules that emit fluorescence (reading process) [8,9]. The excitation process can also proceed through a metastable intermediate S_1 (process b).

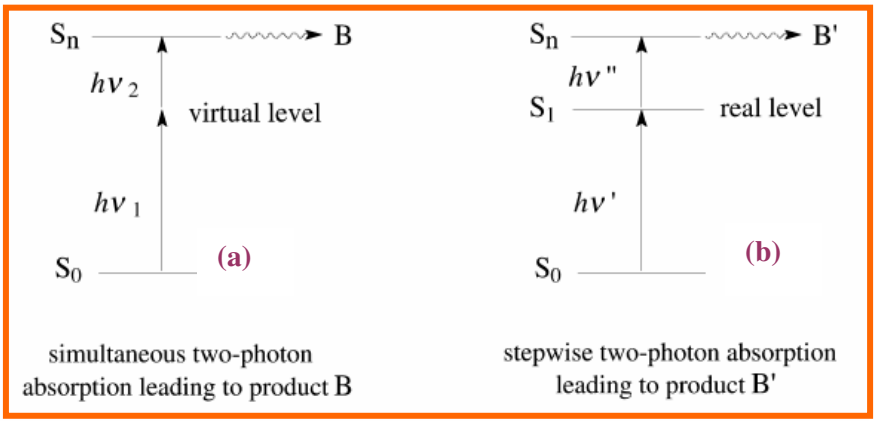

Figure 3.2. *Mechanisms of two-photon absorption. a) simultaneous absorption of two photons, hν1 and hν2, b) stepwise two-photon absorption process.*

3.1.2. Photochromic compounds

Photochromic compounds are chemical species having photochromic properties. The main photo-induced reactions responsible of photochromism are:

a) trans-cis isomerization of azoaromatics and stilbenes, Figure 3.3;
b) opening of the ring in spyrobenzopyranic derivatives, Figure 3.4;
c) ionic dissociation of triphenylmethane leuco-derivatives, Figure 3.5;

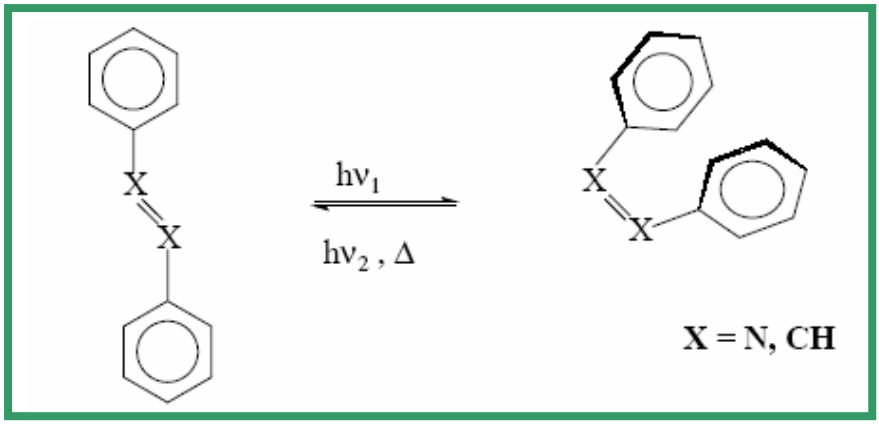

Figure 3.3. *Trans-cis isomerization of azoaromatics (X = N) and stilbenes (X = CH).*

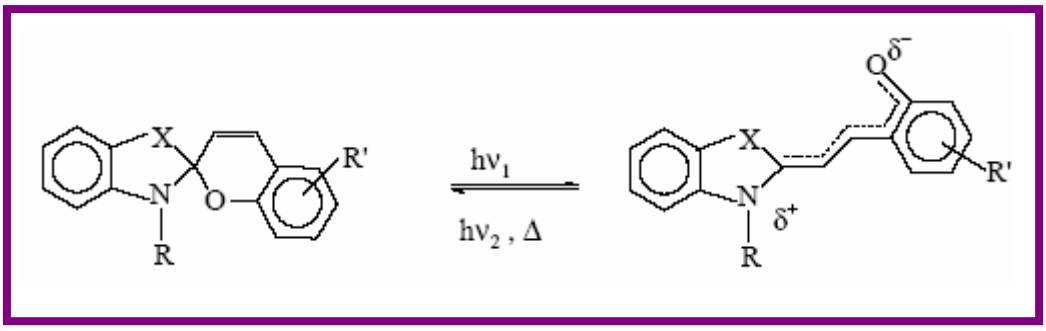

Figure 3.4. *Opening of the ring in spirobenzopyranic derivatives.*

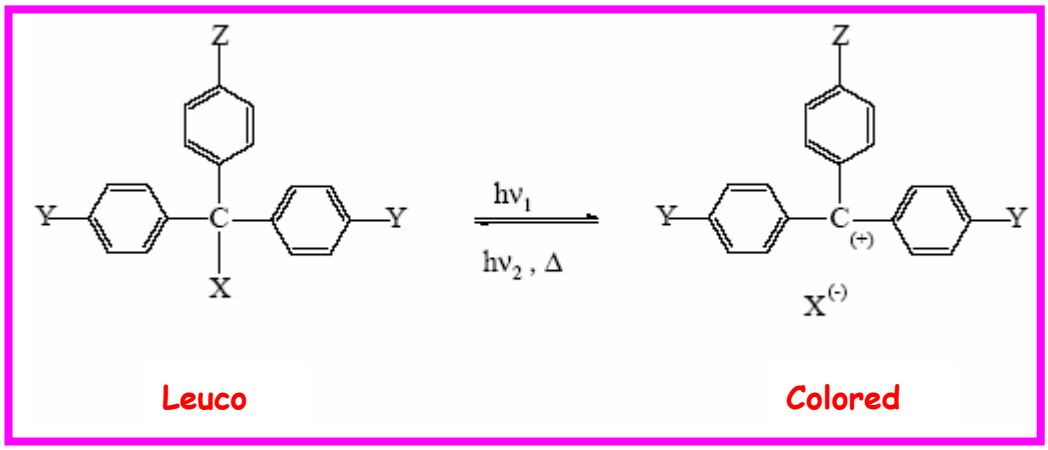

Figure 3.5. *Ionic dissociation of triphenylmethane leuco-derivatives.*

In many cases, the photoinduced isomerization process is completely reversibile, as for azobenzene compounds. These systems return to the original state in the dark.

Azobenzene chomophores have been studied for over 70 years, yet they continue to present new and unique optical effects. Due to their clean photochemistry, and substantial change in material properties during light irradiation, they have been investigated as an active component for a variety of applications, from lithography, to non-linear optical (NLO) devices, to optical switches, and even data storage.

3.2. Photochemistry of Azobenzene

Azobenzene, with two phenyl rings connected by an azo (-N=N-) bond (Figure 3.6), serves as the parent molecule for a broad class of aromatic azo compounds. The strong electronic absorption maximum can be tailored by ring substitution to fall anywhere from the ultraviolet to red-visible regions, allowing chemical fine-tuning of color. Such a property, combined with the fact that these azo groups are relatively robust and chemically stable, has prompted extensive study of azobenzene-based structures as dyes and colorants [10,11].

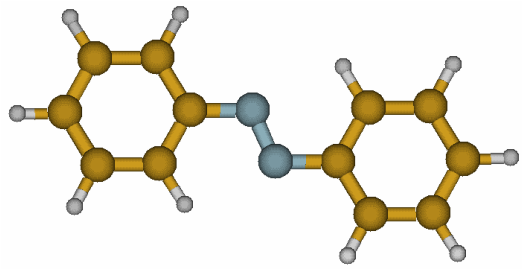

***Figure 3.6**. Schematic representation of the structure of trans azobenzene*

The azos are typically divided into three classes, distinguished by their spectral and photophysical response, which is intimately tied to their substitution patterns. These categories are [12]: a) the azobenzene-type molecules, b) the aminoazobenzene type, and c) the so called pseudo-stilbenes (Figure 3.7). The azobenzene-type molecules are similar to the parent (unsubstituted) azobenzene molecule, and have their most prominent absorption features in the UV. The aminoazobenzenes are substituted at the ortho or para- position with an electron donating group (typically an amino, $–NH_2$), and exhibit strong absorption features in the visible-blue region.

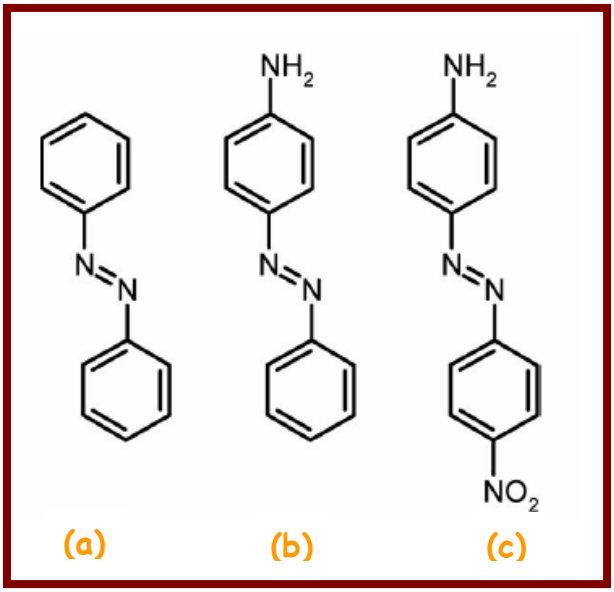

Figure 3.7. *Examples of azobenzene molecules that fall into the three spectroscopic classes: (a) azobenzenes (b) aminoazobenzenes, and (c) pseudo-stilbenes.*

Finally, the pseudo-stilbenes are characterized by a strongly asymmetric electron distribution, due to substitutents at the 4 and 4' positions with electron-donating and electron-withdrawing properties (called a 'push/pull' substitution pattern). The pseudo-stilbenes have a strong and broad absorption feature throughout the visible spectrum, have non-linear optical properties, owing to the asymmetric electron distribution, and often have the best photo-switching response. This makes them ideal candidates for a variety of applications and studies. Without doubt the most interesting feature of the azobenzenes is their ability to undergo fast, efficient, and fully reversible photo-isomerization (Figure 3.8).

Absorption of a photon leads to movement of the phenyl rings about the azo bond, converting the molecule from the trans (E) state to the cis (Z) state. The isomerization is one of the cleanest photoreactions known, and it does not generate side-products even after innumerable isomerization cycles [12]. At a molecular scale, the isomerization leads to extremely large changes in conformation and size. The trans isomer is nearly always the thermodynamically favoured isomer, being more stable by approximately 50 kJ/mol [13,14]. The energy barrier to the photo-excited state is on the order of 200 kJ/mol [15]. As a result, the azobenzenes are found predominantly in the trans form in the dark or under typical ambient illumination. Absorption of a photon in the trans absorption band causes isomerization to the cis state with high quantum yield. A photon in the cis absorption band can then be used to elicit the cis to trans back-isomerization. These photo-isomerization reactions have timescales in the order of picoseconds [16,17].

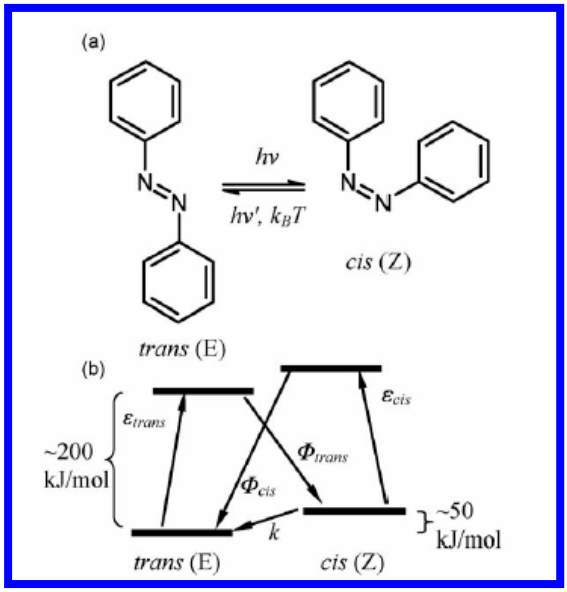

Figure 3.8. *(a) Photoisomerization of azobenzene.*
(b) Simplified state model for azobenzene chromophores. The extinction coefficients are denoted ε, whereas the quantum yields for the photoisomerizations are labelled Φ. The rate of thermal relaxation is denoted by k. Competition between these pathways determines the composition of the photo-stationary state [18].

Even without illumination, however, a population of azo cis isomers will thermally reconvert back to the more stable trans state, with a timescale that depends greatly on the azo's substitution pattern. Lifetimes are typically on the order of hours, minutes, and seconds, for azobenzenes, aminoazobenzenes, and pseudo-stilbenes, respectively. The energy barrier for this thermal isomerization is in the order of 90 kJ/mol [19,20]. Even in the case of the parent azobenzene, the cis lifetime is not long enough for the molecule to be treated as a stable two-state system. Considerable research has gone into elongating the cis lifetime, which would then allow the two states to be selected without unwanted interconversion. This is essential in applications that require two stable states, such as data storage. Typically, bulky substituents have been used to hinder the thermal back reaction. In extreme cases, the cis species can be stabilized by completely preventing isomerization: by synthesis of ring-like molecules [21]. Even in the case of the parent azobenzene, crystallization of the cis form prevents the back reaction [22,23]. These experiments again emphasize that the azo isomerization requires a large geometric change in molecular configuration. The thermal back-relaxation is generally first-order, although the distribution of highly constrained configurations that arise in a glassy polymer matrix can lead to anomalously fast decay components [24-27]. Accordingly, higher matrix crystallinity further increases the decay rate [28]. Again, the relationship between molecular size

constraint and kinetic processes points to the highly geometric nature of the isomerization. In fact, the decay rate can be used to probe the local environment and molecular conformation [29,30]. Under irradiation, a bulk azobenzene will achieve a photostationary state, whose steady-state composition of trans and cis species is based upon the competition between photoisomerization in one or both directions and constant thermal relaxation back into the trans state. Thus, the steady-state composition is unique to each system, depending upon the quantum yields for the two isomerization processes, Φ_{trans} and Φ_{cis}, and the thermal relaxation rate constant (k). Moreover, the composition is affected by irradiation intensity and wavelength, temperature, and the host matrix, be it solution, liquid crystal mixture, monolayer, polymer matrix, etc.. Upon irradiation, an azobenzene sample's spectrum will change as the proportion of cis to trans molecules changes, making the system photochromic. Because of this, the composition of the steady-state and the isomerization kinetics are usually monitored using absorption spectroscopy [31,32], although NMR methods have also been successfully applied [33]. The ring substitution pattern influences both the trans and the cis absorption spectra.

Azobenzene units are extremely sensitive to packing and aggregation, with π–π stacking causing shifts in the absorption spectra, and changes in photophysical properties. When the azos are aligned in a parallel fashion, head-to-head, they are called *J* aggregates, and give rise to a red-shift, bathochromic, compared to the well-isolated chromophore spectrum.

If the dipoles are instead antiparallel, head-to-tail, they are called *H*-aggregates, and one observes a blue-shift, hypsochromic. The local packing can be influenced, of course, by solvent conditions and molecular architecture [18].

3.3. Azobenzene in polymer films

Research on polymers into which azobenzene moieties are incorporated has been motivated by various intriguing potential applications [34-36]. The foremost of these include devices for optical data storage [37], membranes with switch on/off permeability [38], and polymers with controllable solubility [39], miscibility and wettability [40]. It is the possibility to induce stable and erasable birefringence in the polymer which has inspired hopes for optical data storage applications. The birefringence is induced by polarized light,

which causes the azobenzene to align perpendicularly to the direction of the polarization. The birefringence can then be erased by a circularly polarized laser beam. The geometrical change associated with trans to cis isomerization of azobenzenes is significant, and can be used to destroy or rearrange the order in a wide variety of organized media. The conversion from trans to cis azobenzene decreases the distance between the 4 and 4' ring positions from 9.0 to 5.5 Å (see Figure 3.9), increases the average free volume requirement [41], and can produce a substantial change in many of the observable properties of azo-containing systems.

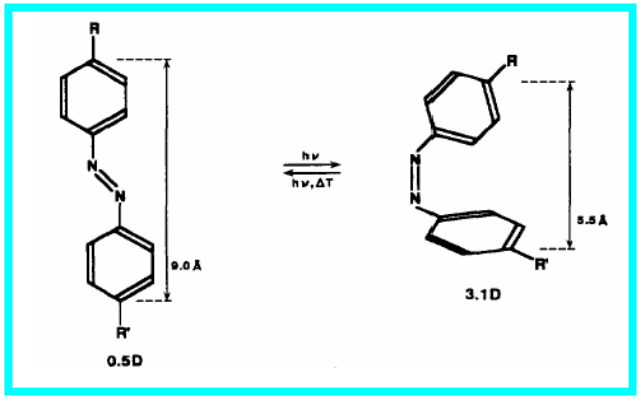

Figure 3.9. *Photoinduced structural change of azobenzene derivatives.*

Azobenzenes can thus be used as efficient, reversible, and high resolution photoswitches. They have been well studied for these applications, especially in the areas of photoinduced phase transitions in liquid crystal media [42-44], and surface properties of Langmuir-Blodgett and self-assembled monolayer films [45,46].

3.3.1. Non-Linear Optics (NLO)

Nonlinear optics (NLO) is the branch of optics that describes the behaviour of light in nonlinear media, that is, media in which the polarization P responds nonlinearly to the electric field E of the light. Nematic liquid crystal doped with azobenzene derivatives possesses the strongest nonlinear and photo-sensitive effects among all the optical materials.

Doping liquid crystals with these particular dopants greatly increases their light sensitivities and lowers the intensity thresholds for molecular reorientation.

The molecular motion of azobenzenes can give rise to a unique form of photo-orientation, shown schematically in Figure 3.10. The process is statistical, occurs when irradiating with polarized light, and is enhanced in systems where repeated isomerizations are facilitated (i.e. the pseudo-stilbenes). An azo molecule will preferentially absorb light polarized along its transition dipole axis (long axis of the molecule). A NLO material requires not merely anisotropy, but non-centrosymmetry. Thus, the azo dipoles must typically be aligned with an electric field, although photo-orientation has proved to be useful in aligning azo materials at lower field strength and temperature [47-50]. However, by using polarized light and its harmonics, a directional electric field results, and a net non-centrosymmetry can be produced entirely optically [51,52].

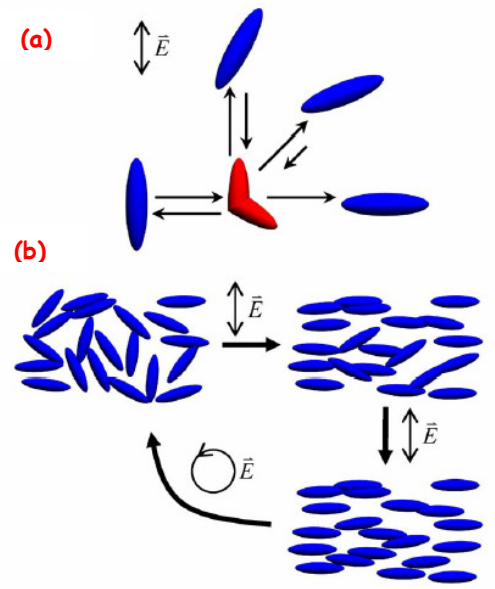

Figure 3.10. *The mechanism of statistical photo-orientation of azo molecules. (a) The molecules aligned along the polarization direction of the incident light will isomerize, and take on a new random orientation. The molecules that lie perpendicular to the polarization of light cannot absorb a photon and remain fixed. (b) An initially isotropic distribution of chromophores will become progressively aligned with polarized irradiation. Irradiation with circularly polarized light can restore isotropy.*

3.3.2. Photobiological experiments

The clean and unique azo photochemistry has been applied to switching biological systems [53]. One of the earliest investigations of azobenzene in a biological context involved embedding azobenzene molecules into a model membrane system [54]. Upon isomerization, the lamella were disrupted and rearranged, which also changed the enzymatic

activity of membrane-bound proteins. The catalytic activity of a cyclodextrin with a histidine and azobenzene pendant group was photo-controllable because the trans version of the azo pendant can bind inside the cyclodextrin pocket, whereas the cis version liberated the catalytic site [55]. Covalent attachment of azobenzene units to enzymes can modify protein activity by distorting the protein structure with isomerization. This was used to control the enzyme activity of papain [56,57] and the catalytic efficiency of lysozyme [58].

Bioengineering has more recently been broadened by expanding the natural protein alphabet with artificial amino acids. This enables novel and non-natural protein sequences to be created, while still exploiting the highly efficient natural synthesis machinery. Chiral azobenzene amino acids have been synthesized, and incorporated into protein sequences [59]. The introduction of artificial photoactive residues opens the possibility of photo-control of biological processes. It has also been suggested that the rapid switching of azobenzene could be used as a 'molecular shuttle' for electron transduction in enzyme systems [60]. This would mean that light could be efficiently used to alter behaviour in yet another class of enzymes. These experiments suggest an overall strategy to control biological systems using light. Azobenzenes thus present unique opportunities in the biological sciences for studying complex biological systems, in addition to controlling them.

3.3.3. Photochromic probes to measure the distribution of local free volume in films.

Photochromism of molecular probes is a technique which should be sensitive to the distribution of local free volume in polymer glasses [61,62]. The technique is based upon the lesser extent of photoisomerization of nonpolar probes in a glass in comparison with in a dilute solution. Indeed, it is hypothesized that photoisomerization in a glassy polymer (relative to that in dilute solution) requires a minimum, critical size of local free volume in the vicinity of the chromophore. Since the isomerization processes need some "sweeping volume" to occur, it is reasonable to expect that the isomerization kinetics are coupled to the free volume available in the polymer matrix. Fundamentally, the isomerization of an azobenzene chromophore is a photo-induced molecular motion and two possible mechanisms compete to it. The first mechanism is the rotation about the σ bond N=N: it implies the weakening of π bond due to the transition of an electron to the π^* anti-bonding orbital ($\pi \rightarrow \pi^*$ transition). The second mechanism is the inversion of a nitrogen of the N=N

bond: it implies the transition of a non-shared electron pair of nitrogen to the π* anti-bonding orbital (n→π* transition *) [63,64], see Figure 3.11.

For the parent azobenzene, this change in geometry results in an increase in the molecular dipole moment, from 0.5 D in the trans state to 3.1 D in the cis form [22]. The free volume requirement of the cis isomer is larger than for the trans isomer [65], with estimates of approximately 0.12 nm^3 required for isomerization to proceed via an inversion of the azo bond [25,63], and 0.28 nm^3 for a rotation about the azo bond [66].

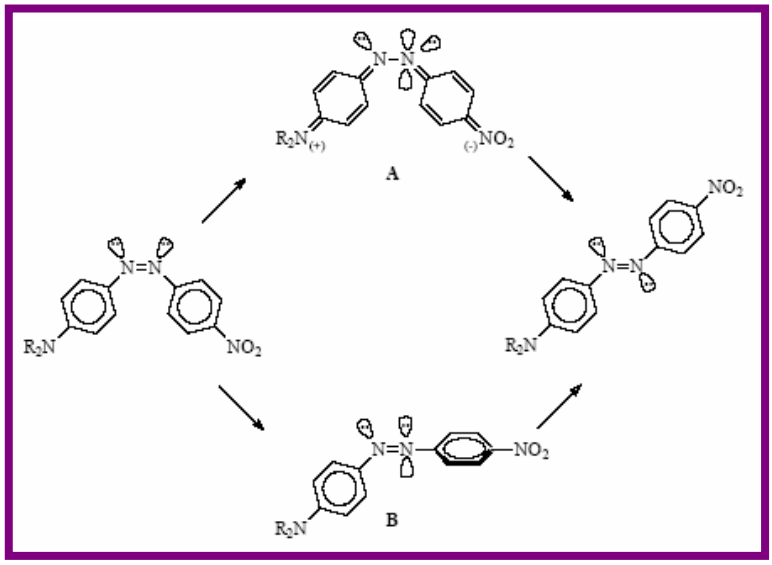

Figure 3.11. *Transition states relative to the rotational mechanism (A) or to the inversion (B) of para, para' substituted azobenzene.*

3.4. Photo-induced switching of macroscopic properties with azobenzene

The photochemical isomerization of azobenzene creates a geometric change of molecular dimensions. This molecular motion can give rise to much larger-scale and even coordinated motion for instance in liquid crystal systems. The type and extent of induced response of course depends upon the system. In some cases the molecular motion enables switching of a macroscopic material property.

The azobenzene moiety is robust and versatile. It has been incorporated into a wide variety of different system types and in different modes, including dissolved in small molecules, doped into polymeric systems, as supramolecular assemblies, as liquid crystals, and covalently bonded to crystalline or amorphous polymers. The isomerization of

azobenzene can be used to induce a phase change [67], a solubility change [68,69], crystallization [70], reverse phase separation [71], or alter the critical micelle concentration (cmc) and surface activity [72]. Experiments on methacrylates [73,74] and polyamides [75] showed that the polymer's chiral helix could be reversibly suppressed on irradiation. In polyisocyanate polymers, it could be selected whether irradiation would suppress or increase chirality [76,77].

There is a growing body of literature analyzing how selfassembled systems can be altered with light. In many cases, the effect of azobenzene isomerization is to disrupt a supramolecular organization. The isomerization of azobenzene has been applied to self-assembly in block-copolymer films. In this case, the microphase separation of the azo block-copolymer could be controlled with light [78]. In solution, azo block-copolymers can be used to create photo-responsive micelles [79-83] and vesicles [84]. Since light can be used to disrupt the encapsulating vesicle, this has been investigated for tunable drug delivery [85]. Careful attention to the self-assembly behaviour, and the change in azo dipole moment upon irradiation in particular, is required to optimize the photo-control of vesicle formation/destruction [86]. Azo colloids have also been prepared, and used as photoresponsive monolayers [87], exhibiting all the usual photophysical phenomena (such as photo-orientation). Although doping is an easy and convenient way to include azobenzene in a matrix of choice, it is usually found that mobility leads to aggregation and crystallization of the azo molecules, making the resultant films heterogeneous and optically cloudy. Thus, by far the most often-employed incorporation strategy is to covalently bind the azo chromophore to a polymer backbone [88].

3.4.1. Change of gas permeation by photoinduced switching of zeolite-azobenzene membranes

One example of photoswitching of transport properties in membrane systems is given by FAU membranes of type Na–X and MFI membranes of type silicalite-1 which contain adsorbed azobenzene [89]. They have photoswitchable permeation properties due to the trans–cis photoisomerization of azobenzene. The change of gas permeation through these host–guest composite membranes depends on the irradiation wavelength, the quality of the membranes and the amount of adsorbed azobenzene. The permeances of the gases in the trans-form of the zeolite-encapsulated azobenzene were higher than those in the cis-form.

The separation factors of equimolar mixtures of N_2/CO_2 and CH_4/CO_2 fed through the FAU–AZB membrane were higher at trans-switching than at cis-switching. This is due to the fact that the bulkier trans isomer partially obstructs the zeolite pores for gas transport.

The changes of the permeances of single gases and of the separation factors of equimolar gas mixtures by photoinduced trans–cis switching were found to be reversible over numerous switching cycles. Because of the reversibility of the photochemical trans–cis switching the AZB-modified membranes could be used as micro-valves in the microreaction technology for dosing of reactants or light-controlled removing of products.

3.4.2. Change of gas permeation by photoinduced switching of polymer-azobenzene membranes

Membrane functions, such as transport/barrier and membrane potential, have been shown to be controllable by light irradiation. Kato et al. initially tried this approach in 1976 and succeeded in photocontrol of membrane potential using acetyl cellulose membrane entrapping photochromic spirobenzopyran [91]. Since then, many studies have been made, mainly in the 1980s, and extensive reviews are available [40,92]. For example Anzai et al. [92] prepared a photoresponsive PVC membrane by entrapping an azobenzene-modified crown ether into the membrane. They used the cis-trans isomerization of the azobenzene derivative to regulate the membrane potential across the PVC membrane. Light irradiation enhances the binding ability of the azobenzene-modified crown ether for larger cations, as a result, the photoresponse in the membrane potential was explained in terms of surface potential changes associated with the adsoption and desorption of ions.

Polymers functionalized with azobenzene chromophores (azopolymers) are among the most investigated photofunctional materials. Kameda and coworkers studied how the photoisomerization of an azogroup, introduced in the side chain of a polymer, can plasticize it and then increase the gas permeability of the membrane [90]. Indeed, the gas permeation property of the polymer film is reversibly changed by photoirradiation. The observed permeability change was at most 10%, and it was observed that azopolymer irradiated with blue light spread out from localized particulate domains and thinly covered the entire surface of the base membrane. This experimental result supports the possible existence of photoinduced plasticization and fluidization of the azopolymer.

References

1. J. Fritzsche, *Comptes Rendus Acad. Sci.*, Paris, **1867**, 69, 1035.
2. E. ter Meer, *Ann. Chem*. **1876**, 181, 1.
3. (a) T. L. Phipson, *Chem. News*, **1881**, 43, 283; (b) J. B. Orr, *Chem. News*, **1881**, 44, 12.
4. W. Markwald, *Z. Phys. Chem*., **1899,** 30, 140.
5. Y. Hirshberg, *Compt. Rend. Acad. Sci.*, Paris, **1950**, 231, 903.
6. G. H. Brown (Ed.), *Photochromism*, Wiley-Intersciences, New York **1971**.
7. R. C. Bertelson, *Mol. Cryst. Liq. Cryst*., **1994**, 246, 1.
8. D. A. Parthenopoulos and P. M. Rentzepis, *Science*, **1989**, 245, 843.
9. A. S. Dvornikov, S. E. Esener, P. M. Rentzepis, *Optical Computing Hardware*, Ch. 11, AT&T and Acad. Press **1994**.
10. H. Zollinger, *Azo and Diazo Chemistry*, Interscience, New York **1961**.
11. H. Zollinger, *Colour Chemistry. Synthesis, Properties, and Applications of Organic dyes*, VCH, Weinheim **1987**.
12. H. Rau, in: J. Rebek (Ed.), *Photochemistry and Photophysics*, vol. 2, CRC Press, Boca Raton, FL, **1990**, p. 119.
13. F.W. Schulze, H.J. Petrick, H.K. Cammenga, H. Klinge, *Z. Phys. Chem.*, **1977**, 107, 1.
14. I. Mita, K. Horie, K. Hirao, *Macromolecules,* **1989**, 22, 558.
15. S. Monti, G. Orlandi, P. Palmieri, *Chem. Phys.* **1982**, 71, 87.
16. T. Kobayashi, E.O. Degenkolb, P.M. Rentzepis, *J. Phys. Chem,*. **1979**, 83, 2431.
17. I.K. Lednev, T.-Q. Ye, R.E. Hester, J.N. Moore, *J. Phys. Chem*., **1996**, 100, 13338.
18. K. G. Yager, Christopher J. Barrett, *J. Photochem. and Photobio. A: Chem*., **2006,** 182, 250–261.
19. E.V. Brown, G.R. Granneman, *J. Am. Chem. Soc*., **1975**, 97, 621.
20. P. Haberfield, P.M. Block, M.S. Lux, *J. Am. Chem. Soc.*, **1975**, 97, 5804.
21. U. Funke, H.F. Gruetzmacher, *Tetrahedron,* **1987**, 43, 3787.
22. G.S. Hartley, *Nature,* **1937**, 140, 281.
23. G.S. Hartley, *J. Chem. Soc. Abst*., **1938**, 633.
24. W.J. Priest, M.M. Sifain, *J. Polym. Sci. Part A: Polym. Chem*., **1971**, 9, 3161.
25. C.S. Paik, H. Morawetz, *Macromolecules*, **1972**, 5, 171.
26. C. Barrett, A. Natansohn, P. Rochon, *Chem. Mater,*. **1995**, 7, 899.

27. C. Barrett, A. Natansohn, P. Rochon, *Macromolecules,* **1994**, 27, 4781.
28. N. Sarkar, A. Sarkar, S. Sivaram, *J. Appl. Polym. Sci*., **2001**, 81, 2923.
29. L.L. Norman, C.J. Barrett, *J. Phys. Chem. B*, **2002**, 106, 8499.
30. K. Tanaka, Y. Tateishi, T. Nagamura, *Macromolecules,* **2004**, 37, 8188.
31. E. Fischer, *J. Phys. Chem*., **1967**, 71, 3704.
32. H. Rau, G. Greiner, G. Gauglitz, H. Meier, *J. Phys. Chem*., **1990**, 94, 6523.
33. S.W. Magennis, F.S. Mackay, A.C. Jones, K.M. Tait, P.J. Sadler, *Chem. Mater*., **2005,** 17, 2059.
34. J. A. Delaire, K., Nakatani, *Chem. Rev.* **2000**, 100, 1817-1845.
35. G. S. Kumar, D. C. Neckers, *Chem. Rev*. **1989**, 89, 1915-1925.
36. A. Natansohn, P. Rochon, *Can. J. Chem.,*. **2001**, 79, 1093-1100.
37. A. Natansohn, P. Rochon, J. Gosselin, S. Xie, *Macromolecules,* **1992**, 25, 2268-2273.
38. K. Weh, M. Noack, R. Ruhmann, K. Hoffmann, P. Toussaint, Caro, *J. Chem. Eng. Technol,*. **1998**, 21, 408-412.
39. M. Irie;H. Tanaka, *Macromolecules* **1983**, 16, 210-214.
40. M. Irie, *Adv. Polym. Sci*., **1990**, 94, 27-67.
41. T. Ubukata, T. Seki, K. Ichimura, *Macromol. Symp.,,* **1999**, 137, 25.
42. L. Brzozowski, E.H. Sargent, *J. Mater. Sci.: Mater. Electron*., **2001,** 12, 483.
43. K. Ichimura, *Chem. Rev.* **2000**, 100, 1847.
44. V. Shibaev, A. Bobrovsky, N. Boiko, *Prog. Polym. Sci*., **2003**, 28, 729.
45. O. Pieroni, and F. Ciardelli, Photoresponsive polymeric materials, *Trends Polym. Sci.,* **1995**, 3, 282-287.
46. I. M. Pepe, and C. Nicolini, Langmuir-Blodgett films of photosensitive proteins, *J. Photochem. and Photobio. B: Biol.*, **1996**, 3, 191-200.
47. P.M. Blanchard, G.R. Mitchell, *Appl. Phys. Lett.*, **1993**, 63, 2038.
48. P.M. Blanchard, G.R. Mitchell, *J. Phys. D: Appl. Phys*., **1993,** 26, 500.
49. Z. Sekkat, C.-S. Kang, E.F. Aust, G. Wegner, W. Knoll, *Chem. Mater.,* **1995**, 7, 142.
50. X.L. Jiang, L. Li, J. Kumar, S.K. Tripathy, *Appl. Phys. Lett.*, **1996,** 69, 3629.
51. J.-M. Nunzi, C. Fiorini, A.-C. Etil´e, F. Kajzar, *Pure Appl. Opt*., **1998,** 7, 141.
52. X. Zhong, X. Yu, Q. Li, S. Luo, Y. Chen, Y. Sui, J. Yin, *Opt. Commun*., **2001**, 190, 333.
53. I. Willner, S. Rubin, *Angew. Chem. Int. Ed. Engl*., **1996**, 35, 367.
54. D. Balasubramanian, S. Subramani, C. Kumar, *Nature,* **1975**, 254, 252.

55. W.-S. Lee, A. Ueno, *Macromol. Rapid Commun.*, **2001**, 22, 448.
56. I. Willner, S. Rubin, A. Riklin, *J. Am. Chem. Soc.*, **1991**, 113, 3321.
57. I. Willner, S. Rubin, *Reactive Polym.*, **1993**, 21, 177.
58. T. Inada, T. Terabayashi, Y. Yamaguchi, K. Kato, K. Kikuchi, *J. Photochem. Photobiol. A,* **2005**, 175, 100.
59. L. Wang, P.G. Schultz, *Angew. Chem., Int. Ed.*, **2004**, 44, 34.
60. M.V. Voinova, M. Jonson, *Biosens. Bioelectron.*, **2004**, 20, 1106.
61. J. Victor, J. M. Torkelson, *Macromolecules*, **1987**, 20, 2241-2250.
62. J. Algers, P. Sperr, W. Egger, L. Liszkay, G. Kogel, J. de Baerdemaeker, F. H. J. Maurer, *Macromolecules*, **2004**, 37, 8035-8042.
63. T. Naito, K. Horie, I. Mita, *Macromolecules,* **1991**, 24, 2907.
64. P. Uznanski, M. Kryszewski, E.W. Thulstrup, *Eur. Polym. J.*, **1991**, 27, 41.
65. T. Naito, K. Horie, I. Mita, *Polymer,* **1993,** 34, 4140.
66. L. Lamarre, C.S.P. Sung, *Macromolecules,* **1983**, 16, 1729.
67. K.I. Aoki, M. Nakagawa, K. Ichimura, *J. Am. Chem. Soc.,* **2000**, 122, 10997.
68. H. Yamamoto, A. Nishida, T. Takimoto, A. Nagai, *J. Polym. Sci. Part A: Polym. Chem.*, **1990**, 28, 67.
69. K. Arai, Y. Kawabata, *Macromol. Rapid Commun.*, **1995**, 16, 875.
70. T.D. Ebralidze, A.N. Mumladze, *Appl. Opt.*, **1990**, 29, 446.
71. J.J. Effing, J.C.T. Kwak, *Angew. Chem., Int. Ed. Engl.*, **1995**, 34, 88.
72. L. Yang, N. Takisawa, T. Hayashita, K. Shirahama, *J. Phys. Chem.*, **1995**, 99, 8799.
73. L. Angiolini, D. Caretti, C. Carlini, E. Salatelli, *Macromol. Chem. Phys.*, **1995**, 196, 2737.
74. J.P. Chen, J.P. Gao, Z.Y. Wang, *J. Polym. Sci. Part A: Polym. Chem.*, **1997,** 35, 9.
75. G.J. Everlof, G.D. Jaycox, *Polymer,* **2000**, 41, 6527.
76. G. Maxein, R. Zentel, *Macromolecules*, **1995**, 28, 8438.
77. M. Muller, R. Zentel, *Macromolecules,* **1996**, 29, 1609.
78. S. Kadota, K. Aoki, S. Nagano, T. Seki, *J. Am. Chem. Soc.*, **2005**, 127, 8266.
79. G. Wang, X. Tong, Y. Zhao, *Macromolecules*, **2004**, 37, 8911.
80. P. Ravi, S.L. Sin, L.H. Gan, Y.Y. Gan, K.C. Tam, X.L. Xia, X. Hu, *Polymer,* **2005**, 46, 137.
81. S.L. Sin, L.H. Gan, X. Hu, K.C. Tam, Y.Y. Gan, *Macromolecules*, **2005**, 38, 3943.

82. E. Yoshida, M. Ohta, *Colloid Polym. Sci.,* **2005**, 283, 872.
83. E. Yoshida, M. Ohta, *Colloid Polym. Sci*., **2005**, 283, 521.
84. H. Sakai, A. Matsumura, T. Saji, M. Abe, *Stud. Surf. Sci. Catal*., **2001**, 132, 505.
85. X.-M. Liu, B. Yang, Y.-L. Wang, J.-Y. Wang, *Chem. Mater*., **2005**, 17, 2792.
86. X. Tong, G. Wang, A. Soldera, Y. Zhao, *J. Phys. Chem. B*, **2005**, 109, 20281.
87. Y. Li, Y. Deng, Y. He, X. Tong, X. Wang, *Langmuir,* **2005**, 21, 6567.
88. N.K. Viswanathan, D.Y. Kim, S. Bian, J. Williams, W. Liu, L. Li, L.Samuelson, J. Kumar, S.K. Tripathy, *J. Mater. Chem*., **1999,** 9, 1941.
89. K. Weh, M. Noack,, K. Hoffmann, K. P. Schroder, J. Caro, *Microporous and Mesoporous Materials,* **2002**, 54, 15–26.
90. M. Kameda, K. Sumaru, T. Kanamori, T. Shinbo, *Journal of Applied Polymer Science*, **2003**, 88, 2068–2072.
91. S. Kato, M. Aizawa, S. Suzuki, *J. Memb. Sci.,* **1976**, 1, 289-300.
92. J. Anzai, T. Osa, *Tetrahedron,* **1994**, 50, 4039-4070.

PART II

Results

4.

Influence of the residual solvent in Hyflon®AD membranes

4.1. Introduction

It is generally known that the performance of dense polymeric gas separation membranes may be strongly affected by traces of solvents or condensable species in the gas mixture.

This is especially true for glassy polymers in which condensable species cause plasticization and consequent loss of the mechanical stability and/or permselectivity. Also the solvents themselves, used during the membrane preparation, can have a significant influence on the membrane transport properties, especially if they are not completely removed from the final membrane. Many researchers have observed the effect of the casting solvent on the membrane performance but this aspect is not well-documented because it is usually not the aim of their research. In the majority of the papers on preparation of new gas separation membranes this aspect is completely ignored. Kesting and Fritzche [1] have recognized the importance of the membrane preparation protocol and have discussed the effect that this can have on the separation performance. Most studies reported in the literature discuss the effect that a specific solvent may have on the final membrane performance in relation to changes in the polymer chain conformation [2-4], to the free volume [5] or to morphological aspects of the obtained membranes, such as the polymer state and the surface roughness [6]. In a comparative study on numerous polycarbonate (PC) membranes from the literature, Hacarlioglu et al. observed variations of over 400% in nitrogen permeability, and they suggested that this might be related to the preparation protocol and to the solvent used [2]. This was confirmed by their own studies which demonstrated strong differences between membranes prepared from chloroform and from dichloromethane solutions. Chloroform generally produced membranes with a higher selectivity, which was attributed to its higher molar volume and to the possibility to form

hydrogen bridges with the polymer chains. Such effects were recently confirmed by Alentiev *et al*. who demonstrated that residual chloroform may change the chain conformation and that slow removal of this chloroform under controlled strain conditions may result in a surprisingly high increase of the permselectivity of polyetherimide membranes [7]. Only few studies have been conducted in order to quantify the amount of the residual solvent in the membranes and the effect that this has on the permeation properties [e.g. 2,8]. Generally the amount of residual solvent does not exceed a few percent, even for solvents with a low volatility. Hacarlioglu et al. reported a residual solvent contents ranging from 0.5 to 3 % in their PC membranes but could not find an unambiguous quantitative relation between the amount of residual solvent and the membrane performance [2]. Joly *et al*. investigated the influence of the type of solvent on the permeation properties of polyimide membranes [8]. After extensive drying at about 100°C below the glass transition temperature they observed a solvent retention in the membranes ranging from 0.6 % to 1.2 %, depending on their boiling point. They showed that the transport parameters are strongly affected by the presence of the residual solvent. In their studies the diffusion coefficient generally decreased, whereas the permeability and solubility coefficients increased with decreasing solvent content in the membrane. The increased diffusion rate in the presence of residual solvent was ascribed to plasticization and increased polymer chain mobility. In contrast, Maeda and Paul observed an antiplasticization effect when they intentionally added various low molar mass diluents to polymeric membranes. This led to increased selectivity and reduced permeability and could be explained in terms of a reduction of the free volume of the polymer films [9-12].

To the best of my knowledge the topic of residual solvent has not been dealt with in the case of high free volume perfluorinated polymer membranes. Nevertheless, comparison of solution cast Teflon AF® 2400 membranes obtained by Pinnau and Toy [13] with melt-pressed membranes prepared by Nemser et al. [14] show that the permeabilities of the solution-cast film were between 30 % (helium) and 80 % (methane) higher than those reported for the melt-pressed Teflon AF 2400 film. These differences may be related either to the thermomechanical history of the samples but also to the effect of the casting solvent.

In this light the remarkable solvent retention observed in Hyflon® AD60X membranes seems particularly interesting [15], the more so because the polymer's high FFV is supposed to facilitate mass transport.

4.1.1. Objectives of the work

The present study shows that Hyflon has an unexpected tendency to retain considerable amounts of solvent. To the best of my knowledge this property has not been described yet in the literature, although Hyflon and other amorphous perfluorinated polymers are currently receiving much attention for their potential as a membrane material. The aim of this chapter of the thesis is to present the first systematic study on the effect of residual solvent in high free volume perfluorinated polymers. The study will focus in particular on two different fluorinated solvents and their effect on the physical and transport properties of Hyflon® AD60X membranes, studied by means of Differential Scanning Calorimetry (DSC) and gas permeation measurements.

The transport properties of the solution-cast membranes are also compared with those of a solvent-free melt-pressed sample. It will be further described a non-destructive procedure for complete solvent removal and for quantification of the solvent content. The presence of the solvent is also studied by solid state NMR analysis of the samples, providing information on the physical state of the solvent in the polymer matrix and on possible polymer-solvent interactions. Finally, the possibility to model the gas transport by molecular simulation studies is evaluated. Experimental results are confronted with simulated data, obtained using the Gusev-Suter Transition State Theory (TST) [18] method and using MD simulations. The advantages and limitations of TST and MD will also be discussed.

4.2. Experimental

4.2.1. Materials.

Hyflon® AD 60X (Scheme 4.1), an amorphous TTD-TFE copolymer containing 60 mol% 2,2,4-trifluoromethoxy-1,3-dioxole (TTD) and 40 mol% tetrafluoroethylene (TFE) was kindly supplied by Solvay-Solexis. Hyflon® AD 60X has a reported density of 1.93 g/cm^3 at 20°C [19]. This polymer shows excellent stability to organic solvents; the only known solvents are pefluorinated compounds. In this study 1 methoxy-nonafluorobutane (3M, commercial name HFE 7100, Bp 60°C, MW 250 g/mol) and Galden HT55 (Solvay-Solexis) were used as the solvents to prepare the solution-cast membranes. Galden HT is a mixture

of oligomeric perfluorpolyethers of which the molar mass depends on its specific grade. Galden HT 55 has a boiling point of 55°C and an average molar mass of 350 g/mol. [20].

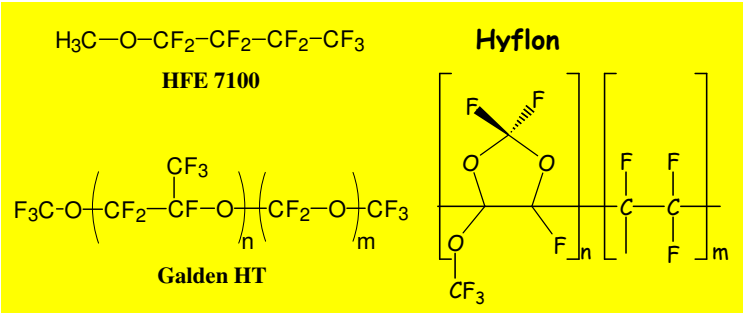

Scheme 4.1. *Chemical structure of the repeating unit in Hyflon AD 60X and of the solvents Galden HT and HFE 7100.*

4.2.2. Membrane preparation

Dense Hyflon® AD 60X gas separation membranes were prepared by the solvent evaporation method from a 5 wt % polymer solution in a Petri dish, using Galden HT55 or HFE 7100 as the solvent. The films were first dried overnight at room temperature and then in a vacuum oven with a very slow heating rate of 0.02°C/min from 50 to 200°C at, in order to avoid foaming during the solvent evaporation. A previously described dense membrane, prepared without the use of a solvent by melt-pressing of the polymer powder, was used as a reference [21]. An overview of the membranes and the fundamental differences in their preparation is given in Table 4.1.

Table 4.1: *Membranes and their main preparation conditions.*

Membrane	Casting solvent	Treatment	Thickness (µm)
H25	HFE 7100	Dried at room temperature	67.7
H200 [a)]	HFE 7100	Dried at 200°C	68.3
G25	Galden HT 55	Dried at room temperature	60.6
G200 [b)]	Galden HT 55	Dried at 200°C	65.2
M170	---	Melt pressed at 170°C	220

[a)] *Same membrane as H25, after drying under vacuum at 200°C.* [b)] *Same membrane as G25, after drying under vacuum at 200°C.*

4.2.3. Gravimetric measurements

In order to quantify the amount of residual solvent and to determine its release rate, a membrane sample was heated slowly in a vacuum oven and its weight was measured periodically. For each weighing the vacuum was temporarily released and the sample was removed from the oven. This operation took only a few minutes and did not interfere significantly with the drying procedure. At various stages of the drying procedure small samples were taken for thermal analysis.

4.2.4. Differential Scanning Calorimetry

Thermal properties of the Hyflon AD60X virgin polymer and that of the solution-cast membranes, at the different stages of the drying process, were evaluated by DSC analysis. Measurements were carried out on a Pyris Diamond Differential Scanning Calorimeter (Perkin Elmer). Samples of about 8-15 mg were subjected to a heating/cooling/heating cycle at a rate of 15°C/min in the range of 50-150°C. An empty pan with two covers was used as the reference. The effect of the solvent was evaluated on the basis of the first heating run while the difference between the first and the second heating run was used to verify the additional solvent loss upon heating. The glass transition temperature was determined as the *half-c_p extrapolated* value, i.e. the temperature corresponding to half of the c_p increase of the complete transition, calculated by baseline extrapolation before and after the glass transition.

4.2.5. ^{1}H High Resolution Magic Angle Spinning Nuclear Magnetic Resonance (^{1}H HRMAS NMR)

The presence of solvent in the polymer was also studied by ^{1}H HRMAS NMR. A membrane specimen was cut into thin slices, and about 20 mg of polymer was packed into a 4 mm MAS zirconium rotor of 50µl total volume, with hemispherical inserts. All HRMAS NMR spectra were recorded at 298 K on an Avance 500 MHz instrument (by Bruker Spectrospin) working at 11.74 Tesla, using a 4 mm HRMAS ^{1}H/^{13}C probe head. The sample was spun at 8000 Hz, a 10 µs 90° pulse, a spectral width of 40000 Hz and a recycle time of 2 s were used. The free induction decays were stored in 32k words of computer memory.

Different spectra of the same membrane were recorded to monitor the solvent evaporation during the thermal treatment.

4.2.6. Mechanical testing

Tensile tests were carried out on a single column Zwicki Z2.5 universal testing machine (by Zwick/Roell) equipped with a 50N maximum load cell and with pneumatic sample grips with flat sanded stainless steel surface. The membrane samples were cut into 10.0 mm wide test strips of with an extremely sharp cutter in order to limit as much as possible craze formation during cutting. The specimen thickness, *l*, was measured with a digital micrometer (Carl Mahr) by taking no less than 5 points and then averaging. Specimens with a thickness variation of more than 5% were discarded. The effective sample length (grip to grip distance) was normally 50 mm and the test speed was 5 mm/min (corresponding to 10% deformation per minute). The test specimens were stretched with a pre-load of 0.2-0.3 MPa before starting the measurements.

The instrument hardware was controlled and the stress-strain curves were recorded and elaborated by the Zwick/Roell *Master TestXpert* software. At least 2 to 5 different specimens of each membrane sample were tested. Clearly failed measurements were excluded from the statistical analysis.

4.2.7. Density measurement

The density of a solvent-free sample was determined by the buoyancy method, measuring the weight of the sample specimen in air, *m*, and immersed in toluene (Carlo Erba Reagenti) as non-absorbing liquid with a known density (m_{immersed}). The observed weight difference is due to the buoyancy and is the product of the sample volume (V_{pol}) and the solvent density (ρ_{solv}):

$$\Delta m = m - m_{immersed} = \rho_{solv} \cdot V_{pol} \tag{4.1}$$

After elimination of the unknown sample volume, $V_{pol} = m / \rho_{pol}$, the polymer density can easily be calculated as follows:

$$\rho_{pol} = \frac{m \cdot \rho_{solv}}{m - m_{immersed}} \tag{4.2}$$

4.2.8. Gas permeation measurements

Low pressure single gas permeation experiments were carried out in a fixed volume-pressure increase instrument, made by GKSS (Geesthacht, Germany) to suit our requirements and schematically displayed in Figure 4.1. The fixed feed volume of the instrument is about 2 litres; the fixed permeate volume is 75.5cm^3 and it is expandable, when high fluxes or long measurement times to reach steady state are needed. Up to eight gas cylinders are connected simultaneously to the instrument and an additional liquid flask can be connected for vapour transport measurements. A feed pressure up to 1.33 bar can be used and the actual value is read with a resolution of 0.1 mbar; the permeate pressure is measured in the range of 0 to 13.3 mbar with a resolution of 0.001 mbar. The membrane cell diameter is 75 mm but the effective area can be reduced by the use of appropriate masks on the membrane. The entire system is computer controlled: the feed gas pressure is set by pneumatic valves and the gases can be alternated automatically.

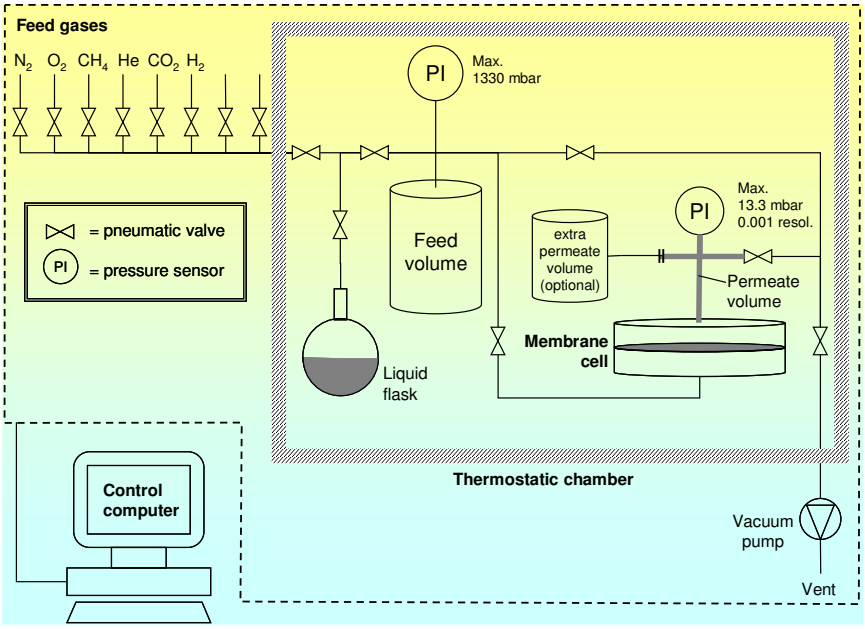

Figure 4.1. *Experimental setup for the pure gas permeation measurements in the fixed-volume/pressure-increase mode.*

The instrumental time lag is less than 0.05 s, so time lags down to 0.5 s can be determined with less than 10% error. The crucial parts of the setup are placed in a thermostatic chamber which allows measurements according to a previously chosen temperature program. Feed pressure, permeate pressure, temperature and the automatically calculated permeance are continuously registered during each measurement run and are exported automatically to an Excel data file. In the present work the membranes were tested over an effective surface area of 11,3 cm^2. Measurements were carried out at 25°C and at a feed gas pressure of 1 bar. Before the first measurement the membrane cell was evacuated for sufficient time (10-20 minutes) with a two-stage rotary pump in order to remove dissolved gases or vapours from the membrane and from the rubber seals. Between two subsequent gases the system was evacuated, flushed with the second gas and evacuated again in order to guarantee complete removal of the previous gas. The measurement of the transport parameters is based on the determination of the pressure increase rate of the fixed permeate volume upon exposure of the membrane to the pure gas. For a constant permeate volume and a constant feed pressure and in the absence of a time-lag the permeate pressure will increase asymptotically to the feed pressure, as shown in Figure 4.2. If a closed feed volume is used then the feed pressure decreases according to the amount of permeating gas. However, if the feed volume is much larger than that of the permeate, and the feed pressure much higher than that of the permeate, then a constant feed pressure can be assumed. In that case the permeance, defined as the gas volume (m^3_{STP}) which penetrates a certain membrane area (m^2) per unit time (h) at a given pressure difference (bar), can be calculated from the permeate pressure increase according to the following equation:

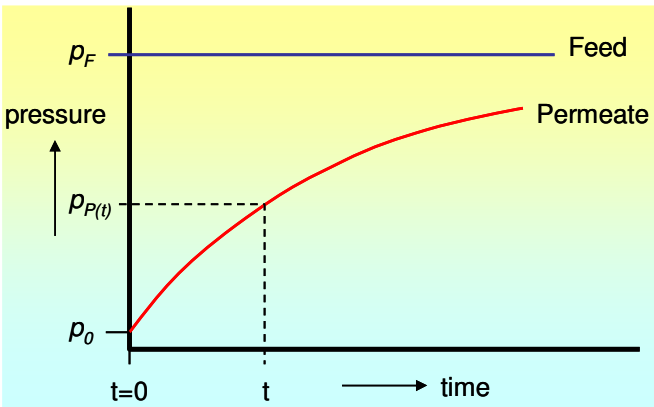

Figure 4.2. *Permeate pressure increase curve described by Eq. (4.3) for a membrane system with a constant feed pressure and a fixed permeate volume.*

$$P = \frac{3600 \cdot V_P \cdot V_m}{R \cdot T \cdot A \cdot t} \cdot \ln\left(\frac{p_F - p_0}{p_F - p_{P(t)}}\right) \qquad \text{in} \quad \frac{\mathrm{m}^3_{\mathrm{STP}}}{\mathrm{m}^2 \cdot \mathrm{h} \cdot \mathrm{bar}} \tag{4.3}$$

in which V_P is the permeate volume [m^3], V_m is the molar volume of a gas at standard temperature and pressure [$22.41 \cdot 10^{-3}$ m^3_{STP}/mol at 0°C and 1 atm], R is the universal gas constant [$8.314 \cdot 10^{-5}$ m^3bar/(mol·K)], T is the absolute temperature [K], A is the exposed membrane area [m^2], t is the measurement time [s], p_F is the feed pressure and p_0 and $p_{P(t)}$ are the permeate pressure at t=0 and at t=t, respectively. The number 3600 is the conversion factor for time [s/h].

If the permeate pressure and the total permeate pressure change is very small and negligible compared to the feed pressure, the logarithmic term in Eq. (4.3) simplifies to:

$$\ln\left(\frac{p_F - p_0}{p_F - p_{P(t)}}\right) = \ln\left(1 - \frac{p_0 - p_{P(t)}}{p_F - p_{P(t)}}\right) \approx -\frac{p_0 - p_{P(t)}}{p_F - p_{P(t)}} \approx \frac{p_{P(t)} - p_0}{p_F} \quad \text{for } p_0 \text{ and } p_{P(t)} << p_F \tag{4.4}$$

This is generally the case in our measurements, with $p_F \approx 1$ bar and p_0 and $p_{P(t)} < 13$ mbar, and Eq. (4.3) can thus be approached by a linear equation:

$$P = \frac{3600 \cdot V_P \cdot V_m}{R \cdot T \cdot A \cdot t} \cdot \frac{p_{P(t)} - p_0}{p_F} \tag{4.5}$$

In the initial linear part of the pressure increase curve (Figure 4.2) the permeance is proportional to the curve slope or permeate pressure increase rate, dp_P/dt , and can thus be calculated straightforwardly by:

$$P = \frac{3600 \cdot V_P \cdot V_m}{R \cdot T \cdot A \cdot p_F} \cdot \frac{dp_P}{dt} \tag{4.6}$$

4.2.9. Solubility and diffusion coefficient

Penetrant transport through a polymer film is commonly described by a three-step solution-diffusion process, characterized by absorption of the gas at the polymer-gas interface at the feed side, followed by diffusion of the dissolved species across the membrane and desorption of the gas species from the polymer-gas interface at the low pressure side. In simple cases where the unidirectional penetrant flux obeys Fick's law and where the downstream pressure is negligible compared to the upstream pressure, the permeability is generally expressed as the product of solubility and diffusion, as already described in par. *1.2.4*:

$$P = D \cdot S \tag{4.7}$$

where D is the diffusion coefficient (cm^2/s) and S is the solubility coefficient ($cm^3_{STP}/(cm^3\ bar)$). A common procedure to determine the diffusion coefficient by permeation experiments is the time lag method, as exposed in par. *1.2.6*.

In the setup of Figure 4.1 the pressure of the fixed permeate volume is proportional to the amount of penetrant permeating through the membrane and the equation describing the pressure increase takes the same form as Eq. (1.17) (Figure 4.3). If the permeate pressure is again negligible compared to the feed pressure, then Eq. (4.5), after some rearrangement and introduction of the time lag describes the steady state permeate pressure increase as follows:

$$p_{p(t)} - p_0 = \frac{R \cdot T \cdot A \cdot p_F \cdot S}{3600 \cdot V_p \cdot V_m \cdot l} \cdot D \cdot (t - \Theta) \tag{4.8}$$

The time lag can thus be obtained by linear extrapolation of the steady state pressure increase curve to the time axis or to the starting pressure (Figure 4.3). Knowing the membrane thickness, the diffusion coefficient can then be obtained from Eq. (1.19) and subsequently the solubility can be obtained from the steady state permeation and Eq. (4.7): $S = P/D$.

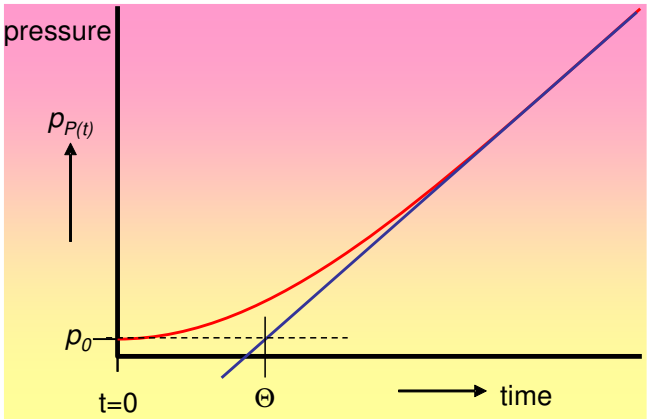

Figure 4.3. *Time lag curve for a membrane system with a fixed permeate volume, valid in the case of $p_0 \approx 0$ and $p_{P(t)} << p_F$. The steady state curve (tangent line) is described by Eq. (4.13).*

4.2.10. Modeling of transport properties.

4.2.10.1. Generation and equilibration of polymer structures.

The TTD and TFE repeating units of Hyflon have been constructed using the BUILDER module of Insight II [23], according to the method already described [15], employing the COMPASS (condensed-phase optimized molecular potentials for atomistic simulation studies) force field [24] to compute interatomic interactions. The comonomer units were minimised for about 500 iteration steps utilising the steepest-descent and conjugate gradient algorithms. Then a single copolymer chain of 770 repeat units with the appropriate molar ratio of TTD and TFE was constructed, using conditional statistics with the Polymerize module [23]. For the construction of periodic cells a correct distribution of conformational angles and global chain geometry was requested. Based on the Rotational Isomeric State (RIS) model the stepwise chain construction scheme of the Amorphous Cell Program of Insight II [23] was employed to generate the initial structure [25,26].

In order to minimize chain end effects, each cell contains only one minimized polymer chain rather than several chains confined to the sane volume, which would lead to increased density of chain ends. Figure 4.4 shows schematically the packing procedure from a single polymer chain to a fully equilibrated three-dimensional box. The details of the chosen procedure were described in ref. [15].

After the cell construction at the initial density, the models were subjected to sequences of energy minimization and dynamics runs at constant number of particles, temperature and volume (NVT-MD), combined with force field parameter scaling. Small deviations may happen in obtaining the experimental density for glassy stiff-chain polymer materials [27,28], especially if the models are rather large. The deviations may reflect minor errors of the parameterization of the respective polymers in the chosen force field, which influence the equilibration of the models. This final equilibration step is carried out for 300 picoseconds (ps). During the dynamics the Andersen [29] temperature control and the Berendsen [30] pressure control methods were used. NPT-MD simulations for the further analysis (collection of data) at 1 bar were performed with the Discover InsightII package of Accelrys [23] employing a time step of 1 fs for the numerical integration for 1.2 ns.

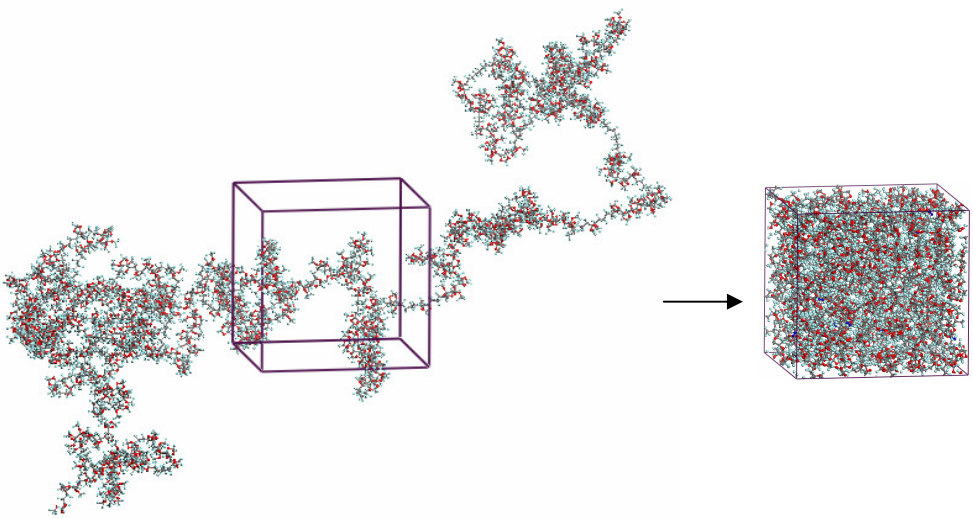

Figure 4.4 *Construction of a fully equilibrated 3-dimensional box, starting with a single Hyflon AD60X polymer chain. Atom colors: grey=carbon, red=oxygen, light blue=fluorine. Ten nitrogen molecules (dark blue) are inserted into the box for the transport studies.*

Positions and velocities of all atoms of the model structures were saved each 500 ps in a history file. Parallel to the MD simulations the reasonably equilibrated packing models were subjected to the Transition State Theory (TST) algorithm using the GSNET and GSDIF programs [31].

4.2.10.2. Generation and equilibration of polymer structures.

The diffusion coefficients (D) for penetrant molecules were calculated via the long term molecular dynamics (MD) method by means of the Einstein relation [32]:

$$D = \frac{1}{6} N_a \lim_{t \to \infty} \frac{d}{dt} \sum_{i=1}^{N_a} \left\langle \left| \mathbf{r}_i(t) - \mathbf{r}_i(0) \right|^2 \right\rangle \tag{4.9}$$

where N_a is the number of diffusing molecules of type a, $\mathbf{r}_i(0)$ and $\mathbf{r}_i(t)$ are the initial and final positions of molecules (of centres of mass of particle *i*) over the time interval *t*, and $\left\langle \left| \mathbf{r}_i(t) - \mathbf{r}_i(0) \right|^2 \right\rangle$ is the mean squared displacement (MSD), averaged over the possible ensemble. The Einstein relation assumes a random walk motion for the diffusing particle.

The anomalous diffusion, generally observed for glassy polymers in the range of short times, is characterized by the mean squared displacement [33]:

$$\left\langle \left| \mathbf{r}_i(t) - \mathbf{r}_i(0) \right|^2 \right\rangle \propto t^n \tag{4.10}$$

with $n<1$. In the short simulation time the MSD may be quadratic due to the fact that the penetrant molecule is restrained in its motion in the rigid structure.

The dissolved gas is assumed to be at infinite dilution. However, in order to enhance the sampling efficiency, ten molecules of each gas type have been inserted into the polymer structure. For the given boxes this corresponds to a slightly higher nitrogen and oxygen concentration than the experimental solubilities, while the helium concentration is notably higher than the experimental solubility at 1 bar in the melt-pressed membrane. Nevertheless, for the simulations this does not give any complications. The concentrations are still sufficiently low and there are no significant mutual interactions between the dissolved gas molecules. It is also experimentally known that these very low concentrations still have no effect on the polymer matrix. Only highly soluble gases at elevated pressures may cause plasticization, and thus significant modification of the polymer structure. This is for instance the case with CO_2 at pressures higher than 10-20 bar.

4.2.10.3. Theoretical calculation of diffusion and solubility coefficients with the TST.

TST is used to calculate the rate constants, k_{jump}, of each possible jump from cavity to cavity in a polymer microstructure and it is used to compute diffusion and solubility coefficients. Gusev and Suter implemented the original TST method giving the polymer some flexibility [34,35] and assuming that the polymer atoms in a sorption site execute uncorrelated harmonic vibrations around their equilibrium positions to accommodate the guest molecules. These motions are termed elastic motions and they occur at a much shorter time scale than the time elapsing between penetrant jumps. The behaviour and properties of the solute can be described with the time-independent single particle distribution function $\rho(\vec{\tau})$, where $\vec{\tau}$ is the location [34,35], thus allowing for modelling the transport of small molecules in solids on time scales far beyond the reach of MD. The thermal fluctuations of the position of all atoms are described by the isotropic Gaussian functional form, using the mean squared deviation of host atoms from their average positions, given by:

$$W(\{\Delta\}) \propto \exp\left\{-\sum \frac{\Delta^2}{2\langle\Delta^2\rangle}\right\} \tag{4.11}$$

The smearing factor $<\Delta^2>$ is a parameter in the homogeneous isotropic approximation and can be evaluated from atomistic trajectories of the polymeric matrix by means of short–scale MD simulations of the host matrix without dissolved molecules. It is assumed that the averaging time for the determination of the smearing factor $<\Delta^2>$ should be the most frequent residence time τ of a probe molecule in the void. Since the value of the average residence time of diffusing molecules in the void depends on the thermal vibrations of the polymer matrix an iterative procedure is used, starting with the rather arbitrary setting $<\Delta>$ = 0.3-0.4 Å and computing $\rho(\log\tau, <\Delta^2>)$. A new iteration with the new values for $<\Delta^2>$ is used and the function is recalculated until the convergence criterion is fulfilled and the smearing factor does not change the position of the maxima of the probability function.

The behaviour and properties of the small gas molecules is described by a time independent single-particle distribution function $r(\mathbf{r})$, where $\mathbf{r}$ is the position [18,36,37].

This allows the modelling of the transport of probe gases also in glassy polymers on time scales exceeding the diffusive regime and it requires much less computational time than MD. The application of TST requires (a) preparation of the host polymeric matrix, determining the positions of all atoms in the matrix; (b) evaluation of the interactions between the diffusant guest molecule and the host matrix that determine the probability of finding the guest particle at each point of the host matrix; (c) random walk of the diffusing molecules through the matrix.

The TST method was thus used to study the thermodynamics and transport of the small gas molecules, hydrogen, oxygen, nitrogen, methane and carbon dioxide, respectively, in the version of InsightII (400P+) [23]. Diffusion coefficients (D) and gas solubility (S) in the matrix were computed and then the permeability coefficients (P) were calculated as the product of D and S (Eq. (4.7)). The calculations were carried out in two steps. In the first step the solubility of the respective gas was evaluated. A 3D orthogonal lattice grid with a constant spacing of 0.3 Å was used to estimate the solute distribution function in the matrix by calculating the Helmholtz free energy between the gas molecule inserted at each grid point and all the atoms of the polymer matrix that are subject to elastic fluctuations.

These data were used to identify minimum energetic sites and to determine transition probabilities from site to site, together with the residence time in each site. In the second step a Monte Carlo simulation of gas diffusion by a 'hopping' mechanism was performed, based on the energy as well as the connectivity of available sites and on the transition jump probabilities. In this study, the smearing factor was calculated by means of the self-consistent field (SCF) procedure. The mean squared displacement of all subsets of atoms in the amorphous cell was obtained as a function of time from a short NVT dynamics run (30 ps with 1 fs time step at 300°K).

4.3. Results and discussion

4.3.1. Quantitative analysis of the residual solvent.

Membranes were prepared by a standard solution-casting procedure, followed by evaporation of the solvent at room temperature, first at atmospheric pressure until a solid dense film was obtained, and then under vacuum. Subsequently the amount of residual

solvent in the membranes was monitored by periodically weighing the film while it is slowly heated under vacuum. Figure 4.5a shows the weight loss as a function of the drying temperature for two membranes cast from different solutions. The membrane with Galden HT 55 contains more solvent after drying at room temperature and reaches constant weight at a higher drying temperatures than the membrane with HFE 7100. Evidently, complete removal of Galden is more difficult due to its higher molar mass: 350 g/mol, compared to 250 g/mol for HFE. In both cases the complete evaporation of the solvent within reasonable time is achieved at temperatures well above 130°C, the Tg of the polymer, measured as the half c_p value (see below).

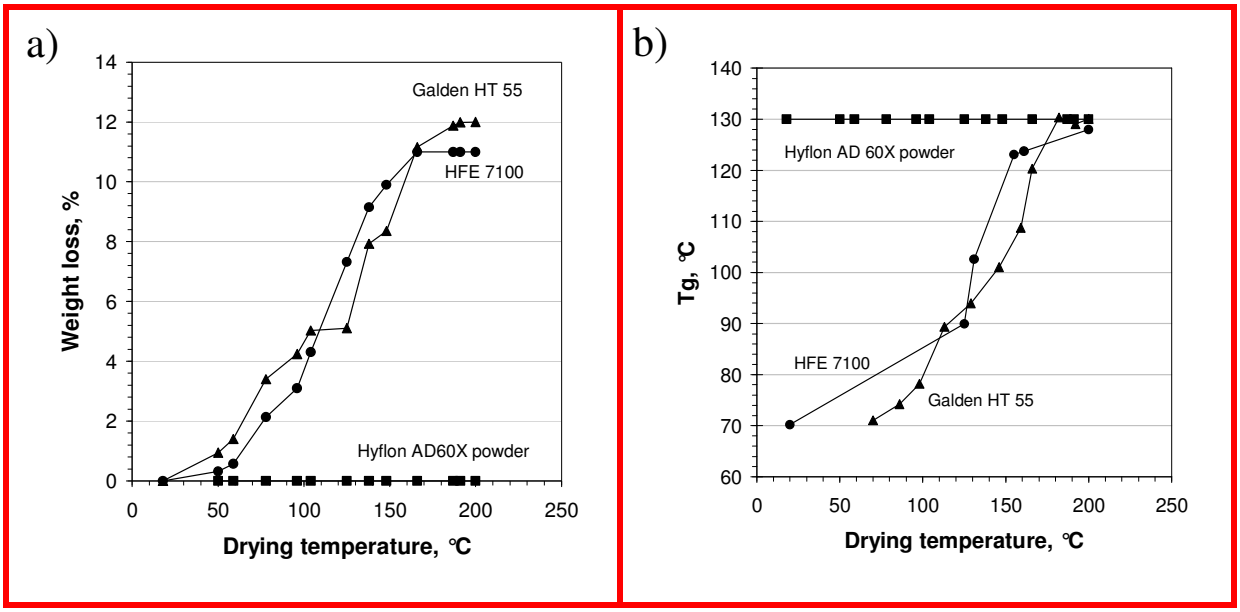

Figure 4.5 *a) Weight loss and b) glass transition temperature of the Hyflon AD60X membranes and of Hyflon powder as a function of the drying temperatures during very slow heating at 0.02°C/min under vacuum. Tg determined by DSC from the first heating run at a heating rate of 15°C/min.*

Only the increased polymer chain mobility in the rubbery state enables a sufficiently fast diffusion of the solvent, while solvent removal from the glassy state seems to be particularly difficult. It was previously found that thin Hyflon® AD60X membranes may retain up to about 3% of solvent even after 3 years at room temperature [21].

4.3.2. Density.

The density of the solvent-free melt-pressed membrane was determined by the buoyancy method, as described in the experimental part, using toluene as the non-absorbing liquid. At 20°C the average density determined by 3 measurements was 1.917 ± 0.012 g/cm^3, in good agreement with the value of 1.93 reported in the literature [19].

4.3.3. Influence of the residual solvent on the thermal properties.

DSC analysis of the samples shows a strong increase of the *Tg* with increasing drying temperature and decreasing solvent content (Figure 4.5b).

Near 200°C the *Tg* reaches the same value as the starting polymer powder, which itself does not show any weight loss or change of the *Tg* over the entire range of drying temperatures. Evidently the residual solvent strongly plasticizes the polymer, reducing the *T*g of the freshly cast films to more than 50°C below that of the pure polymer. Although the trend is clear, the data in Figure 4.5b are somewhat scattered. This is because the effect of residual solvent must necessarily be evaluated on the first heating run, which is usually more noisy due stress relaxation above the *Tg* and to further evaporation of residual solvent.

The second heating curve usually shows a more smooth curve but gives a higher *Tg* because of partial evaporation of the residual solvent in the first heating-cooling cycle (Figure 4.6). The relation between the heating temperature and the *Tg* (Figure 4.5b) is determined both by the amount of the solvent, related to the evaporation rate, and by the relative effect of the solvent on the *Tg*, related to molecular properties. In the present case both solvents seem to affect the *Tg* in a similar way.

In quantitative terms the plasticizing effect of HFE and Galden can be evaluated better if the *Tg* is plotted against the weight fraction of solvent in the film (Figure 4.7).

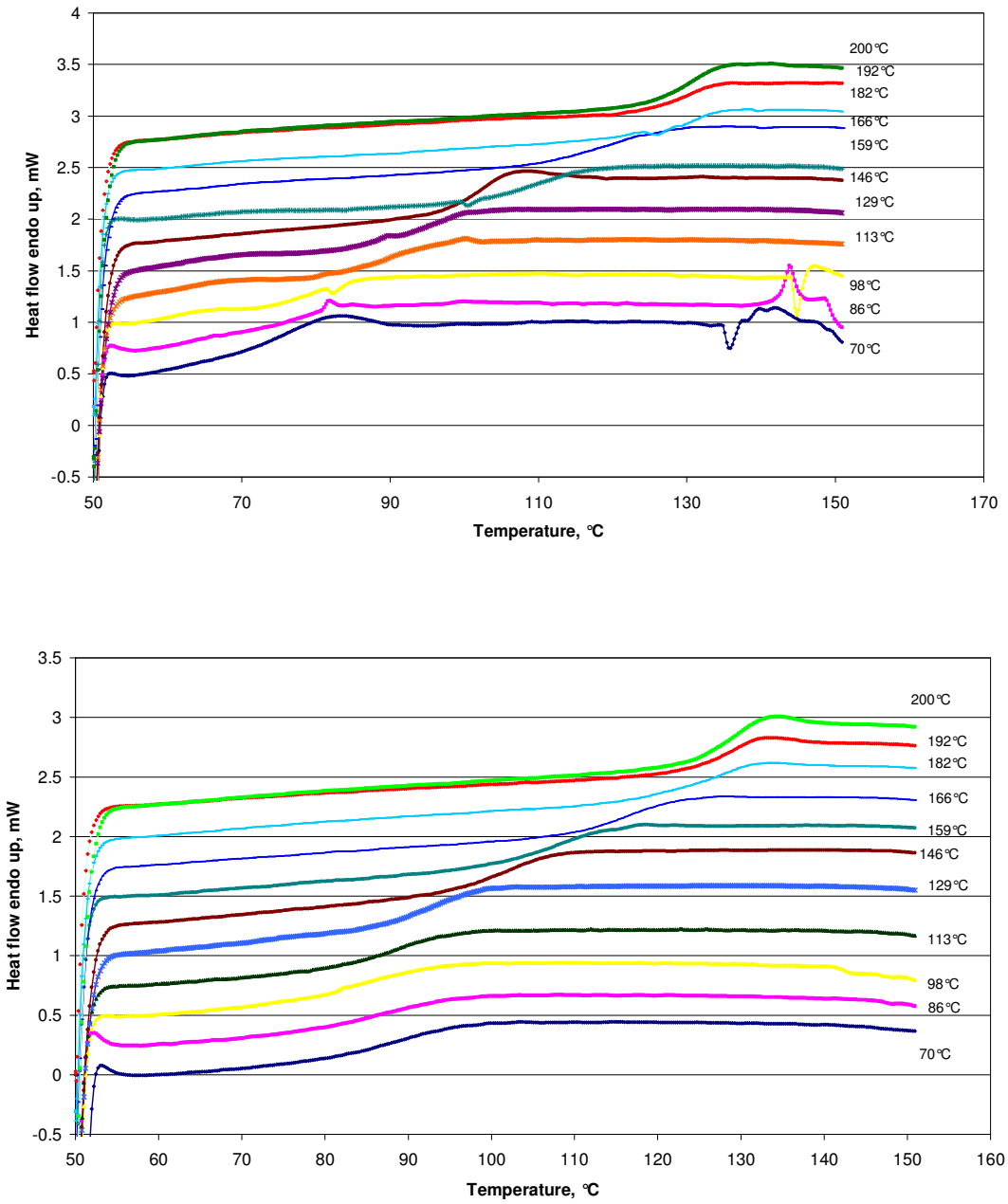

Figure 4.6. *DSC curves of the membrane prepared from a solution in Galden HT55, after heating of the sample under vacuum to the indicated temperature at 0.02°C/min. First heating run (top) and second heating rung (bottom) at 15°C/min. Curves are shifted vertically for clarity.*

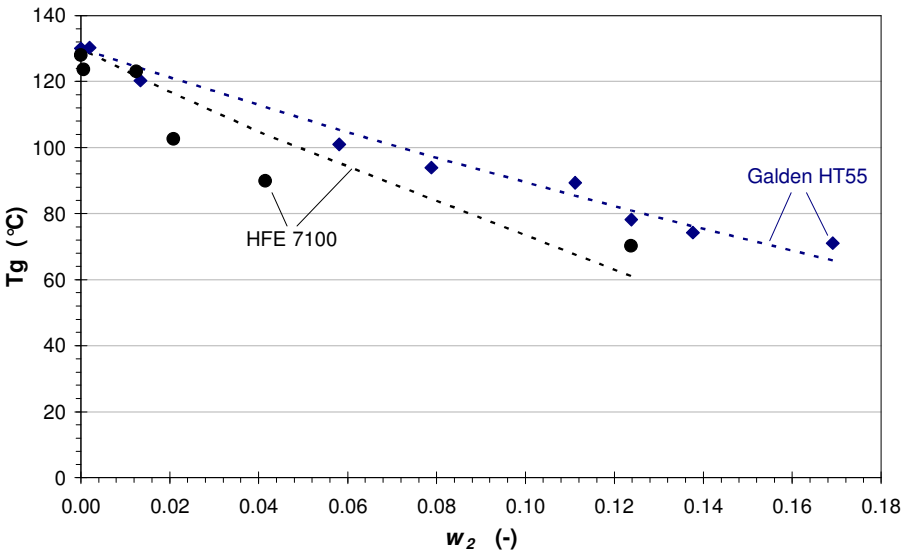

Figure 4.7 *Glass transition temperatures as a function of the weight fraction of the solvent in the dense film for Galden HT 55 (♦) and HFE 7100 (●). Dashed curves: Nonlinear regression curve of the Fox equation (Eq. (19)), solving for the unknown value of* Tg_2 *for Galden and for HFE 7100.*

Many different equations have been proposed to describe the glass transition temperature of miscible binary polymer blends or polymer/diluent mixtures [38]. One of the most popular relations describing the *Tg* as a function of the blend composition is the Kwei equation, which is particularly valid for systems with strong interactions between the constituents of the blend [39-41]:

$$T_g = \frac{w_1 T_{g_1} + k w_2 T_{g_2}}{w_1 + k w_2} + q w_1 w_2 \qquad (4.12)$$

in which w_1 is the weight fraction of the first component with glass transition temperature Tg_1 and w_2 is the weight fraction of the second component with glass transition temperature Tg_2; k and q are two adjustable empirical parameters, related to the excess energy of backbone stabilization and to incipient phase inversion [41]. Ruiz-Treviño and Paul, successfully used the Gordon-Tailor equation in their work on membranes with low molecular weight diluents [42-44]. This is a somewhat simplified form of the Kwei equation, with just one adjustable parameter.

$$T_g = \frac{w_d T_{gd} + k w_p T_{gp}}{w_d + k w_p} \tag{4.13}$$

in which *d* and *p* represent the diluent and the polymer, respectively. Probably the most frequently used and simplest relation, without adjustable parameters, is the Fox equation, which will be evaluated in the present work [45]:

$$\frac{1}{T_g} = \frac{w_1}{T_{g_1}} + \frac{w_2}{T_{g_2}} \tag{4.14}$$

Due to the reciprocal terms, the *Tg* of the mixture according to the Fox equation is always below the weighted average of the two individual *Tg*'s. If we choose the index 1 for the polymer and 2 for the solvent, then after substitution of $w_1=1-w_2$ the Fox equation can be rewritten in a linearized form:

$$\frac{1}{T_g} - \frac{1}{T_{g_1}} = w_2 \left(\frac{1}{T_{g_2}} - \frac{1}{T_{g_1}} \right) \tag{4.15}$$

A plot of $\frac{1}{T_g} - \frac{1}{T_{g_1}}$ against the weight fraction of solvent, w_2, should thus yield a straight line through the origin, with slope $\frac{1}{T_{g_2}} - \frac{1}{T_{g_1}}$. If the *Tg* of the solvent is not known, then it can be estimated by a linear least squares fit of the experimental data according to Eq. (4.15) or it can be obtained directly by a nonlinear fit according to Eq. (4.14). On the other hand, if both Tg_1 and Tg_2 are known, then the Fox equation allows the determination of the solvent content by measurement of the *Tg*.

The experimental values of *Tg* as a function of the residual solvent content are plotted in Figure 4.7. The dotted lines represent the nonlinear fit of the Fox equation, resolving for the unknown value of Tg_2, using the experimental weight fractions of solvent and Tg_1= 130°C for pure Hyflon AD60X. Thus the estimated values of the *Tg* of HFE is -120°C and that of Galden HT55 is -80°C. The latter is somewhat overestimated, because its actual *Tg* is below -100°C [46] and indicates that the Fox equation fits reasonably well but not perfectly the

experimental data. Nevertheless below 10-15% of residual solvent this fit provides a reasonable estimation of the solvent content if the *Tg* of an unknown sample is measured.

At the same concentration HFE appears to plasticize Hyflon slightly more than Galden HT, probably because of the $-CF_3$ side groups (Scheme 4.1), which reduce the chain mobility of Galden. Nevertheless, HFE may be more suitable for preparation of dense membranes because of its easier removal.

4.3.4. Influence of the solvent on the mechanical properties.

The mechanical properties of a freshly prepared film and a vacuum-dried film are listed in Table 4.2. Remarkably both the Young's modulus, the maximum elongation and maximum strength decrease as a result of the drying procedure. Especially the lower Young's modulus seems to be in contradiction with the strong plasticization found by DSC analysis. Paul and coworkers observed a similar effect in a series of membranes with different low molar mass diluents, defining the phenomenon as antiplasticization [43,44,47-50].

Table 4.2. *Mechanical properties of the solvent cast film before and after drying at 200°C under vacuum.* [a)]

		Average	Standard deviation	Variance
Fresh film	Young's Modulus (MPa)	761	32	4.2
	Maximum load (MPa)	8.82	1.22	13.8
	Elongation at break (%)	1.46	0.31	21.3
Dried film	Young's Modulus (MPa)	323	42	13
	Maximum load (MPa)	2.43	0.53	21.8
	Elongation at break (%)	0.85	0.16	18.9

[a)] *Average of 4 samples*

They further observed that the increase in strength was accompanied by a decrease of the free volume.

For this reason their diluent molecules caused a decrease in the gas permeability and an increase in the selectivity, in sharp contrast with the observations in this paper (see transport properties below). In the present work it was furthermore observed that drying at elevated

temperature is usually accompanied by a contraction of the sample specimen of up to about 20% of its original diameter, and by a slight increase of the film thickness. The predominance of contraction in the in-plane direction suggests that in the last stage of the solvent evaporation process the chains have undergone a net orientation as a result of the unidirectional diffusion of the solvent to the membrane surface (Figure 4.8). This orientation then relaxes upon heating of the sample above the Tg, resulting in the observed contraction. We can thus attribute the observed results to two distinct phenomena. The first, true plasticization by the residual solvent, dominates the thermal properties and the gas transport. The second, the introduction of anisotropy in the polymer sample by the solvent evaporation, dominates the mechanical properties.

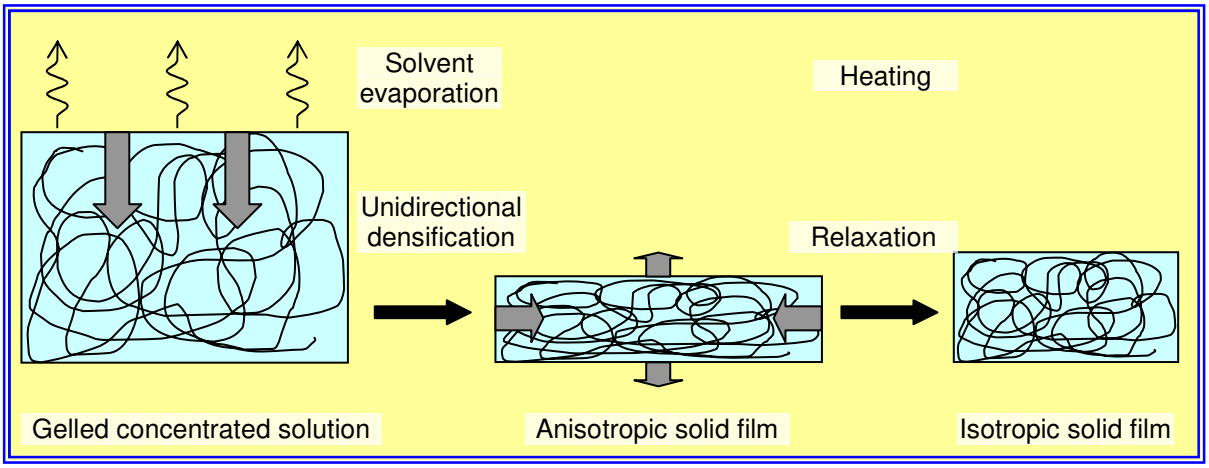

Figure 4.8. *Schematic representation of the orientation and relaxation phenomena of the polymer during solvent evaporation from the film below and above the Tg, respectively.*

4.3.5. Influence of residual solvent on gas permeation.

In order to quantify the effect of the residual solvent on the transport properties, permeation measurements were carried out on membranes cast from solutions in HFE as well as Galden, before and after thorough removal of the residual solvent under vacuum.

A melt pressed membrane, prepared in the complete absence of solvent, was investigated for comparison. The automated gas permeation setup (Figure 4.1) has such a rapid response that it enables accurate measurements of the time lag of very fast gases such as helium and hydrogen. An example of the experimental time-lag curves of membrane H25 is given in Figure 4.9. The time lag is obtained by extrapolation of the steady state pressure increase curve to the starting pressure while the diffusion coefficients of the gases in the polymer are

calculated from the time lag according to Eq. (1.19). The permeability and solubility are then obtained from the steady state pressure increase rate, as described above. An overview of all experimental data of the different membranes is given in Table 4.3 and Table 4.4.

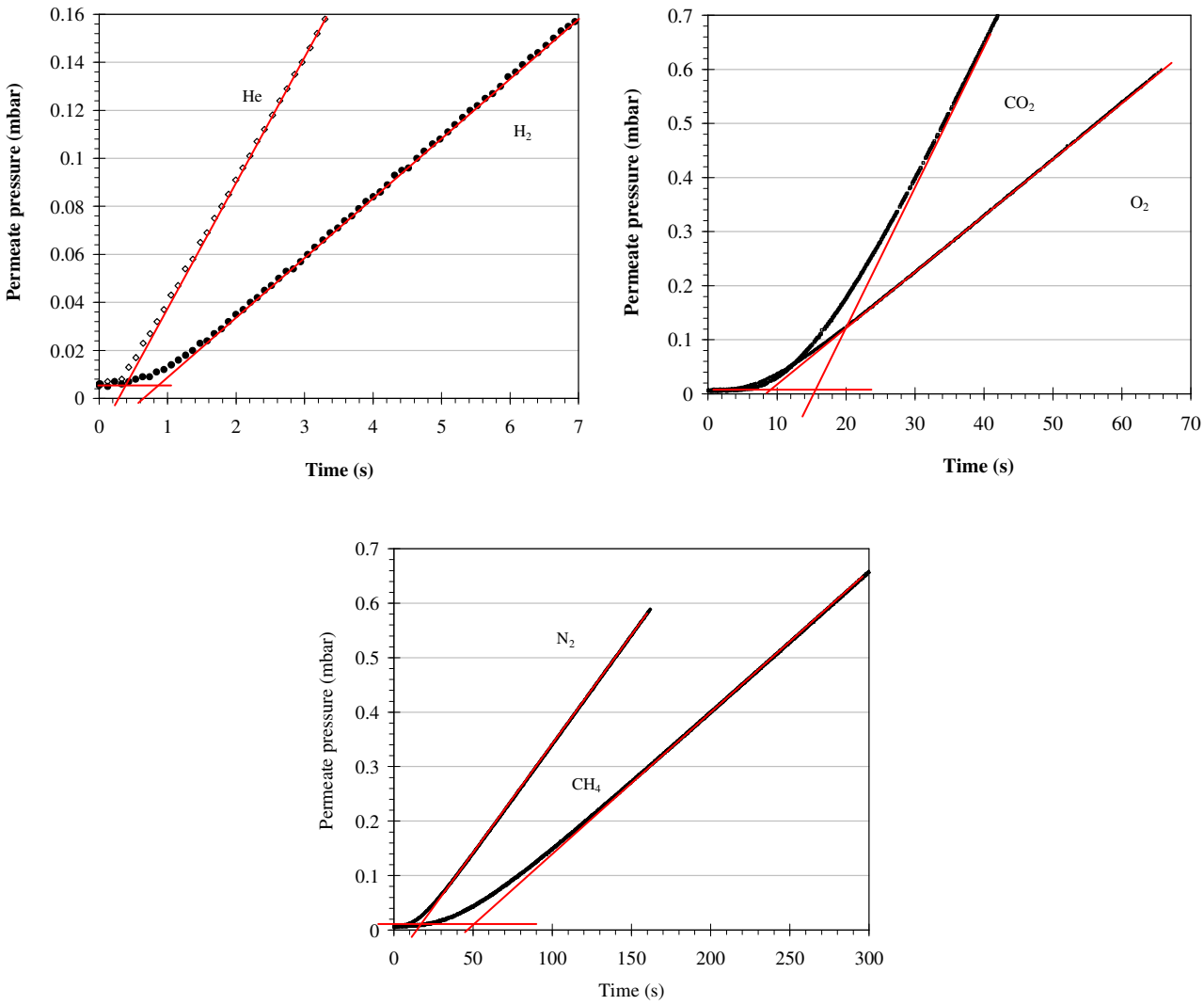

Figure 4.9. *Pressure increase curves of the freshly cast membrane H25 for six different gases at 25°C and a feed pressure of 1 bar. Membrane area 11.3 cm^2, permeate volume 75.5 cm^3.*

Table 4.3 *Experimental transport parameters at 25°C and 1 bar of feed gas pressure for solution-cast membranes from casting solutions in Galden HT 55 or HFE 7100 before and after vacuum drying at 200°C.*

Membrane	Gas	Permeability coefficient, P		Time lag, Θ	Diffusion coeff., D	Solubility, S	Selectivity		
		10^{-6} m^3_{STP} m / (m^2 h bar)	Barrer [a)]	s	10^{-6} cm^2/s	m^3_{STP}/m^3bar	P_i/P_{N2} (-)	D_i/D_{N2} (-)	S_i/S_{N2} (-)
Membrane G25 Solvent Galden Freshly cast Thickness 60.6 µm	Helium	0.976	357	0.21	29.1	0.093	9.37	37.62	0.249
	Hydrogen	0.515	188	0.41	14.9	0.0958	4.94	19.27	0.256
	CO_2	0.576	210	7.5	0.816	1.96	5.52	1.05	5.24
	Oxygen	0.232	84.7	4.6	1.33	0.484	2.22	1.72	1.30
	Nitrogen	0.104	38.1	7.9	0.775	0.374	1.00	1.00	1.00
	Methane	0.0844	30.8	15.5	0.395	0.593	0.81	0.51	1.59
Membrane G200 Solvent Galden Dried at 200°C Thickness 65.2 µm	Helium	1.3	476	0.23	30.8	0.117	50.3	187.0	0.269
	Hydrogen	0.511	187	0.7	10.1	0.140	19.72	61.4	0.321
	CO_2	0.211	77.0	35	0.202	2.89	8.14	1.23	6.62
	Oxygen	0.0948	34.6	17	0.417	0.632	3.66	2.53	1.45
	Nitrogen	0.0259	9.46	43	0.165	0.436	1.00	1.00	1.00
	Methane	0.00828	3.03	290	0.0244	0.941	0.32	0.15	2.16
Membrane H25 Solvent HFE 7100 Freshly cast Thickness 67.7 µm	Helium	0.928	339	0.29	26.3	0.0978	12.93	53.5	0.242
	Hydrogen	0.461	169	0.51	15.0	0.0856	6.43	30.4	0.212
	CO_2	0.455	166	11.8	0.647	1.95	6.34	1.31	4.83
	Oxygen	0.189	69.1	7.4	1.03	0.509	2.63	2.09	1.26
	Nitrogen	0.0718	26.2	15.5	0.493	0.404	1.00	1.00	1.00
	Methane	0.0549	20.1	66	0.116	1.32	0.77	0.23	3.26
Membrane H200 Solvent HFE 7100 Dried at 200°C Thickness 68.3 µm	Helium	1.24	455	0.3	26.3	0.131	41.0	126.7	0.323
	Hydrogen	0.509	186	0.62	12.7	0.111	16.8	61.3	0.273
	CO_2	0.220	80.3	37	0.214	2.86	7.24	1.03	7.05
	Oxygen	0.106	38.7	15	0.527	0.559	3.49	2.53	1.38
	Nitrogen	0.0304	11.1	38	0.208	0.406	1.00	1.00	1.00
	Methane	0.00916	3.35	260	0.0304	0.837	0.30	0.15	2.06

[a)] *1 barrer = 10^{-10} cm^3_{STP} cm /(cm^2 s cmHg)*

Table 4.4. *Experimental transport properties at 25°C and 1 bar of feed gas pressure for a melt-pressed membrane prepared at 170°C, and transport properties at 25°C obtained by TST and MD simulations.*

Membrane	Gas	Permeability coefficient, P		Time lag, Θ	Diffusion coeff., D	Solubility, S	Selectivity		
		10^{-6} m^3_{STP} m / (m^2 h bar)	Barrer	s	10^{-6} cm^2/s	m^3_{STP}/ m^3bar	P_i/P_{N2} (-)	D_i/D_{N2} (-)	S_i/S_{N2} (-)
Membrane M170 [17] Melt-pressed at 170°C Thickness 220 µm	Helium	1.11	405	1.57	51.4	0.0599	48.9	385.4	0.127
	Hydrogen	0.382	140	6.2	0.130	0.0815	16.9	97.6	0.173
	CO_2	0.173	63.3	400	0.202	2.39	7.65	1.51	5.06
	Oxygen	0.0786	28.7	185	0.436	0.501	3.47	3.27	1.06
	Nitrogen	0.0226	8.27	605	0.133	0.472	1.00	1.00	1.00
	Methane	0.00664	2.43	2710	0.0297	0.620	0.29	0.22	1.32
Pure Hyflon AD60X TST simulations	Helium								
	Hydrogen	19.3	$7.13 \cdot 10^3$		103	0.527	3.38	12.6	0.269
	CO_2	33.8	$1.25 \cdot 10^4$		2.13	44.7	5.94	0.260	22.8
	Oxygen	15.5	$5.74 \cdot 10^3$		14.3	3.05	2.72	1.75	1.55
	Nitrogen	5.7	$2.11 \cdot 10^3$		8.18	1.96	1.00	1.00	1.00
	Methane	15.9	$5.90 \cdot 10^3$		5.66	7.93	2.80	0.69	4.04
Pure Hyflon AD60X MD simulations	Helium				76.8			175.3	
	Hydrogen								
	CO_2								
	Oxygen				0.401			0.916	
	Nitrogen				0.438			1.00	
	Methane								

[a)] *1 barrer = 10^{-10} cm^3_{STP} cm /(cm^2 s cmHg)*

4.3.6. Gas diffusion - experimental.

The diffusion coefficient strongly decreases with increasing molecular size of the gas, indicating a considerable size-sieving character of Hyflon AD60X (Figure 4.10).

Furthermore, depending on the specific gas species, the diffusion coefficient may change dramatically upon drying of the membrane. Diffusion in the freshly cast membrane is generally much faster than in the solvent-free membrane, in particular for the gases with a large kinetic diameter, such as CO_2 and methane. As discussed above on the basis of the thermal properties, this is due to plasticization of the polymer by the residual solvent, which

favours especially the motion of the bulkier molecules. Both the polymer and the solvent are highly hydrophobic and lack the molecular interactions which are responsible for the antiplasticization observed by Paul and coworkers [43,44,47-50]. The membranes prepared from HFE and from Galden demonstrate similar behaviour, although the latter has initially a higher permeability and a lower selectivity due to a slightly higher residual solvent content.

After complete removal of the solvent under vacuum the solution cast membranes have nearly the same properties as the melt-pressed sample. Since both types of membrane have been treated above the *Tg*, the sample history is cancelled and becomes irrelevant, in contrast to what can be observed if the solvent is removed below the *Tg* [8].

The increase in permselectivity of the membranes upon removal of the residual solvent can be ascribed entirely to the increase of diffusion selectivity. In the absence of residual solvent the Hyflon membranes have a CO_2/CH_4 selectivity of about 25. Although this is not exceptionally high, the combination with a relatively high CO_2 permeability and an excellent resistance to swelling by condensable species such as higher hydrocarbons, makes this material nevertheless attractive for natural gas treatment.

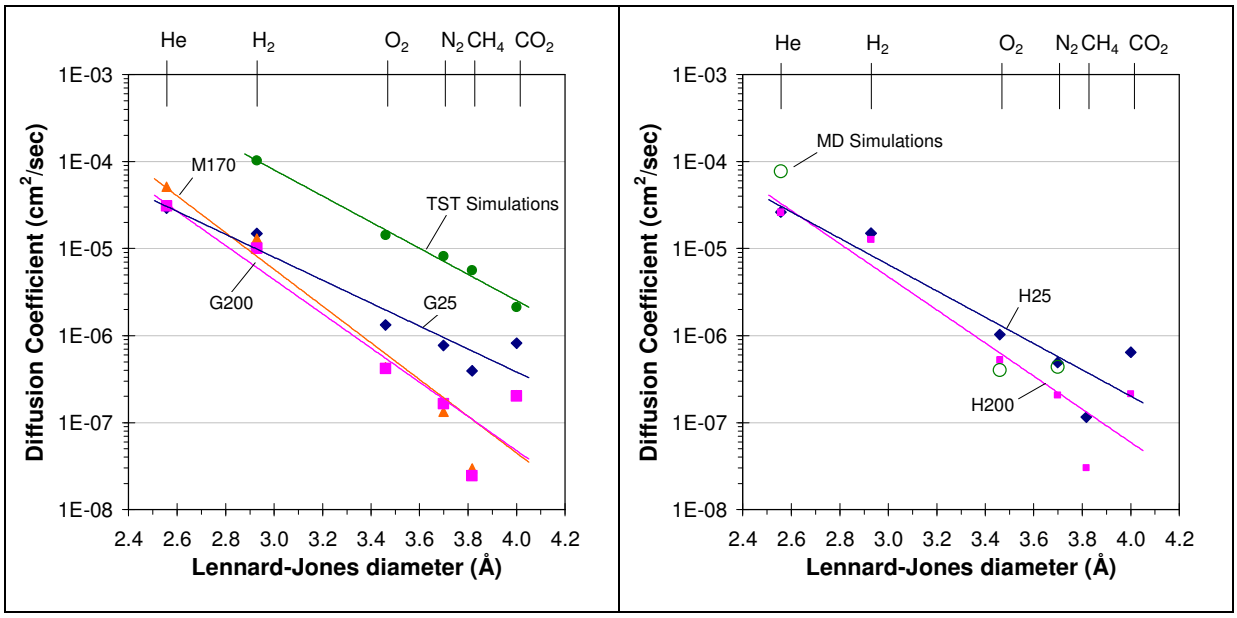

Figure 4.10. *Diffusion coefficients of six gases in a solution-cast membrane, obtained with Galden HT 55 (left) and HFE 7100 (right) before (♦) and after (■) drying under vacuum. Comparison with a melt-pressed membrane, M170 (▲), and with theoretical data from TST (●) and from MD simulations (○).*

4.3.7. Gas diffusion - simulations.

The theoretical diffusion coefficients were also obtained from simulations by using the TST method and by MD runs at 300 K. The data obtained by TST studies are plotted together with the experimental data in Figure 4.10. They follow the same trend as the experimental results, although the absolute values of all diffusion coefficients obtained by TST are about one order of magnitude higher. The discrepancy between the experimental and theoretical data may have several reasons. The first is related to the construction of the model, where small deviations may occur in the density. This happens especially for glassy stiff-chain polymer materials [27,28] and when the model is rather large. These deviations may reflect minor errors of the parameterization of the respective polymers in the chosen force field, which influence the equilibration of the models. The second one is related to assumptions about the diffusing species and the polymer. It must be emphasized that the TST calculations assume that the penetrant molecules are spherical united atoms, defined by effective Lennard–Jones parameters, σ (Å) and ε (kcal/mol). It is furthermore assumed that the polymer packing does not undergo structural relaxation (e.g. resulting from torsion transitions) to accommodate an inserted particle. Therefore, this simulation technique is restricted to small molecules.

The large deviations for CO_2 and CH_4 may be explained by their relatively large dimensions, necessitating a certain dilation of the polymer matrix for their insertion. An additional reason for the deviation of CO_2 may be the well known experimental fact of plasticization of the glassy membrane due to specific interactions of CO_2 with the polymer matrix, leading to membrane structural relaxations. This behaviour "violates" the assumption of the TST in which the dynamics of the dissolved molecules is coupled only to the elastic thermal motion of the dense polymer.

The results for CO_2 clearly show the necessity to develop improved TST-methods which permit the matrix to be locally flexible in order to accommodate larger penetrant molecules that are described in all-atom representation with partial charges.

A better agreement between simulated and experimental D and S for N_2 and O_2 would require a re-parametrisation of the Lennard-Jones parameters of both gas molecules, and improvement of the force field for the polymer.

The gas diffusion was further calculated using Eq. (4.9) from the MSD over the range of simulation times from 0.5 to 1.2 ns where Einstein diffusion is observed. The results are indicated in Figure 4.10 and clearly show a better agreement with the experimental data than the values obtained with the TST method. The difficulties for MD simulations in glassy polymers lie in the extremely broad distribution of gas molecule jump rates. It is known that the diffusion of a penetrant in a glassy polymer involves occasional jumps between cavities through the opening of a channel [27,28]. Jumps are rare events and the time between them is often shorter than the times governing matrix relaxation processes. In spite of these limitations, MD simulations are a very powerful technique and preliminary calculations on oxygen, nitrogen ad helium molecules were therefore carried out in the present work. Since the quality of MD results strongly depends on the box construction, studies are currently in progress to improve the box construction and to make MD calculations more feasible, so that a better correlation between the experimental and the theoretical results can be achieved.

4.3.8. Gas solubility - experimental.

The penetrant solubility of all gases in the different membranes is calculated from the corresponding diffusion constant and the steady state permeability according to equation (4.7) and is listed in Table 4.3 and Table 4.4. It tends to increase with increasing condensability (i.e. higher critical temperature or higher normal boiling point) of the gas and in the presence of more favourable interactions with the polymer. Often a linear trend is observed between the logarithm of the solubility and the critical temperature of the absorbed gas [51]. The present results indeed show a clear correlation between solubility and critical temperature (Figure 4.11). Unlike the diffusion coefficient, the solubility hardly changes in the presence or absence of residual solvent. This is because the solubility is mainly related to the interactions between the penetrant and the polymer matrix. Since the solvent has similar physical-chemical properties as the polymer, its presence has little effect on the gas solubility. The differences between the membranes prepared from the two solvents, either before or after vacuum drying, are within the range of the experimental error. Furthermore, the gas solubilities in the solution-cast membranes are nearly identical to those of the melt-

pressed sample. It is evident that the sample history has a much stronger effect on the diffusion than on the gas solubility.

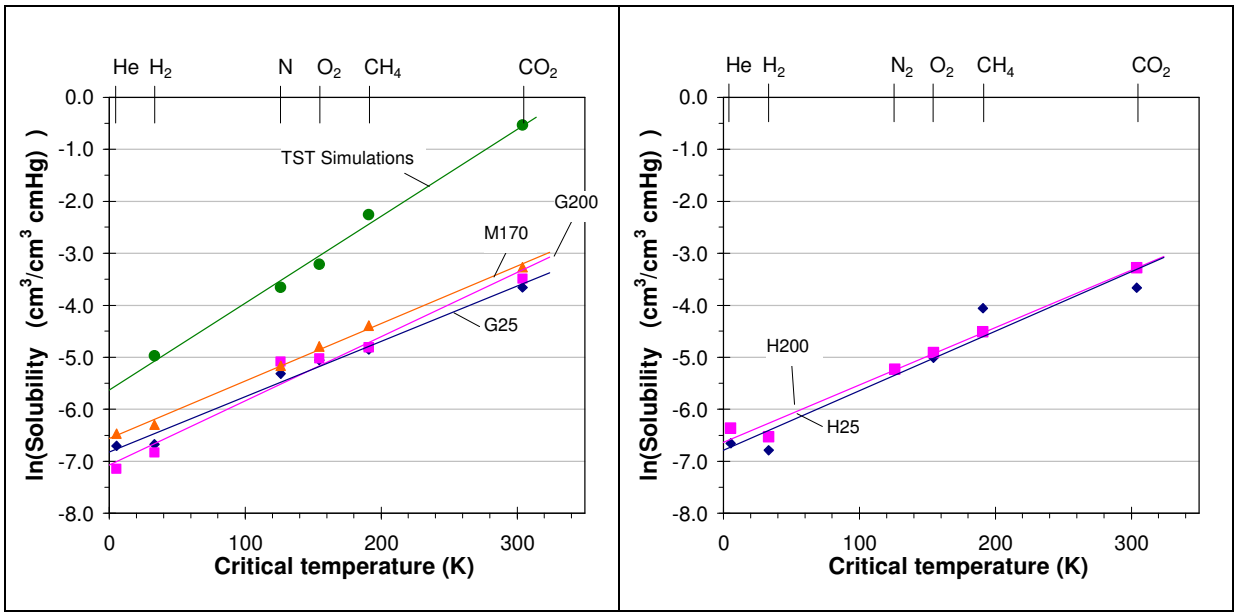

Figure 4.11. *Solubility coefficients of six gases in a solution-cast membrane, obtained with Galden HT 55 (left) and HFE 7100 (right) before (♦) and after (■) drying under vacuum. Comparison with a melt-pressed membrane, M170 (▲) and with theoretical data from TST simulations (●).*

4.3.9. Gas solubility - simulations.

The simulated solubility values are substantially higher than the experimental data (Figure 4.11 and Table 4.4). This is to some extent due to the thermodynamic non-equilibrium state of glassy polymers, which modifies the polymer-penetrant interactions and thus provokes relatively high deviations of simulated and experimental solubility coefficients. An additional reason could be related to the packing procedure and to the available data for the modelling: even relatively small errors in the insertion energy, which are determined by the quality of the model and of the applied force fields, may lead to rather high deviation in the simulated solubilities [52]. For these reasons developments to obtain new or improved models are in continuous evolution [53].

Summarizing it may be concluded that we have two clearly distinct phenomena. A) True plasticization by the residual solvent dominates the thermal properties and the gas transport properties, reducing both the *Tg* and the permselectivity. B) The anisotropy of the sample, induced by the solvent evaporation, dominates the mechanical properties with an increase of

the Young's modulus and the tensile strength of the sample. In this light the results of Yampolskii et al., who observe that thorough drying under strain causes an even stronger increase in the selectivity than in the present work are particularly interesting [4,54] Their so-called strained ageing in conditions where the polymer is not allowed to relax [3,7], also suggests the introduction of a certain anisotropy in the sample. However, they explained the results entirely in terms of conformational changes in the polymer chain.

4.3.10. Solid-state NMR spectroscopy.

The ^{1}H HRMAS NMR spectra in Figure 4.12 of the solution-cast membrane, dried at different temperatures, give clear evidence of the presence of the solvent HFE and show a qualitative picture of the progress of the solvent removal. The spectrum of the freshly prepared membrane shows two major peaks. The most intense line is attributed to the methoxy group of HFE. Its intensity decreases with the drying temperature and the peak disappears at 200°C, evidencing the complete removal of the solvent. The few small peaks, centred around a less intense second line can be attributed to the presence of protonated impurities in Hyflon, and in particular to traces of the initiator or of the surfactants used during the polymerization [46].

Besides this qualitative information on the amount of solvent, the NMR spectra give important extra information about the state of the solvent. The single sharp solvent peak indicates that only one kind of solvent exists in the polymer matrix, *i.e.* either bound or unbound, or that the dynamics of the transition between the bound and the unbound state of the solvent molecules is faster than the time scale of the NMR analysis. The latter hypothesis can be excluded by the fact that no change in the chemical shift of the methoxy peak occurs at different solvent concentrations. If the solvent were present in two different states with a very fast interchange, then the average chemical shift would be expected to depend on the relative amount of the two states and, most likely, on the total amount of solvent present. NMR analysis thus seems to confirm that the origin of the particular solvent retention by the Hyflon membranes must not be found in special interactions between solvent and polymer matrix but only in the kinetics of the solvent diffusion. This is reasonable, considering the very high molar mass of the solvent molecules. Extrapolation of the curves in Figure 4.10 to much higher Lennard-Jones diameter indeed suggests that the

diffusion of the solvents is several orders of magnitude slower than that of the permanent gases studied in this work.

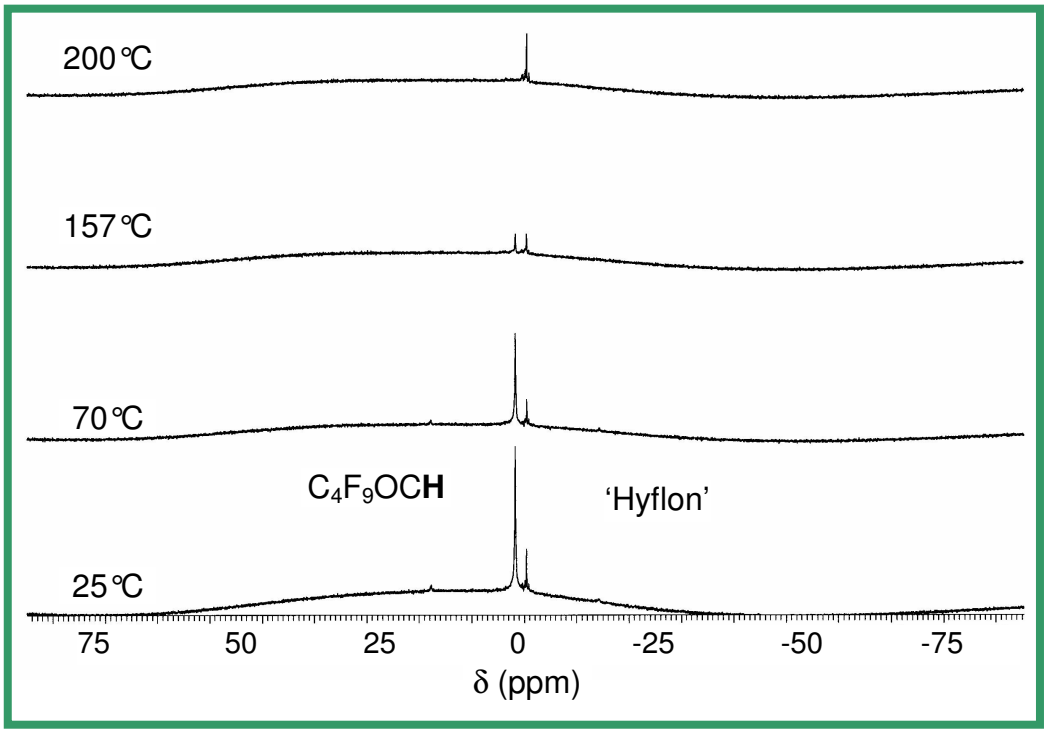

Figure 4.12. *HR MAS ^{1}H NMR spectra of a Hyflon film after drying at room temperature at atmospheric pressure and of three films after drying under vacuum at the indicated temperatures (vertical scales not normalized).*

References

1. R. E. Kesting, A. K. Fritzche, "Polymeric gas separation membranes", Ch. 3, Wiley, New York **1993**.
2. P. Hacarlioglu, L. Toppare, L. Yilmaz, Effect of preparation parameters on performance of dense homogeneous polycarbonate gas separation membranes, *J. App. Polym. Sci.*, **2003**, 90, 776-785.
3. Yu. Kostina, G. Bondarenko, A. Alentiev, Yu. Yampolskii, The influence of conformation composition of polyheteroarylenes on their transport properties, *Desalination*, **2006**, 200, 34–36.
4. Yu. Kostina, G. Bondarenko, A. Alentiev, Yu. Yampolskii, Effect of chloroform on the structure and gas-separation properties of poly(ether imides), *Polym. Sci. Ser. A*, **2006**, 48, 32-38.
5. J. Bi., G. P. Simon, A. Yamasaki, C. L. Wang, Y. Kobayashi, H. J. Griesser, Effects of solvent in the casting of poly(1 trimethylsilyl-1 propyne) membranes, *Rad. Phys. Chem.*, **2000**, 58, 563-566.
6. K. C. Khulbe, T. Matsuura, G. Lamarche, H. J. Kim, The morphology characterisation and performance of dense PPO membranes for gas separation, *J. Membr. Sci.,* **1977**, 135, 211-223.
7. A. Alentiev, Y. Yampolskii, Yu. Kostina, G. Bondarenko, New possibilities for increasing the selectivity of polymer gas separating membranes, *Desalination*, **2006**, 199, 121–123.
8. C. Joly, D. Le Cerf, C. Chappey, D. Langevin, G. Muller, Residual solvent effect on the permeation properties of fluorinated polyimide films, *Sep. Purif. Techn.*, **1999**, 16, 47-54.
9. Y. Maeda, D. R. Paul, Effect of antiplasticization on selectivity and productivity of gas separation membranes, *J. Membr. Sci.*, **1987**, 30, 1-9.
10. Y. Maeda, D. R. Paul, Effect of antiplasticization on gas sorption and transport. I Polysulfone, *J. Polym. Sci. B: Polym. Phys.,* **1987**, 25, 957-980.
11. Y. Maeda, D. R. Paul, Effect of antiplasticization on gas sorption and transport. II Poly(phenylene oxide), *J. Polym. Sci. B: Polym. Phys.*, **1987**, 25, 981-1003.

12. Y. Maeda, D. R. Paul, Effect of antiplasticization on gas sorption and transport. III Free volume interpretation, *J. Polym. Sci. B: Polym. Phys.,* **1987**, 25, 1005-1016.
13. I. Pinnau, L. G. Toy, Gas and vapor transport properties of amorphous perfluorinated copolymer membranes based on 2,2-bistrifluormethyl-4,5 difluoro-1,3 dioxole/tetrafluoroethylene, *J. Membr. Sci.*, **1996**, 109, 125-133.
14. S. M. Nemser, I. C. Roman, Perfluorinated membranes, US Patent, **1991**, 5,051,114.
15. M. Macchione, J. C. Jansen, G. De Luca, E. Tocci, M. Longeri, and E. Drioli, Experimental analysis and simulation of the gas transport in dense Hyflon® AD60X membranes: Influence of residual solvent, *Polymer*, **2007**, 48, 2619-2635.
16. V. Arcella, P. Colaianna, P. Maccone, A. Sanguineti, A. Gordano, G. Clarizia, E. Drioli, A study on a perfluoropolymer purification and its application to membrane formation, *J. Membr. Sci*., **1999**, 163, 203-209.
17. R. S. Prabhakar, B. D. Freeman, I. Roman, Gas and vapor sorption and permeation in poly(2,2,4-trifluoromethoxy-1,3-dioxole-co-tetrafluoroethylene), *Macromolecules,* **2004**, 37, 7688-7697.
18. A. A. Gusev, F. Mueller-Plathe, W. F. van Gunsteren, U. W. Suter, Dynamics of small molecules in bulk polymers, *Adv Polym Sci*., **1994**, 116, 207-247.
19. I. Pinnau, Z. He, A.R. Da Costa, K. D. Amo, R. Daniels, Gas separation using organic-vapor-resistant membranes, US Patent **1992**; 6361583.
20. Solvay-Solexis, "Galden® HT Low-Boiling" Safety Data Sheets.
21. J. C. Jansen, M. Macchione, E. Drioli On the unusual solvent retention and the effect on the gas transport in perfluorinated Hyflon AD® membranes, *J Membr Sci.,* **2007**, 287, 132-137.
22. J. Crank, G.S. Park, Diffusion in Polymers, Academic Press, London, **1986**.
23. Insight II (400P+) software package (2004), Accelrys Inc., San Diego, CA, USA.
24. J. R. Maple, M. J. Hwang, T. P. Stockfish, U. Dinur, M. Waldman, C. S. Ewig, A. T. Hagler, Derivation of class II force fields. I. Methodology and quantum force field for the alkyl functional group and alkane molecules, *J Comput Chem*., **1994**, 15, 162-182.
25. D. N. Theodorou, U. W. Suter, Detailed molecular structure of a vinyl polymer glass, *Macromolecules*, **1985**, 18, 1467-1478.
26. D. N. Theodorou, U. W. Suter, Atomistic modeling of mechanical properties of polymeric glasses, *Macromolecules,* **1986**, 19, 139-154.

27. D. Hofmann, L. Fritz, J. Ulbrich, C. Shepers, M. Boehning, Detailed-atomistic molecular modeling of small molecule diffusion and solution processes in polymeric membrane materials, *Macromol Theory Simul*, **2000**, 9, 293-327
28. E. Tocci, D. Hofmann, D. Paul, N. Russo, E. Drioli, A molecular simulation study on gas diffusion in a dense poly(ether- ether- ketone) membrane, *Polymer,* **2001**, 42, 521-533.
29. T. A. Andrea, W. C. Swope, H. C. Andersen, The role of long range forces in determining the structure and properties of liquid water, *J Chem Phys*., **1983**, 79, 4576-4584.
30. H.J.C. Berendsen, J.P.M. Postma, W.F. van Gunsteren, A. DiNola, J.R. Haak, Molecular dynamics with coupling to an external bath, *J Chem Phys.,* **1984**, 81, 3684-3690.
31. A. R. Tiller, GSNET program, *Biosym Technologies*, **1993**; A. R. Tiller GSDIF program, *Biosym Technologies,* **1993**.
32. J. M. Haile, Molecular dynamics simulations, elementary methods, Wiley-Interscience, New York, **1992**.
33. F. Mueller-Plathe, S. C. Rogers, W. F. van Gunsteren, Computational evidence of anomalous diffusion of small molecules in amorphous polymers, *Chem Phys Lett.,* **1992,** 199, 237-243.
34. A. A. Gusev, S. Arizzi, U. W. Suter, D. J. Moll, Dynamics of light gases in rigid matrices of dense polymers, *J Chem Phys*., **1993**, 99, 2221-2227.
35. A. A. Gusev, U. W. Suter, Dynamics of Small Molecules in Dense Polymers Subject to Thermal Motion, *J Chem Phys*., **1993**, 99, 2228-2234
36. A. A. Gusev, U. W. Suter, D. J. Moll, Relationship between helium transport and molecular motions in a glassy polycarbonate, *Macromolecules,* **1995**, 28, 2582-2584.
37. A. A. Gusev, U. W. Suter, A model for transport of diatomic molecules through elastic solids, J Comput-Aided Mater, *Desalination,* **1993**, 1, 63-73.
38. H. A. Schneider, Conformational Entropy Contributions to the Glass Temperature of Blends of Miscible Polymers, *J Res Natl Inst Stand Technol,* **1997**, 102, 229-248.
39. T. J. Kwei, Effect of hydrogen bonding on the glass transition temperatures of polymer mixtures, *J Polym Sci Polym Lett.,* **1984**, 22, 307-313.

40. T. K. Kwei, E. M. Pearce, J. R. Pennacchia, M. Charton Correlation between the Glass Transition Temperatures of Polymer Mixtures and Intermolecular Force Parameters, *Macromolecules,* **1987**, 20, 1174-1176.
41. A. A. Lin, T. K. Kwei, A. Reiser, On the Physical Meaning of the Kwei Equation for the Glass Transition Temperature of Polymer Blends, *Macromolecules*, **1989,** 22, 4112-4119.
42. F. A. Ruiz-Treviño, D. R. Paul, A quantitative model for the specific volume of polymer-diluent mixtures in the glassy state, *J Polym Sci B Polym Phys.,* **1998**, 36, 1037-1050.
43. F. A. Ruiz-Treviño, D. R. Paul, Modification of polysulfone gas separation membranes by additives, *J. Appl. Polym. Sci*., **1997**, 66, 1925-1941.
44. F. A. Ruiz-Treviño, D. R. Paul, Gas permselectivity properties of high free volume polymers modified by a low molecular weight additive, *J. Appl. Polym. Sci*., **1998**, 68, 403-415.
45. T. G. Fox, Influence of diluent and copolymer composition on the glass transition temperature of copolymers, *Bull Am Phys Soc*., **1956**, 1, 123-135.
46. Solvay-Solexis, personal communication.
47. Y. Maeda, D. R. Paul, Effect of antiplasticization on selectivity and productivity of gas separation membranes, *J Membr Sci.*, **1987**, 30, 1-9.
48. Y. Maeda, D. R. Paul, Effect of antiplasticization on gas sorption and transport. I Polysulfone, *J Polym Sci B Polym Phys.,* **1987**, 25, 957-980.
49. Y. Maeda, D. R. Paul, Effect of antiplasticization on gas sorption and transport. II Poly(phenylene oxide), *J Polym Sci B Polym Phys*., **1987**, 25, 981-1003.
50. Y. Maeda, D. R. Paul, Effect of antiplasticization on gas sorption and transport. III Free volume interpretation, *J Polym Sci B Polym Phys.,* **1987**, 25, 1005-1016.
51. D. W. Van Krevelen,. Properties of Polymers, 3rd ed., Elsevier, Amsterdam, **1990**.
52. D. Hofmann, M. Entrialgo-Castano, A. Lerbret, M. Heuchel, Y. Yampolskii, Molecular Modeling Investigation of Free Volume Distributions in stiff chain polymers with conventional and ultra-high free volume: Comparison between Molecular Modeling and Positron Lifetime Studies, *Macromolecules,* **2003**, 36, 8528-8538.

53. European Commission 6th Framework Program Project MultiMatDesign "Computer aided molecular design of multifunctional materials with controlled permeability properties "Contract Number: NMP3-CT-2005-013644"
54. A. Alentiev, Yu Yampolskii, M. Vidyakin, A. Rusanov, A. Chalykh, 5th Intern. Symposium "Molecular mobility and order in polymer systems", St. Petersburg, **2005**, p.1

5. Analysis of the distribution of local free volume in Hyflon®AD membranes by photochromic probes.

5.1. Introduction

The search for novel polymeric materials with optimized combinations of gas permeability and permselectivity is an important challenge in membrane science. In many cases glassy polymers are the most useful materials for gas separation membranes because of their superior permeability- selectivity balance. Polymeric glasses are in a non-equilibrium state [1], with a continuous evolution towards equilibrium through spontaneous, but usually very slow, molecular rearrangements at temperatures far below the glass transition temperature, Tg. Since macroscopic properties of glassy polymers depend on their inefficiency of packing or free volume [2,3], a rational determination of relationship between chemical structure and transport parameters, such as permeability and diffusion coefficients, becomes important. The concept that free volume in polymer glasses is composed of local free volume elements of different sizes has a broad theoretical support [1-4]. Only recently more experimental data on the distribution of local free volume are gradually becoming available. Free volume in polymers can be determined by various methods, as already said in chapter 3, as PALS [5,6], IGC [7], ^{129}Xe-NMR [7] electrochromic [9], and spin probe [9] methods, but data on high free volume perfluorinated polymers are rather rare [10,11].

For Hyflon AD polymers only the total FFV, estimated by the group contribution method [12] and experimentally determined by ^{129}Xe-NMR spectroscopy [7] has been published in the literature. The reported FFV value of Hyflon®AD60X and Hyflon®AD80X of 23 %, poses these polymers near other high FFV polymers such as Teflon®AF 2400, 33%, and Teflon®AF1600, 30%, [13] and clarifies the reason of the high permeability of these polymers, significantly above for instance polysulfone membranes with a FFV ranging between 12-17 %, [14].

5.1.1. Theoretical background of the photochromic probe method

Photochromism of molecular probes is a phenomenon which is sensitive to the distribution of local free volume in polymer glasses [16]. Photochromic molecular probes in glassy polymer were first used by Gardlund [17]. Since then they have been successfully used in evaluating FV of various matrices including polycarbonate[18], polystyrene [19], epoxy resin [20,21] and other polymers. For this purpose, photochromic or photo-isomerizable molecules, usually stilbenes and azobenzenes, are dispersed homogenously into the polymer matrix. Upon irradiation with UV or visible light with the proper wavelength and/or upon heating, the photochromic molecules may undergo trans-cis isomerization and back. The crucial hypothesis, at the basis of this technique, is that photoisomerization in the glassy state requires a minimum, critical size of local free volume in the vicinity of the chromophore. This isomerization requires a certain amount of extra volume during the rotation of the molecule from the trans to the cis configuration [16] not only because the molecular volume of the cis and the trans isomers may be different, but also because the rotation itself requires some freedom of motion. This is schematically displayed in Figure 5.6. If this volume is available, i.e. if the photochromic molecule is located in a sufficiently large free volume element, then photoisomerization will occur, otherwise it will not, see Figure 5.1. This procedure thus allows the qualitative determination of the free volume distribution if a series of photochromic molecules is used which requires each a different volume for the trans-cis isomerization reaction. An important assumption is that the dye molecule does not influence the free volume itself and that it does not interact with the polymer matrix. Furthermore, the polymer chain dynamics must be sufficiently slow that there is no significant relaxation of the free volume elements on the time scale required to realize the trans-cis transition. In practice the amount of probe photoisomerization in a glassy polymer relative to that in dilute solution in a non-viscous model solvent, where free volume is not a constraint to isomerization, is measured as a function of the volume required for photoisomerization of the probe.

5.1.2. Perfluorinated polymers and free volume

Hyflon®AD polymers are amorphous perfluorinated copolymers of tetrafluoroethylene (TFE) and 2,2,4-trifluoro-5-trifluorometoxy-1,3-dioxole (TTD) (see chapter 1). In contrast

to the semi-crystalline PTFE, Hyflon®AD polymers are amorphous glasses with a modestly high Tg, as a result of the bulky TTD units in the polymer chain. These amorphous glassy PFPs, such as also those of the Teflon®AF family, are known for their high FFV [10] or high void fraction, which is the reason for their exceptional gas permeability [11,12].

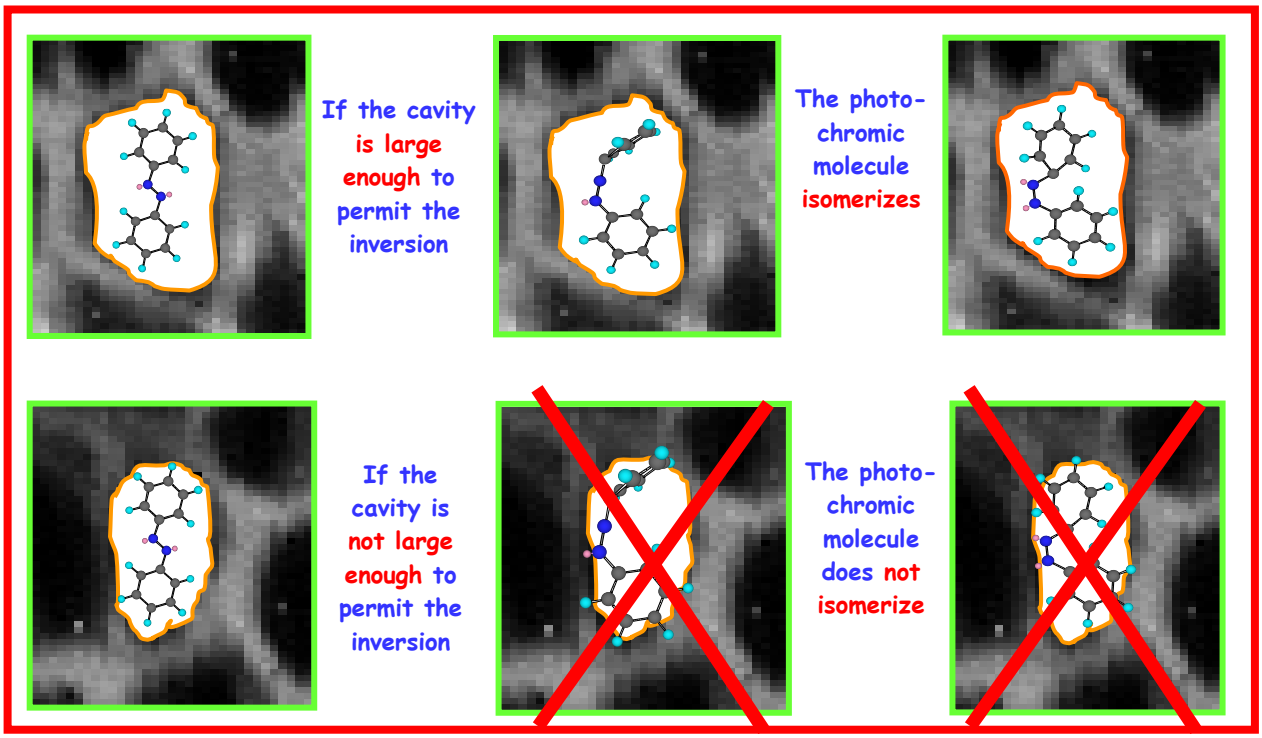

Figure 5.1. *Schematic representation of the photoisomerization of an AZB molecule in a cavity of local free volume of the membrane.*

The aim of this chapter of the thesis is to use the photochromic probe technique to obtain quantitative values of the size distribution of local free volume elements in Hyflon®AD 60X and Hyflon®AD80X. A total of six probes with different required isomerization volumes ranging from 127 $Å^3$ for azobenzene to 350 $Å^3$ for 3[N-Ethyl-4-(4-nitrophenylazo)-phenyl-amino]propionitrile (Disperse Orange 25) was used.

5.2. Experimental section

5.2.1. Materials

Hyflon® AD60X and Hyflon® AD80X (Solvay solexis), have glass transition temperatures of 130°C [22] and 134°C[23] respectively. Even in this study HFE 7100 was used as solvent

for Hyflon AD to prepare solution-cast films. Photochromic molecules were purchased from Aldrich and were used without further purification.

Figure 5.2 shows the molecular probes used in this study and Table 5.1 reports their physical properties. Dichloromethane (Carlo Erba Reagenti, DCM), used as received, was the solvent for the photochromic molecules.

Table 5.1. *Azobenzene and stilbene derivatives used as molecular probes in the present thesis.*

	Azobenzene derivatives[a)]		Stilbene derivatives[a)]	
	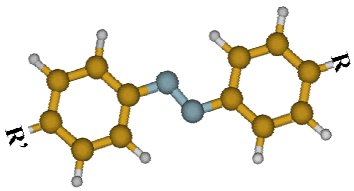		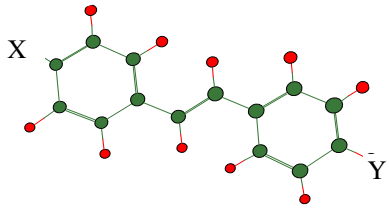	
	R	**R'**	**X**	**Y**
Azobenzene (AZB)	H	H	-	-
Stilbene (STIL)	-	-	H	H
Disperse orange 3 (DO3)	NO_2	NH_2	-	-
4, 4' dinitrostilbene (DNStil)	-	-	NO_2	NO_2
Disperse red 1 (DR1)	NO_2	$N(CH_2CH_3)CH_2CH_2OH$	-	-
Disperse orange 25 (DO25)	NO_2	$N(C_2H_5)CH_2CH_2CN$	-	-

a) Structures obtained by Molden Program.

5.2.2. Membrane preparation

The polymer solution was prepared as a 5 wt.-% solution of Hyflon® AD in HFE 7100 (0.25 g in 5.0 g of total solution). A $5.9 \cdot 10^{-3}$ M mother solution of trans isomer of the dye molecules was prepared separately in DCM. Photochromic solutions were prepared and stored in foil-wrapped flasks to avoid light exposition responsible for the photoisomerization. The photochromic polymeric solution was finally prepared by addition of 0.05 g of the dye solution to the Hyflon solution under rapid stirring. Photochromic dense Hyflon® AD membranes were made by the solvent evaporation method in a Petri dish. Evaporation of the solvent yielded completely transparent films. An AZB containing membrane is shown as an example in Figure 5.3.

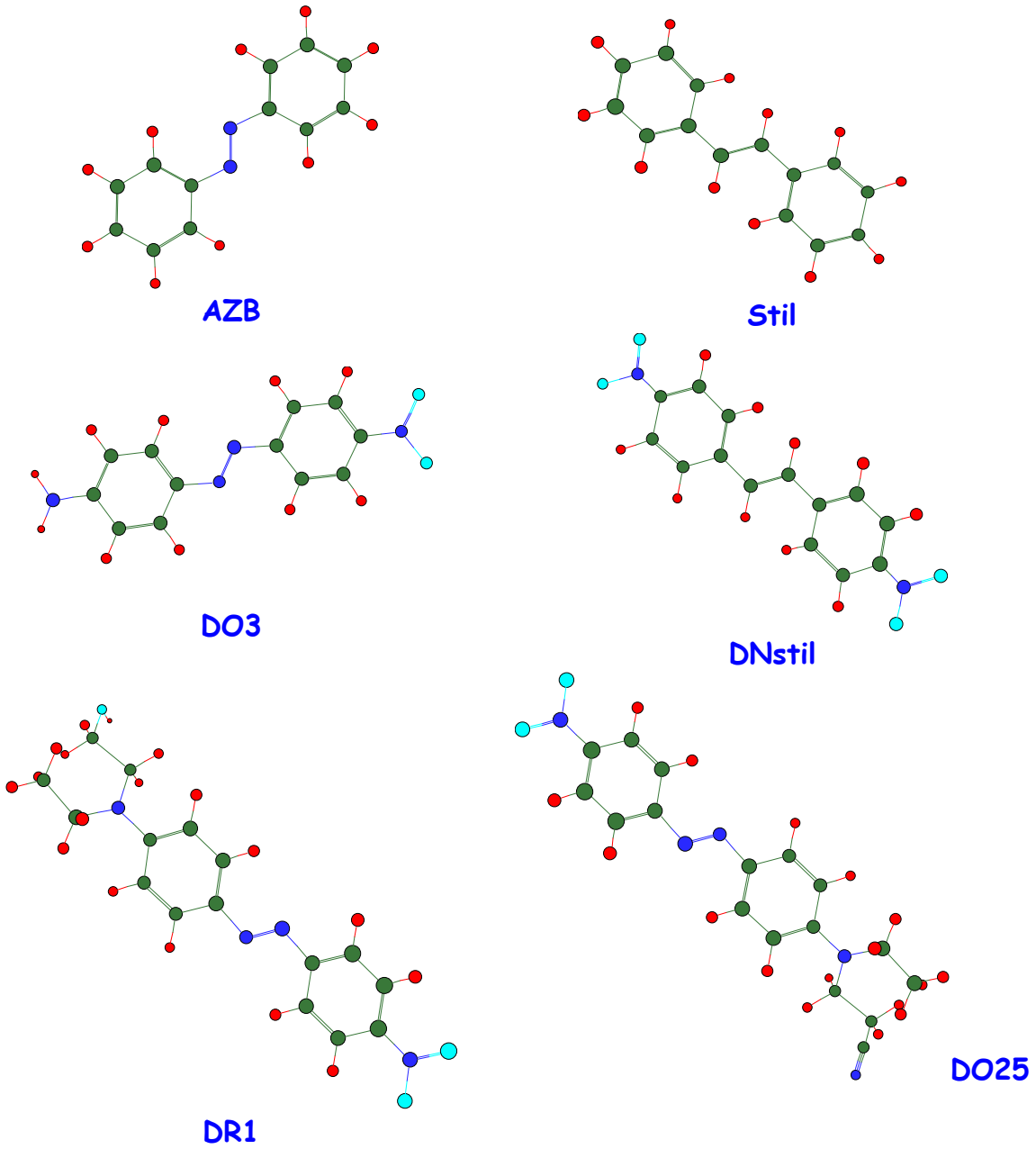

Figure 5.2. *Structures of photochromic probes used, obtained by ChemDraw 3D Pro, showing an impression of the differences in size.(red = H, green = C, blue = N, light blue = O)*

Films were first dried for at least 48 h at room temperature and then in a vacuum oven at 50 °C for 6 h. In all operations the exposure of the dyes to ambient light was minimized in order to prevent uncontrolled photo-isomerization. The resulting dye concentration in the membrane is 0.06 wt.-% based on the polymer dry weight. It is assumed that during evaporation of the solvent the rapidly increasing viscosity of the solution could immobilize the photochromic molecules, and that the dye concentration is sufficiently low to prevent

noticeable aggregation or crystal nucleation of the dye. A ternary phase diagram of Hyflon® AD60X, HFE 7100 and DCM was constructed according to the method described previously [23] by drop-wise addition of DCM to a Hyflon solution in HFE, in order to determine the maximum amount of DCM in the polymer solution without inducing phase separation. This amount (≥ 18%) was found to be well above the maximum DCM concentration in the casting solution (ca 1%) used for membrane preparation.

Figure 5.3. *Photograph of a dense azobenzene containing Hyflon® AD60X membrane.*

5.2.3. UV-Visible characterization

The trans-cis isomerization reaction (Figure 5.4) of all chromophores was realized by a UV Visible lamp (GRE 500W, Helios Italquartz) using a quartz filter (OptoSigma) for irradiation at 350 nm and the back reaction was induced by irradiation at 440 nm, using a blue glass filter (OptoSigma).

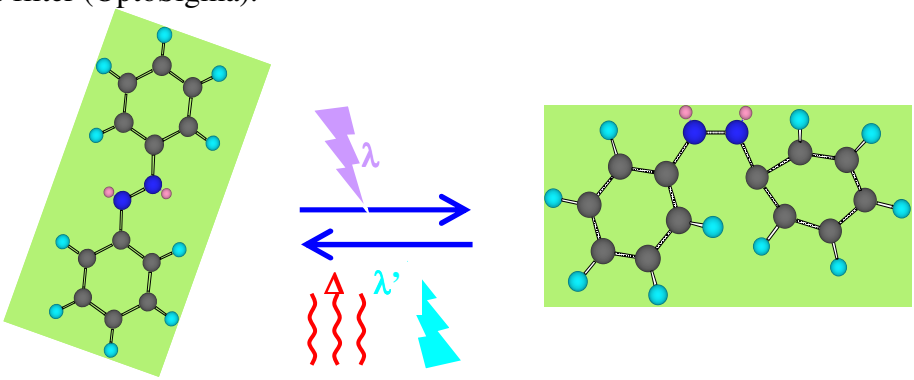

Figure 5.4.Azobenzene can be photochemically converted from the trans to the cis state, and will revert back to the stable trans state thermally. Alternately, the cis to trans conversion can be induced with a distinct wavelength of light.

Study of kinetics of the trans-cis photisomerization recommended an irradiation time of 15 minutes to have the maximum of photoconversion for all type of dyes; lamp to film distance was 15 cm. Band pass filters were placed directly onto the sample surface to avoid

irradiation of the films by unfiltered scattered light from the sides, which may compromise the efficiency of the photo-isomerization. Molar absorption coefficients, ε_{trans} and ε_{ciss}, of photochromic molecules dispersed in the polymer matrix at a concentration, C, were calculated by absorbance measurements, by using the Lambert-Beer law:

$$A = C \cdot \varepsilon \cdot d \tag{5.1}$$

where A is the value of the absorbance peak at the maximum absorption wavelength, λ, of the dye and d is the path length of the UV beam, i.e. the thickness of the membrane. All absorbance measurements were done at ambient temperature. The optical experiments were performed by means of a UV-Visible spectrophotometer (Mod. Shimadzu UV 1601), interfaced to a PC for the data recording and elaboration. The efficiency of trans-cis isomerisation in the films, i.e. the cis isomer fraction, Y, was determined by UV absorption spectroscopy, considering the isomerization in dilute solution as a reference (about 85%) [16], using the following equation:

$$Y = \frac{1 - A / A_{dark}}{1 - \varepsilon_{cis} / \varepsilon_{trans}} \tag{5.2}$$

where A_{dark} is the initial peak absorbance with only trans isomer present, A is the actual peak absorbance in the photostationary state and ε_{cis} and ε_{trans} are the molar absorption coefficients of the cis and trans isomers, respectively.

5.3. Results and discussion

5.3.1. Fractional Free Volume (FFV) by the group contribution method

The FFV of Hyflon AD was first calculated by means the following equation:

$$FFV = \left(\frac{V_{sp} - V_0}{V_{sp}} \right) * 100 \tag{5.3}$$

where V_{sp} is the specific volume of the membrane obtained by measurements of density [22], and V_0 is the occupied volume of the polymer. The occupied volume is generally calculated by the following empirical equation [14,25]:

$$V_0 = 1.3V_W \tag{5.4}$$

where V_w is the van der Waals volume which can be estimated by the groups contribution method described by Bondi [15]. This equation relates the zero point molar volume $V_0(0)$ to van der Waals volume V_w, *i.e.* the volume occupied by a molecule, impenetrable for other molecules. The calculation of V_w assumes a knowledge of bond distances, bond angles, and the contact distances, *i.e.* intermolecular van der Waals radii (r_w), from reliable X-ray diffraction data in the literature, and characteristic shapes of atoms in various molecular configurations. For calculating the van der Waals volume V_w of Hyflon AD polymers according to the procedure of Bondi, the data listed in the Table 5.2 were taken into account [15]:

Table 5.2. *Values of van der Waals molar volume of the groups present in Hyflon AD60X and Hyflon AD80X.*

Groups	V_w cm^3/mol	Bond Type
Oxygen	5.20	Heterocycloaliphatic ethers
C	3.33	sp^3 hybrid
CF_3	21.3	C sp^3 hybrid, F polyhalide of alkane
F	6.20*	Attached to alkane in secondary or tertiary positions
CF_2	14.33	Perhalide of alkane

**In a previous work [12], the value of Van der Waals molar volume of fluorine atoms was mis-interpreted because the F atoms were considered attached to alkane in primary positions.*

The group contribution method gives the van der Waals molar volume, V_w, of a polymer by means of the following expression [9]:

$$V_w = \Sigma n_i V_{wi} \tag{5.5}$$

In which n_i is the number of each specific group present and V_{wi} is its van der Waals volume which is listed in Table 5.2. According to this, we obtained the values of V_w listed in Table 5.3:

Table 5.3. *Values of van der Waals molar volume of the comonomers present in Hyflon AD60X and of Hyflon AD80X.*

	V_w cm^3/mol	N of monomer in 1 mol n_i
TTD	65.09	
TFE	30.66	
Hyflon AD60X	51.32	0.6TTD + 0.4TFE
Hyflon AD80X	58.20	0.8TTD + 0.2TFE

and substituting in Eq. (6.4) we obtain $V_0\ (0)$= 1.3*51.32 = 66.716 cm^3/mol for Hyflon® AD60X and $V_0\ (0)$= 1.3*58.20 = 75.660 cm^3/mol for Hyflon® AD80X.

The density of a dense Hyflon® AD60X membrane, obtained by melt pressing of the polymer powder, was measured experimentally according the buoyancy procedure and was found to be equal to 1.917 ± 0.012 g/cm^3 [22]. Instead, the density of a dense Hyflon® AD80X membrane was found in literature [23] to be equal to 1.92 g/cm^3. Substituting the experimental values of V_{sp}, in Eq. (6.3) we obtained a *FFV* of 23 % for Hyflon® AD60X.

Since experimental evaluation of Hyflon® AD80X density was not carried out by us, the value of V_{sp} is not available, even though literature data [23] report the value of 23% also for *FFV* of Hyflon® AD80X.

5.3.2. Membrane preparation and phase diagram

Dissolving photochromic dyes in the perfluorinated matrix was the most critical step in the membrane preparation. Indeed, no common solvents exist for the hydrocarbon photochromic dye and the perfluorinated polymer Hyflon®AD. This could compromise dramatically the possibility to prepare a stable homogeneous solution. Also the solid polymer is normally incompatible with the hydrocarbon photochromic dyes. Both problems were overcome by the use of a solvent mixture and very low dye concentrations.

Solubility tests and the ternary phase diagram of the system polymer/DCM/HFE7100 demonstrated that a 10 wt.-% Hyflon solution may contain at least 18 wt.% of DCM without

inducing phase separation. In practice much lower DCM concentrations are reached during the membrane preparation procedure and thus DCM does not compromise the polymer solubility. In addition DCM is also very volatile, so it will evaporate together with HFE7100.

5.3.3. Progress of the photoisomerization reaction.

Strictly, 'azobenzene' refers only to the parent molecule, although the term is frequently used to refer to the entire class of substituted azobenzene derivatives with different substituents and functional groups. The common characteristic of the azobenzene molecules is the clean and efficient photochemical isomerization that can occur about the azo linkage when the chromophore absorbs a photon. The two states are a thermally stable trans, and a meta-stable cis configuration. The cis configuration will then typically relax thermally back to the trans state with a lifetime that depends sensitively upon the particular azo's substitution pattern, as well as on local conditions, see Chapter 3.

Irradiation of the cis form with light within its absorption band can also induce the photochemical cis-to-trans isomerization (Figure 5.4). The extent of the photoisomerization, i.e. the maximum of the trans-cis conversion, depends strongly on the time of exposure at UV light. It is therefore very important to set the proper time of irradiation. For this purpose photochromic Hyflon® AD membranes were irradiated at different times (5, 10, 15, 20 min) and for each time of irradiation, a UV spectrum was recorded. Generally the maximum absorbance was reached within 15 min of irradiation. Figure 5.5 shows, as examples, the absorbance spectra of the Hyflon® AD80X membranes containing AZB (left) and DO25 (right) after irradiation for 15 min. It is evident how the extent of the photoisomerization strongly depends on the size of photochromic molecule. At room temperature the back reaction in the films was sufficiently low to allow normal manipulation and characterization of the film. No significant isomerization occurred for the entire duration of the spectroscopic analysis and the permeability measurements.

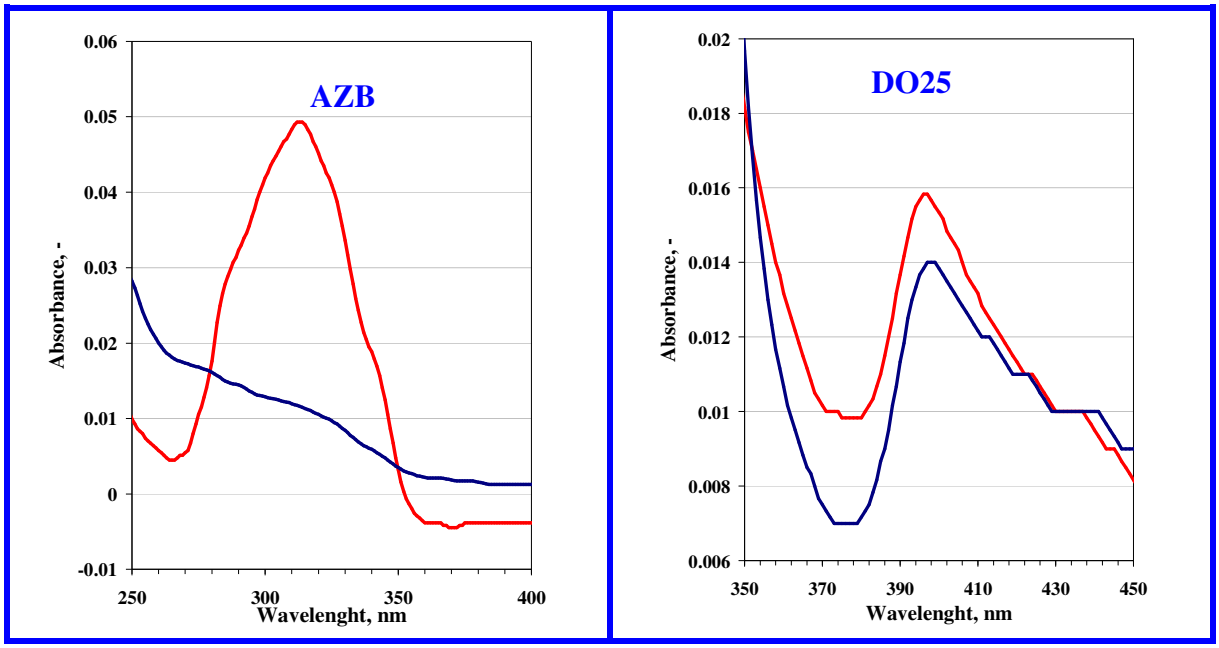

Figure 5.5. *Absorption spectra of azobenzene and DO25 dispersed in Hyflon membranse, before (red curve) and after (blue curve) photoirradiation at 350 nm for 15 min.*

5.3.4. Determination of molar absorption coefficients

Lambert-Beer's law (or Beer's law) is the linear relationship between absorbance and concentration of an absorbing species. The general Lambert-Beer's law is usually written as Eq. (5.1). The length of the light path (thickness of the membrane) and the extinction coefficient (ε) determine the slope of the linear plot of A versus C. The Lambert-Beer Law however is valid only for diluted solutions. The limits for its validity differ for different materials. As a general rule, every material showing absorption of/up to 0.5 - 0.6 still obeys the Lambert-Beer Law. In the case of the dyes dispersed in Hyflon membranes their low concentration ensures the validity of Beer's law. Molar absorption coefficients of cis and trans isomers were calculated in Hyflon® AD membranes, while, as said above, the commonly used efficiency of isomerization in dilute solution of about 85% [16] was considered as reference.

Indeed, the cis isomer of some molecular probes in solution is not sufficiently stable to allow the recording of the spectrum. For probes in Hyflon membranes, molar absorption coefficients were very difficult to measure as well; part because of the variation in the film thickness part because of small loss of probe during film drying. This problem was also observed by other researchers who carried out the same type of experiments [16]. Table 5.4

is an overview of the characteristics of photochromic membranes in terms of their spectroscopic properties.

Table 5.4. *Wavelength of peak absorbance of probe molecules, absorbance values of photochromic membranes and $\varepsilon_{cis}/\varepsilon_{trans}$ ratio in membranes.*

	Wavelength nm	Absorption peak in Hyflon® AD60X		Absorption peak in Hyflon® AD80X		$\varepsilon_{cis}/\varepsilon_{trans}$	
		Before irradiation	After irradiation	Before irradiation	After irradiation	Hyflon® AD 60X	Hyflon® AD 80X
azobenzene	310	0.05	0.016	0.05	0.012	0.050	0.050
stilbene	290	0.046	0.018	0.07	0.0224	0.151	0.147
Disperse orange 3	460	0.062	0.039	0.059	0.029	0.183	0.181
4, 4' dinitrostilbene	310	0.034	0.03	0.121	0.082	0.245	0.238
Disperse red 1	510	0.0525	0.051	0.097	0.085	0.456	0.401
Disperse orange 25	395	0.012	0.011	0.015	0.0143	0.354	0.352

5.3.5. Determination of the total volume of photochromic molecules

A probe molecule has an associated van der Waals volume which represents the volume occupied by the molecule, impenetrable for other molecules. This volume can be calculated using van der Waals radii tabulated by Bondi [15]. The extra volume needed by a dye molecule to isomerize is the volume swept by the van der Waals area, see Figure 5.6. Trans azobenzene and stilbene are planar molecules. In the case of azobenzene and AZB derivatives during the inversion the phenyl is swept trough a total angle of 114° and twists 30° to assume the equilibrium conformation of the cis isomer [16,26] The volume required for isomerization consists of two components: phenyl ring twist and the volume swept by the area comprised of the product of the phenyl thickness and the length. In the case of stilbene and stilbene derivative, upon irradiation, one of the central carbons twists 90° to the geometry of the excited state. The double bond disappears allowing rotational diffusion about a single C-C bond [16,27,28]. The van der Waals volume of photochromic molecules used in this work and the extra volume needed to isomerize are reported in Table 5.5.

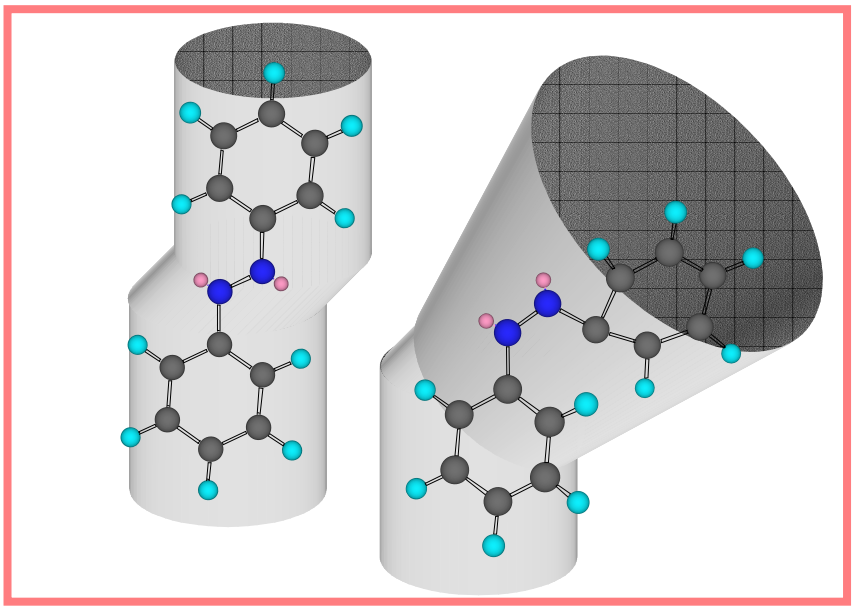

Figure 5.6. *Schematic representation of the volume occupied by a probe molecule (left) and extra volume needed to isomerizes (right).*

Table 5.5. *van der Waals volume of photochromic probes and extra volume needed to isomerize*

	Volume of the molecule, Å^3	Volume extra to isomerize, Å^3	Total volume[b)], Å^3
azobenzene	144[a)]	127[a)]	271
stilbene	151[a)]	222[a)]	373
Disperse orange 3	171	250	421
4, 4' dinitrostilbene	187[a)]	262[a)]	449
Disperse red 1	207	310	517
Disperse orange 25	224	350	574

[a)] Found in the literature [16]. [b)] The sum of the van der Waals volume of the molecule and the extra volume

5.3.6. Determination of local free volume distribution

The size distribution of free volume elements can be derived from the degree of isomerization from the trans- to the cis-isomer. The ratio of cis isomer fraction in film and cis isomer fraction in solution gives a quantitative measurement of the efficiency of photoisomerization for each phototchromic probe. Figure 5.7 shows the dye cis film/cis solution ratio as a function of the total isomerization volume of dye molecules defined as in

Table 5.5. In Hyflon® AD60X the size of free volume elements ranges from about 250-520 Å^3 while in Hyflon® AD80X from ca. 380-600 Å^3. This means that, if we assume to be spherical the shape of the membrane cavities, the averaged value of radii ranges between 3.9 and 5.0 Å in Hyflon® AD60X and between 4.5 and 5.2 Å in Hyflon® AD80X. These values are in agreement with the results obtained by Golemme *et al.* who obtained 6 Å for Hyflon® AD60X and 6.12 Å for Hyflon® AD80X, by ^{129}XeNMR [8] The results clearly reveal that Hyflon AD80X membranes possess bigger local free volumes than Hyflon AD60X. This can explain the higher gas permeability of Hyflon AD80X, otherwise hardly to understand since the two grade of Hyflon AD have equal Fractional Free Volume (FFV) and density.

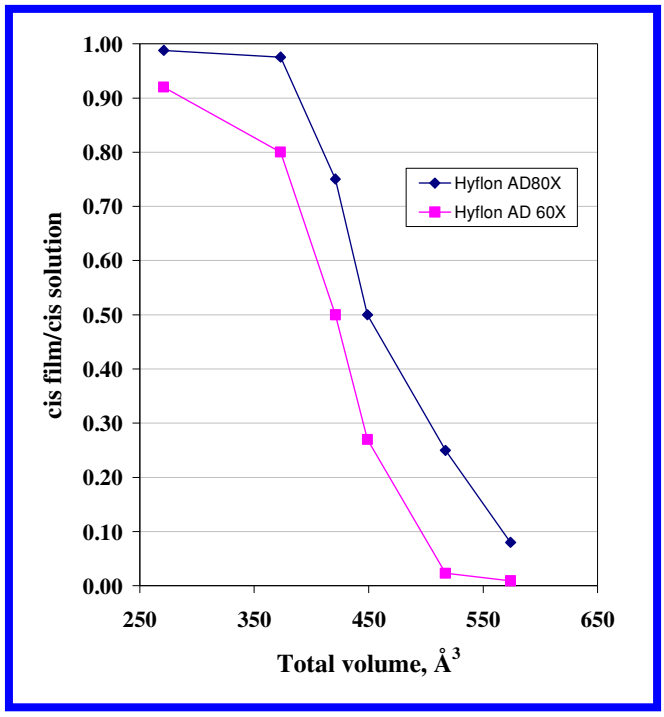

Figure 5.7. *Ratio of the cis isomer in the film and the cis isomer in solution as a function of the total isomerisation volume in Hyflon AD membranes.*

5.4. Conclusions

In spite of some limitations the photochromic probe method is a suitable method to obtain semi-quantitative information of the free volume distribution in Hyflon AD polymers. The main limitations consist in the uncertainly of the isomerization efficiency in solution, generally assumed to be 85 % [16] and the relative inaccuracy in the determination of the

molar absorption coefficient of the least stable isomer in solution. Furthermore the method assumes that the dye molecules do not interfere with the polymer matrix and that no aggregation occurs. Especially the first assumption may not always be true (see chapter 6).

Nevertheless the method describes with success the higher FV size in Hyflon®AD80X compared to Hyflon®AD60X.

References

1. Huang, Y.; Paul, D. R., Physical aging of thin glassy polymer films monitored by gas permeability *Polymer*, **2004**, *45,* 8377–8393
2. Robertson, R. E., Segmental Mobility in the Equilibrium Liquid below the Glass Transition, *Macromolecules* **1985**, *18*, 953-958.
3. Chow, T. S., Kinetics of Free Volume and Physical Aging in Polymer Glasses, *Macromolecules* **1984**, *17*, 2336-2340.
4. Curro, J. G.; Lagasse, R. R.; Simha, R., Diffusion Model for Volume Recovery in Glasses, *Macromolecules* **1982**, *15*, 1621-1626.
5. Shrader, D. M.; Jean, Y. C. *Positron and positronium chemistry*; Elsevier; Amsterdam, 1988.
6. Dlubek, G.; Clarke, A. P.; Fretwell, H. M.; Dugdale, S. B.; Alam, M. A., *Phys. Stat. Sol. A,* **1996**, *157*, 351.
7. Yampolskii, Y. P.; Kaliuzhnyi, N. E.; Durgaryan, S. G., *Macromolecules* **1986**, *19,* 846.
8. Golemme, G.; Nagy, J. B.; Fonseca, A.; Algieri, C.;. Yampolskii, Y., ^{129}Xe-NMR study of free volume in amorphous perfluorinated polymers: comparsion with other methods, *Polymer* **2003**, *44*, 5039-5045.
9. Yampolskii, Y. P.; Shantarovich, V. P.; Chernyakovskii, F. P.; Kornilov, A. I.; Plate, N. A., Estimation of free volume in poly(trimethylsilyl propyne) by positron annihilation and electrochromism methods, *J Appl Polym Sci* **1993**, *47*, 85-92.
10. Alentiev A.Yu., Yampolskii Yu.P., Shantarovich V.P., Nemser S.M., Platé N.A., High transport parameters and free volume of perfluorodioxole copolymers, *J Membr Sci* **1997**; 126: 123-132.
11. Merkel T.C., Pinnau I., Prabhakar R., Freeman B.D., Gas and vapor transport properties of perfluorpolymers, in Yampolskii Yu, Pinnau I and Freeman BD (Eds.), Materials science of membranes for gas and vapor separation, Chichester, England, John Wiley & Sons, 2006 (chapter 9).
12. Arcella, V., Colaianna, P., Maccone, P., Sanguineti, A., Gordano, A., Clarizia, G., Drioli, E.. A study on a perfluoropolymer purification and its application to membrane formation, *J. Membr. Sci*. **163**, 203-209 (1999).

13. Prabhakar, R. S., Freeman, B. D., Roman, I. Gas and Vapor sorption and permeation in poly(2,2,4-trifluoromethoxy-1,3-dioxole-co-tetrafluoroethylene),*Macromolecules,* **2004**, 37, 7688
14. Hu, C.-C.; Chang, C.-S.; Ruaan, R.-C.; Lai, J.-Y., Effect of free volume and sorption on membrane gas transport, *J. Membr. Sci*., **2003**, 226, 51-61.
15. A. Bondi, *J. Phys. Chem.*, **1964**, 68, 441-451.
16. Victor JG, Torkelson JM. On measuring the distribution of local free volume in glassy polymers by photochromic and fluorescence techniques, *Macromolecules,* **1987**, 20, 2241-2250.
17. Gardlund, Z. G.,*J. Polym. Sci., Polym. Lett. Ed*. **1968**, B6, 57.
18. I. Mita, K. Horie, K. Hirao, *Macromolecules,* **1989**, 22, 558.
19. C. S. P. Sung, I. R. Gould, N. J. Turro, *Macromolecules,* **1984**, 17, 1447.
20. M. Ueda, H. B. Kim, T. Ikeda, K. Ichimura, *Chem. Mater.*, **1992**, 4, 1229.
21. M. Ueda, H. B. Kim, T. Ikeda, K. Ichimura, *J. Non-Cryst. Solids,* **1993**, 163, 125.
22. Macchione, M., Jansen, J.C., De Luca, G., Tocci, E., Longeri, M., Drioli, E., Experimental analysis and simulation of the gas transport in dense Hyflon® AD60X membranes. Influence of residual solvent, *Polymer,* **2007**, 48, 2619-2635.
23. Yu. Yampolskii, I. Pinnau, B. D. Freeman, "Materials Science of Membranes" Wiley, NY, **2007**.
24. J.C. Jansen, M. Macchione and E. Drioli, High flux asymmetric gas separation membranes of modified poly(ether ether ketone) prepared by the dry phase inversion technique, *J. Membrane Sci.,* **2005**, 255, 167-180.
25. Park JY, Paul DR. Correlation and prediction of gas permeability in glassy polymer membrane materials via a modified free volume based group contribution method, *J Membr Sci.,* **1997**, 125, 23-39.
26. Traetteberg M., Hilmo I., Hagen K., *J. Mol. Struct.*, **1977**, 39, 231.
27. Orlandi G., Siebrand W., *Chem Phys. Lett*., **1975**, 30, 352.
28. Birks J.B., *Chem. Phys. Lett*., **1976**, 38, 437.

6.

Smart light-switchable Hyflon®AD membranes

6.1. Introduction

Nowadays, a significant part of all industrial processes is still carried out using thermally-driven methods. It is estimated that over an order of magnitude reduction in energy use can be achieved by replacing thermally driven processes with membrane processes that can operate at room temperature [1].

One of the main challenges in the search for new membranes with improved performance for increasingly demanding applications is the development of smart membranes with tunable permeability and selectivity [1]. Photochromic membranes offer the possibility to achieve this goal. Their principle is based on strong structural changes of the photochromic molecules upon photo-isomerization, as described in the previous chapter. In porous materials such as zeolites [2], meso- [3] or nanoporous films [4] the tuning of transport properties may be based on steric effects, if one of the isomers of the dye molecule partially obstructs the pores. In liquid processes differences in permeability can be induced by a change of electrostatic repulsion [5] and degree of swelling [6] of the membrane material upon photoisomerization of the attached photochromic molecules.

Gas separation, subject of numerous reviews [7-10] and forecasts [11-13], is one of the applications where membranes might have a major impact. Intelligent dense polymeric membranes require that the bulk polymer properties change by external stimuli in order to have effect on the permeability. For this application the photochromic molecules may be either attached to the polymer chain or dispersed in the material bulk [14,15] but the latter is reported to have no effect on the permeability [15]. Kameda et al. suggest that photoinduced plasticization may be responsible for permeability modulation in azobenzene functionalized glassy polymer films [14]. The dye concentrations are usually quite high, up to 30 wt.-% in the free dispersion or 60 wt.-% when covalently linked to the polymer backbone [15].

However, reported effects on the transport of light gases are very small, generally not more than about 10 percent [14]. In studies on the determination of the free volume

distribution in glassy perfluorinated Hyflon® AD membranes [16], it has been found by complete surprise that dissolved azobenzene causes unprecedented changes in the permeability upon trans-cis photoisomerization, even at extremely low concentrations of only 0.06 wt.-%.

6.2. Experimental

6.2.1 Photochromic membrane preparation

Photochromic membranes of Hyflon®AD60X and Hyflon®AD80X were prepared according to the method already described in par. *5.2.2*.

6.2.1.1 Phase diagram

A ternary phase diagram of Hyflon® AD60X, HFE 7100 and DCM was constructed according to the method described previously [17] by drop-wise addition of DCM to a Hyflon solution in HFE, in order to determine the maximum amount of DCM in the polymer solution without inducing phase separation.

6.2.1.2 Preparation of reference membranes

Reference membranes for each polymer without photochromics were prepared under exactly the same conditions. These identical conditions are essential in order to avoid differences in the sample history, which may have a strong influence on the gas transport properties [18]. Furthermore, in order to verify the potential effect of DCM as a cosolvent on the gas transport properties of the final membranes, a series of dense Hyflon® AD60X membranes was prepared by casting the polymeric solution, composed of HFE 7100, different amounts of DCM and Hyflon® AD60X. All the membranes were further dried at room temperature over night to remove the solvents.

6.2.2 Photoisomerization and spectroscopic analysis

Membranes were irradiated with a UV Visible Zh type lamp, (GRE 500W, Helios Italquartz) and the proper wavelengths were selected by band pass filters (OptoSigma). The trans-cis isomerization reaction was realized by irradiation at 350±10 nm, using a quartz filter, and the back reaction was induced by irradiation at 440 nm, using a blue glass filter.

The irradiation time was 15 minutes and the lamp to film distance was 15 cm. Band pass filters were placed directly onto the sample surface to avoid irradiation of the films by unfiltered scattered light from the sides, which may compromise the efficiency of the photo-isomerization. Under the given conditions the temperature increase of the sample was limited to a few degrees centigrade. Irradiated membrane samples were always kept in the dark until the UV spectroscopic analysis and the gas permeation measurements.

UV spectra of the solid films were recorded by a Shimadzu UV-1601 spectrophotometer. A membrane without photochromic dye, prepared under identical conditions, was placed in the reference beam.

6.2.3 Permeation measurements

Gas permeability was determined according the already described procedure [17] (see chapter 4), in a fixed volume-pressure increase instrument, constructed by GKSS (Germany). The diffusion coefficient was determined by the time lag method and the gas solubility was calculated from the steady state permeability and the diffusion coefficient according to Eq. (1.13). The UV spectrum was recorded before and after the gas permeation measurement, in order to check that no spontaneous or thermal isomerization occurred during the permeation measurements. The experimental error in the time lag and permeation measurements is less than about 5-10%. The time lag for He and H_2 in a 34 micron film is too short to be determined with the present setup, which has an instrumental time lag of approx. 0.05 s. Therefore also He and H_2 solubility could not be determined.

6.3. Results and discussion

6.3.1 Photochromic membrane preparation

As already anticipated in the previous chapter, a quite difficult task, successfully faced in this thesis, has been the dissolution of the photochromic dye in the perfluorinated matrix. In polymers such as polystyrene [19], poly(methyl methacrylate) [20], polycarbonate and poly(vinyl acetate) [21] this is usually straightforward since it is possible to use the same solvents for both polymer and dye molecule. However, no common solvents exist for the hydrocarbon AZB and stilbene dye at the one hand and perfluorinated polymers at the other hand. This compromises dramatically the possibility to prepare a stable homogeneous solution. Also the perfluorinated polymer is macroscopically incompatible with the hydrocarbon photochromic dyes. Both problems were resolved elegantly with the use of a solvent mixture and very low dye concentrations of only 0.06 wt.-%. The polymer was dissolved in a partially fluorinated solvent, methoxy-nonafluorbutane, which is fully miscible with DCM, a good solvent for all dyes used in this work. A homogeneous dye/Hyflon solution could be prepared by addition of a small quantity of a mother solution of the photochromic compound in DCM to the Hyflon solution in HFE under continuous stirring. The final DCM concentration was low enough to avoid phase inversion of the polymer. Solubility tests demonstrated that a 10 wt.-% Hyflon solution may contain up to 18 wt.% of DCM without inducing phase separation. Evaporation of the solvent yielded completely transparent colorless films.

During evaporation of the solvent the rapidly increasing viscosity of the solution could immobilize the photochromic molecules, and the dye concentration was sufficiently low to prevent noticeable aggregation or crystal nucleation.

6.3.2 Photoisomerization and spectroscopic analysis

The photochromic molecules were homogeneously dissolved in the polymer matrix in the most stable trans isomer. As an example, Figure 6.1 shows the typical absorption peak of azobenzene in Hyflon® AD60X around 300 nm. The membrane was prepared and the spectrum was recorded in dark conditions to avoid undesired conversion to the cis form.

Generally the trans-cis photoconversion in solutions occurs in few seconds of irradiation.

Unless the photochromic molecule is equipped with a flexible chain which provides a local rubbery environment [22], in a glassy polymer membrane a total irradiation time of several minutes is necessary for having the maximum of the photo-conversion because of the constraints of the polymer chains [19]. In our case at least 15 minutes of irradiation were applied to reach maximum conversion.

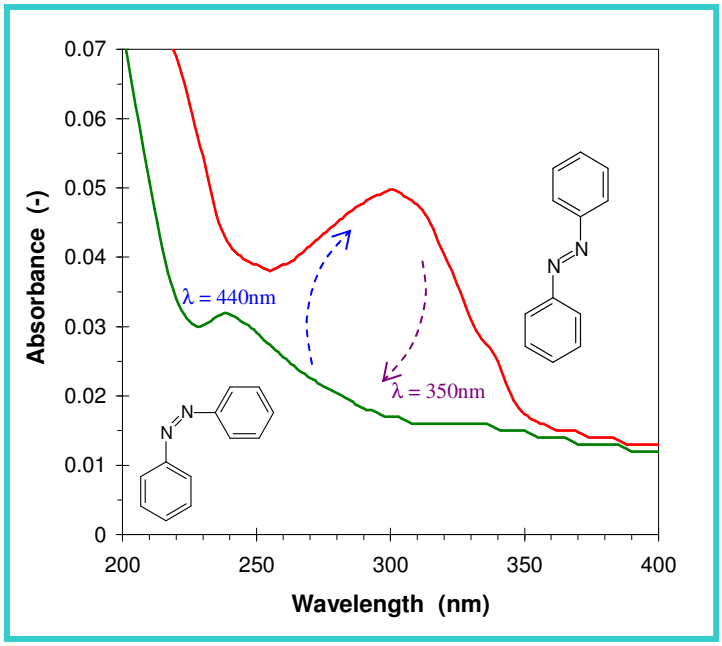

Figure 6.1. *UV spectra of a Hyflon® AD60X membrane containing 0.06 wt.-% of AZB before (red) and after (green) irradiation for 20 min at 350 nm. The original spectrum returns after irradiation with blue light of 440 nm. A film without AZB was used as the reference for the absorption measurements. This film is highly transparent for UV [23].*

Disappearance of the strong absorption peak around 300 nm witnesses the nearly complete conversion to the cis-isomer. The trans-cis isomerization efficiency of the dye in film varies depending on the type of photochromic compound and it can be calculated according to the method reported by Victor and Torkelson [19] (see chapter 5). The subsequent exposition of the membrane to blue light of 440 nm promotes the reverse cis-trans photo-isomerization and the return of the absorption peak. Several cycles of irradiation at 350 nm for the trans-cis conversion and at 440 nm for the reverse reaction were performed without loss in efficiency, indicating the complete reversibility of the process.

6.3.3 Permeation measurements

The effect that dispersing of photochromic dyes in the polymer matrix may cause on transport properties of membranes, can strongly depend both on the type of polymer and on the type of the dye itself. In our case, six different photochromic compounds were dispersed in two grades of Hyflon AD polymers: Hyflon®AD60X and Hyflon®AD80X.

Transport properties of both types of photochromic membranes were compared, while dye free Hyflon®AD60X and Hyflon®AD80X membranes with the same thermal history of the photochromic membranes were used as reference.

6.3.3.1 Photochromic membranes of Hyflon® AD60X

The permselectivity of Hyflon® AD60X membranes containing azobenzene, stilbene, disperse orange 3 and 4,4' dinitrostilbene was studied. Transport properties of photochromic membranes were also compared to those one of a dye free Hyflon® AD60X membrane. In general, in spite of the very low dye concentration, it is evident in Figure 6.2 that the mere addition of dyes in the polymer matrix is responsible for a weak change of the membrane permselectivity and this effect is more or less evident depending on the type of photochromic compound. Before irradiation with UV light, Hyflon membranes containing stilbene and 4,4' dinitrostilbene show selectivity for some gas pairs, higher than the fresh membrane without dye (HAD60X), whereas membranes containing AZB and AZB derivative (DO3) show a lower selectivity. On the other hand, the simple addition of photochromic compounds in the polymer matrix strongly affect also the gas permeability of membranes. Indeed, the dye containing Hyflon® AD60X membranes present a higher CO_2, He and O_2 permeability than the membrane without dye (HAD60X), see Figure 6.2. In particular, permeation of gases seems to be a little bit slower through stilbene and stilbene derivative containing membranes than the AZB and AZB derivative containing membranes.

The reason for this behaviour is not clear and is still subject of further investigations. In any case this is an interesting phenomenon, because it seems in contrast with the hypothesis that the dye molecules used for the free volume analysis do not influence the properties of the polymer matrix. To some extent it might also be related to slight differences in residual solvent in the different membranes, which was shown to have a marked effect on the transport properties. Therefore this will be studied in more detail.

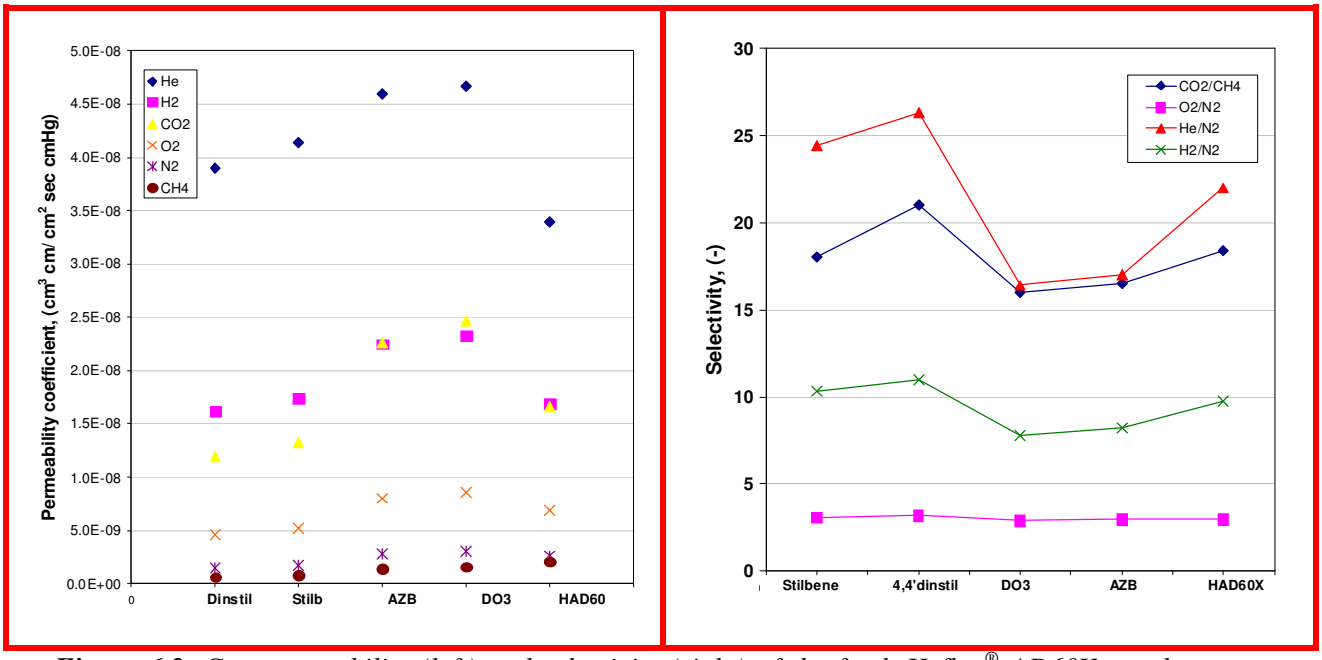

Figure 6.2. *Gas permeability (left) and selectivity (right) of the fresh Hyflon® AD60X membranes containing different photochromic compounds. Dye free membrane (HAD60X) prepared under the same conditions is reported as reference.*

Unfortunately, stilbene derivative containing membranes don't show a significant change in their transport properties after irradiation. This could be ascribed to the low photo-isomerization efficiency, *i.e.* low concentration of cis isomer in the polymer matrix. Indeed, stilbene and stilbene and AZB derivatives are too sterically hindered for a substantial trans to cis photo-conversion as confirmed previously in chapter 5.

6.3.3.2 Effect of photoisomerization on gas transport

An even more interesting aspect of these membranes is that the photoisomerization of the dye molecules may have a noticeable effect on the permeability, in spite of the very low dye concentration. This phenomenon was most clearly observed for the Hyflon® AD60X membrane with AZB dye (Figure 6.4)but is completely absent in the pure membrane without dye, see Figure 6.3. The Hyflon® AD60X membrane containing the AZB cis-isomer exhibits a five times higher CO_2 permeability than the membrane with the trans-isomer and a four times higher O_2 permeability (Figure 6.4, Table 6.2). The N_2 and CH_4 permeability increases less strongly, whereas only marginal differences are observed for He and H_2. The CO_2 and O_2 permeability of a freshly prepared membrane with the trans-isomer and the

same membrane after irradiation at 350 and 440 nm is displayed in Figure 6.4. The process is highly reproducible and reversible over various cycles, even after several months.

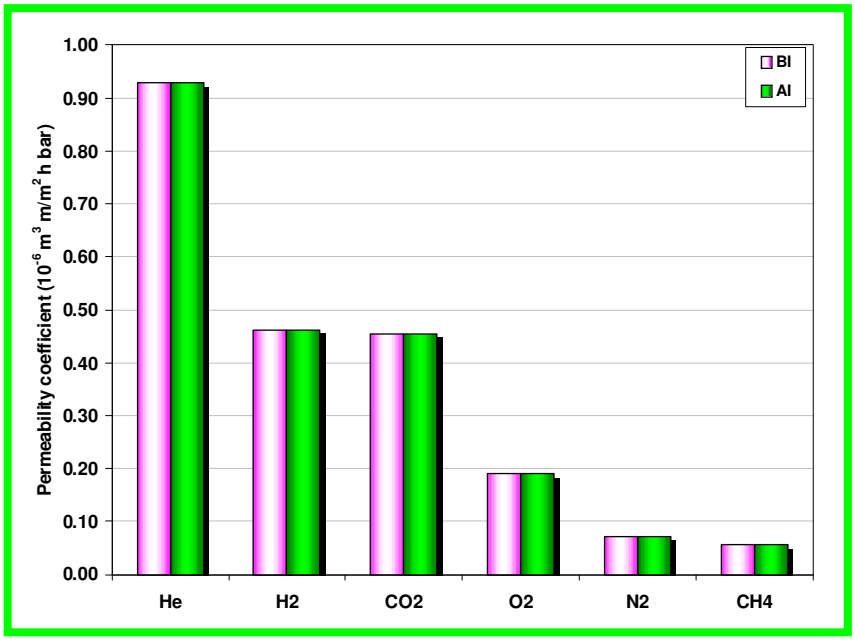

Figure 6.3. *Permeability coefficient of six pure gases in the Hyflon® AD60X membrane without azobenzene molecules before (BI) and after (AI) irradiation at 350 nm for 15 min..*

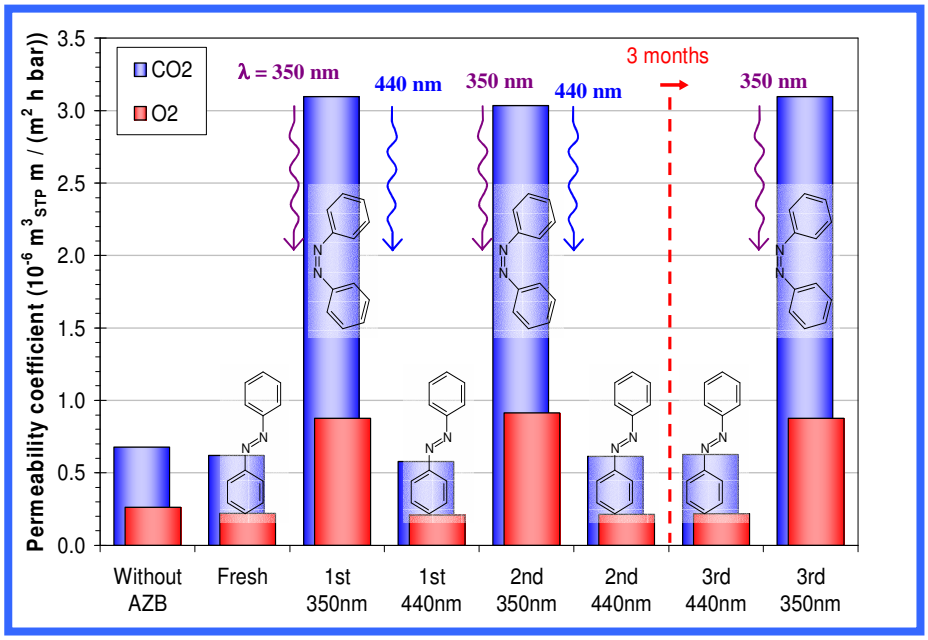

Figure 6.4. *Pure CO2 and O2 permeability coefficients of a fresh Hyflon AD60X membrane doped with AZB and of the same membrane after repeated irradiation at 350 nm and 440 nm. The isomerization reaction and the effect on permeability are completely reversible. A reference membrane without AZB has nearly the same permeability as a membrane with trans-AZB but its permeability is not influenced by UV irradiation (Figure 6.3).*

The effect of the cis-trans isomerization on methane is weaker than that on CO_2, resulting in a significant increase of the CO_2/methane permselectivity (Figure 6.5). Simultaneous increase of the CO_2 permeability and the permselectivity is quite unusual and pushes the performance of the membrane well beyond the famous 1991 Robeson upper bound. The unusual behavior of the membranes is also reflected in the CO_2/hydrogen gas pair. In glassy polymers the size-sieving normally dominates the separation process and the smaller species permeate more rapidly. Remarkably, the present membranes become selective for CO_2 over hydrogen in the presence of cis-AZB, suggesting that sorption selectivity dominates the separation process. In contrast to the present work, Weh and coworkers did not observe any UV-induced switching of the gas transport properties in PMMA in which AZB was physically dispersed, but only when it was chemically linked to the polymer backbone [19]. In addition, they used much higher amounts of AZB and their effects were much weaker. The most remarkable aspect of the work, besides the phototunability of the permeability as such, is the extremely low concentration of the photochromic molecule responsible for a so prominent effect. The precise origin of this phenomenon is not yet understood and is still under evaluation. As a first step the individual contributions of the gas diffusivity and solubility have been evaluated.

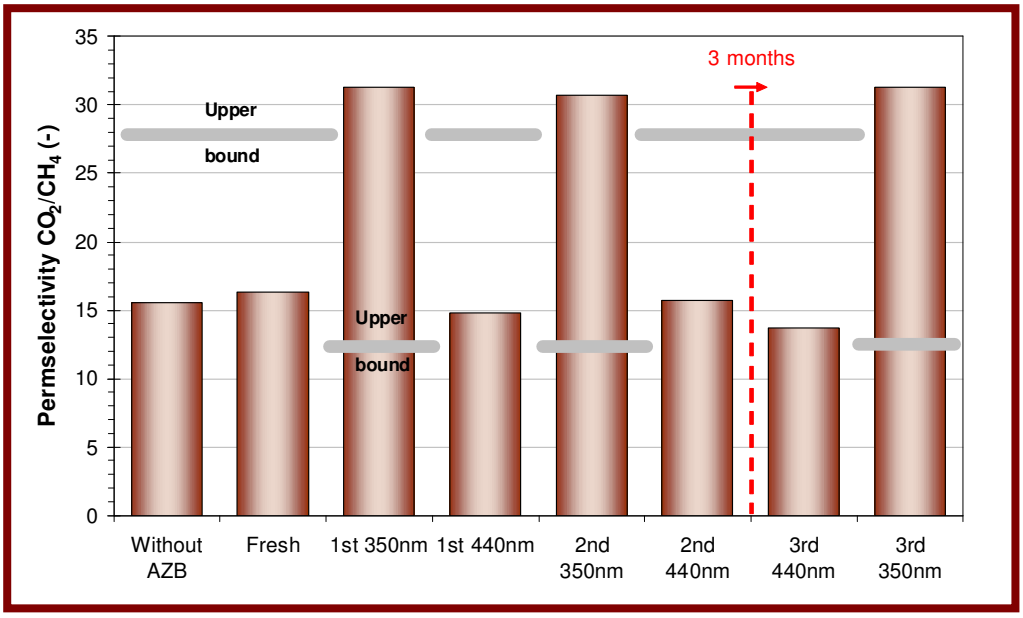

Figure 6.5. *Ideal CO_2/CH_4 selectivity of the same membranes of Figure 6.4. The horizontal lines indicate the selectivity according to the Robeson upper bound [24] at the given CO_2 permeability. The membrane with cis-AZB is clearly located far beyond the Robeson upper bound.*

6.3.3.3 Diffusion and solubility of AZB containing Hyflon® AD60X membrane

A common procedure to determine the diffusion coefficient from permeation data is the time lag method, based on the penetration theory [25]. The time lag, Θ, depends on the penetrant's diffusion coefficient according to Eq. (1.19).

The time lag can be determined for instance from the pressure increase curve in a fixed volume setup, as described previously [17]. Measurement of the membrane thickness then allows for the calculation of the diffusion coefficient. In turn, the gas solubility can then be calculated from the diffusion coefficient and the steady state permeability according to Equation (6.1). Two experimental pressure increase curves for CO_2 after irradiation at 350 nm and after irradiation at 440 nm are given in Figure 6.6. The steady state pressure increase rate is much higher in the presence of the cis-isomer of AZB than in the presence of the trans-isomer. On the other hand, the time lag, and thus the diffusion coefficient, is nearly identical for both samples. The same is true for oxygen, which shows very similar behavior (not shown here).

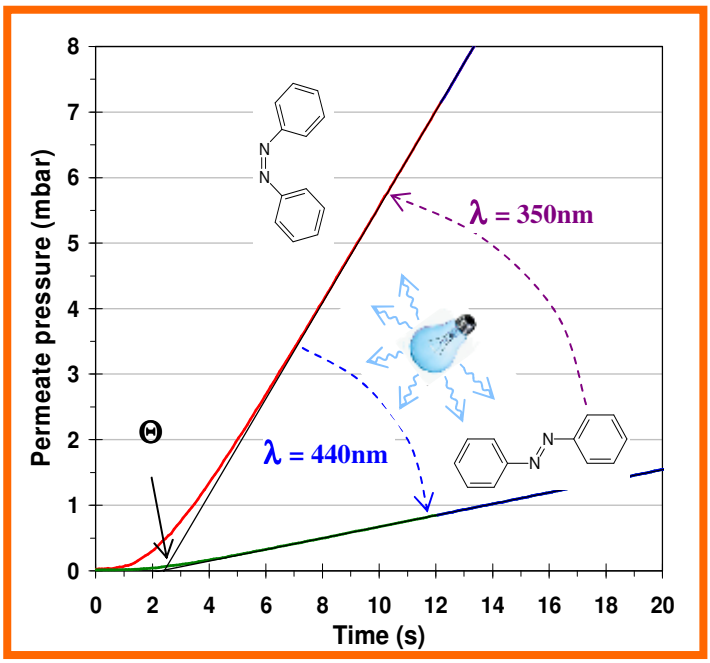

Figure 6.6 *Pressure increase curves of CO_2 permeation as a function of time and irradiation. The sample with the AZB cis-isomer exhibits a much higher pressure increase rate but a nearly identical time lag as the sample with the trans-isomer. Tangents are obtained from a linear least squares fit of the steady state section of the curve.*

So far this is in agreement with the assumption that the size of local cavities of the membrane does not change with the photoisomerization reaction of the dye molecule. [26,16]. In this case the increased permeability upon trans-cis isomerization must be attributed almost entirely to the enhanced solubility of the gas in the polymer matrix. The exact mechanism is still subject of further studies but it seems evident that the change in gas solubility is related to the much higher dipole moment of the cis-isomer than that of the trans isomer, 3.1 Debye against 0.5 Debye, respectively [27,28]. The situation is much more complicated for nitrogen and methane. A freshly prepared sample shows a normal time lag curve for methane permeation, but after irradiation at 350 nm it presents very unusual behavior (Figure 6.7). Permeation starts instantaneously, evidenced by the high initial slope of the permeation curve. This suggests ultra-rapid diffusion through micro- or nanoscale channels or through large, interconnected free volume elements. A weak 'kink' in the curve indicates that part of the flux still occurs according to the solution-diffusion mechanism, with a typical time lag very close to that of the polymer before irradiation.

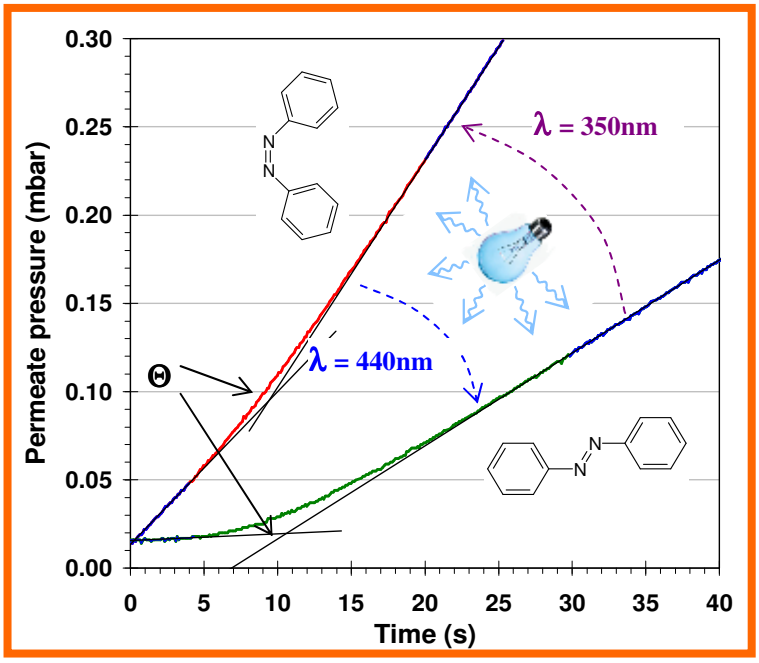

Figure 6.7. *Pressure increase curves of CH_4 permeation as a function of time and irradiation. The irradiated sample with cis-AZB exhibits a much higher pressure increase rate. Both curves show a nearly identical time lag, but the sample with cis-AZB also permeates without time lag, suggesting a different transport mechanism. Tangents are obtained from a linear least squares fit of the steady state section of the curve.*

It must be stressed that the initial slope is reproducible and completely reversible, and not related to the presence or the introduction of defects in the membrane. In fact, that would have given a drastic reduction of the selectivity, which is not the case here. After irradiation at 440 nm the normal behavior returns and after irradiation at 350 nm the anomalous effect reappears. Qualitatively the same behavior is observed for nitrogen (not shown here). An overview of all P, D and S values and corresponding selectivities is listed in Table 6.2, which confirms that for all gases the permeability increases in the presence of the cis-isomer. For CO_2 and O_2 this increase is almost exclusively due to an increase in solubility. It indeed seems evident that the increased solubility is related to the strong difference in dipole moment of the azobenzene molecule in the cis- and the trans-isomeric forms. There are two possible mechanisms: A) Direct interaction of the dissolved gas with the strong dipole of cis-AZB (3.1 D, compared to 0.5 D for trans-AZB). B) Change of the bulk polymer properties induced by the strong dipole of cis-AZB and subsequent interaction of the gas with the polymer bulk. The first hypothesis may be ruled out if the number of gas molecules per dye molecule is considered (Table 6.1). Trans-cis isomerization causes an increase of 15 sorbed oxygen molecules per AZB molecule present and over 200 CO_2 molecules. This definitely excludes a direct coordination of the gas molecules with AZB. Therefore the second hypothesis is more likely: increased sorption by dipole-induced change of the bulk polymer properties. The entity of the effect suggests that it is some kind of collective phenomenon, similar to the effect of dope molecules which change the mesophase in liquid crystals. The difference with liquid crystals, where dope molecules influence the spatial arrangement of the surrounding liquid crystals, is that Hyflon AD is an isotropic material. Therefore it is supposed that cis-AZB induces a collective electronic effect, which leads to an increased polymer-penetrant interaction and higher gas solubility.

Table 6.1. *Number of gas molecules per molecule of AZB dissolved in Hyflon AD60X at 1 bar of gas pressure.*

Gas	CO_2	O_2	CH_4	N_2
mol gas / mol trans-AZB [a)]	55	11	8.0	15
mol gas / mol cis-AZB [b)]	273	26	< 24 [c)]	< 35 [c)]

[a)] Fresh membrane, before irradiation. [b)] After irradiation at 350 nm. [c)] Extreme values if permeability is ascribed only to the solution-diffusion mechanism. In reality a competing transport mechanism is present and the real CH_4 and N_2 solubilities are lower.

Table 6.2. *Experimental transport parameters at 25°C and 1 bar of feed gas pressure of a solution-cast membrane containing 0.06% of azobenzene. Membranes dried at atmospheric pressure and room temperature for at least 48 h and under vacuum at 50°C for 6 h. Membrane thickness is 34 μm*

Membrane	Gas	Permeability coefficient, P		Time lag, Θ	Diffusion coeff., D	Solubility, S	Selectivity		
		10^{-6} m^3_{STP} m / (m^2 h bar)	Barrer [a)]	s	10^{-6} cm^2/s	m^3_{STP} / m^3bar	P_i/P_{N2} (-)	D_i/D_{N2} (-)	S_i/S_{N2} (-)
Memb. H60azoBI Before irradiation trans AZB	Helium	1.26	459	n.d.	-	-	16.7	-	-
	Hydrogen	0.614	224	n.d.	-	-	8.15	-	-
	CO_2	0.620	227	2.4	0.803	2.12	8.23	1.21	6.81
	Oxygen	0.220	80.2	1.4	1.38	0.437	2.91	2.07	1.41
	Nitrogen	0.075	27.5	2.9	0.664	0.311	1.00	1.00	1.00
	Methane	0.038	14.0	10.6	0.182	0.581	0.50	0.27	1.84
Memb.H60azoAI350 After 1x irr at 350 nm cis AZB	Helium	1.90	702	n.d.	-	-	7.20	-	-
	Hydrogen	0.97	359	n.d.	-	-	3.68	-	-
	CO_2	3.10	1147	2.4	0.803	10.7	11.7	1.04	> 11.3 [b)]
	Oxygen	0.88	325	1.03	1.87	1.30	3.33	2.43	> 1.37 [b)]
	Nitrogen	0.264	97.6	2.5	0.771	< 0.950 [b)]	1.00	1.00	1.00 [b)]
	Methane	0.099	36.6	9.4	0.205	<< 1.34 [b)]	0.375	0.266	< 1.41 [b)]
Memb.H60azoAI440 After 1xirr at 440 nm trans AZB	Helium	1.25	455	n.d.	-	-	16.3	-	-
	Hydrogen	0.602	220	n.d.	-	-	7.89	-	-
	CO_2	0.578	211	2.5	0.771	2.06	7.57	1.20	6.31
	Oxygen	0.209	76.5	1.7	1.13	0.506	2.74	1.76	1.55
	Nitrogen	0.0763	27.9	3.0	0.642	0.326	1.00	1.00	1.00
	Methane	0.0390	14.2	10.9	0.177	0.604	0.51	0.28	1.86
Reference membrane without AZB Thickness 27 micron	Helium	1.79	663	n.d.	-	-	20.2	-	-
	Hydrogen	1.04	387	n.d.	-	-	9.76	-	-
	CO_2	0.676	250	1.3	0.935	1.98	7.64	1.23	6.21
	Oxygen	0.261	96.7	0.70	1.74	0.412	2.95	2.29	1.29
	Nitrogen	0.0884	32.7	1.6	0.759	0.319	1.00	1.00	1.00
	Methane	0.0434	16.1	6.4	0.190	0.627	0.49	0.25	1.97

[a)] *1 Barrer = 10^{-10} cm^3_{STP} cm /(cm^2 s cmHg)*
[b)] *Extreme values if permeability is ascribed only to the solution-diffusion mechanism. In reality a competing transport mechanism is present and the real CH_4 and N_2 solubilities are lower.*

In this light it is interesting that one of the fundamental hypotheses of the use of photochromic probes for determination of the free volume distribution in polymeric glasses, is that the isomerization reaction has no influence on the cavity size and on the spatial

arrangement of the polymer chains [26]. This hypothesis is compatible with the constant diffusivity observed for CO_2 and oxygen. However, it seems in strong contrast with the results of methane and nitrogen, which exhibit a strong increase in permeability by a mechanism which does not involve a time lag. The latter is typical for porous membranes and suggests the presence of nanoscale channels through which transport occurs via the Knudsen diffusion mechanism. How only 0.06 wt.-% of cis-AZB could induce the formation of nanoscale channels can only be subject of strong speculation at the moment. In any case, formation of such channels must necessarily involve a rearrangement of the free volume elements in the polymer bulk. In this light the work of Merkel et al. seems remotely related to the present results. Incorporation of silica nanoparticles in amorphous glassy perfluorpolymer membranes caused higher gas permeability by increasing the accessible free volume [29]. However, their particle loadings were more than two orders of magnitude higher than in the present work. The unique advantages of AZB-doped Hyflon membranes are that the film remains basically homogeneous, that both the permeability and the selectivity of the membrane increase simultaneously and that the effect is tunable in a perfectly reversible way by light as an external stimulus.

6.3.3.4 Influence of the solvent

In chapter 4 it was shown that the presence of the casting solvent in the matrix can strongly affect the transport, mechanical ad thermal properties of the membrane, and that a very controlled thermal treatment at high temperature (up to 200°C) it is necessary to eliminate all traces of solvent [18]. Since photochromic membranes were not subjected to such a thermal treatment, because high temperatures can degrade the dye molecules, it was reasonable to verify how much the presence of the solvents (HFE7100 and DCM) in the polymer matrix influenced the transport properties of the membranes and whether the use of DCM as a cosolvent results in changes in the transport parameters compared to membranes prepared with only HFE. For this aim a series of membranes of Hyflon® AD60X was prepared using different amounts of DCM in the casting solution. Transport properties of these membranes were thus compared with those of photochromic Hyflon® AD60X membranes in order to verify whether the use of DCM as a cosolvent during the preparation of the photochromic membranes could have any influence on the transport properties.

Figure 6.8 shows that the permeability coefficients of six permanent gas (CH_4, N_2, O_2, H_2, CO_2, He) do not change significantly as a function of the DCM content. Thus the permeability does not depend significantly on the concentration of DCM in the casting solution. Nevertheless, a slight difference with respect to the AZB containing membrane and the membrane without AZB was the separation between CO_2 and H_2 permeabilities which seems characteristic of membranes containing DCM in the casting solution. Any way, we can exclude that the anomalous behaviour of the photochromic membranes is caused by the use of DCM as a cosolvent in their preparation. Indeed, the trans AZB containing photochromic membrane presents basically the same transport properties as the membranes without azobenzene, prepared with or without DCM.

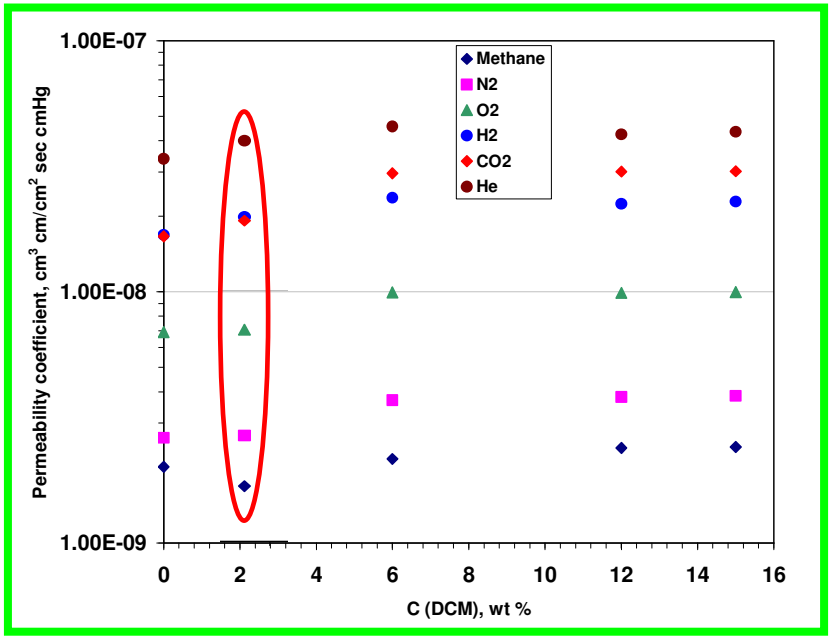

***Figure 6.8**. Permeability coefficients of six pure gases in Hyflon membranes containing different amounts of DCM. The points inside the ellipse represent the gas permeabilities of a Hyflon® AD60X membrane containing azobenzene and dried for both at 50°C under vacuum.*

Moreover, since the membrane without azobenzene does not present any change in gas permeability coefficient, upon irradiation (Figure 6.3), without any doubt the very unusual behaviour showed by the photochromic membranes after UV irradiation is only due to the photoisomerization of azobenzene molecules dispersed in the polymer matrix.

6.3.3.5 *Influence of the polymer*

Transport properties of photochromic membranes of Hyflon AD80X were also studied. In this case the addition of chromophore molecules in the polymer matrix produces a strong reduction of permselectivity with respect to the dye free membrane (HAD80), see Figure 6.9. Moreover, gas permeability of photochromic membranes is lower than that in the dye free membrane (HAD80). In addition, the effect of trans-cis photoisomerization by UV light strongly depends on the type of photochromic molecules. Indeed depending on the type of chromophore, the permeability of some gas increases or decreases.

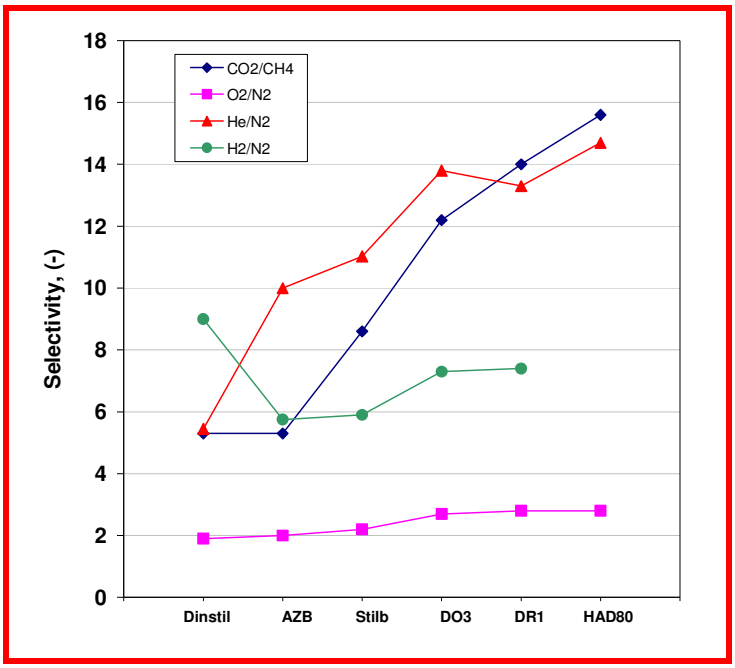

Figure 6.9. *Gas selectivity of the fresh Hyflon® AD80X membranes containing different photochromic compounds. Dye free membrane (HAD80) prepared under the same conditions is reported as reference.*

For example the permeability of hydrogen, methane and oxygen increases after phototisomerization in the AZB containing membrane, while it strongly decreases (of about 20 %) in the case of stilbene or stilbene derivative containing membranes. In general the effect decreases with increasing dye molecule size which is directly linked to the reduced switching efficiency.

References

1. W. J. Koros, Evolving beyond the thermal age or separation processes : Membranes can lead the way, *AIChE Journal* **2004**, 50, 2326-2334.
2. K. Weh, M. Noack, K. Hoffmann, K. P. Schroder, J. Caro, Change of gas permeation by photoinduced switching of zeolite-azobenzene membranes of type MFI and FAU, *Microporous Mesoporous Mater.* **2002**, 54, 15-26.
3. S. Yagi, N. Minami, J. Fujita, Y. Hyodo, H. Nakazumi, T. Yazawa, T. Kami, A.H. Ali, Light-controlled gas permeability of mesoporous silica glass bearing spironaphthoxazine on its surface, *Chem. Commun.*, **2002**, 2444-2445.
4. N. Liu, D.R. Dunphy, P. Atanassov, S.D. Bunge, Z. Chen, G.P. López, T.J. Boyle, C.J. Brinker, Photoregulation of mass transport through a photoresponsive azobenzene-modified nanoporous membrane, *Nano Lett.,* **2004**, 4, 551-554.
5. M. Aoyama, J. Watanabe, S. Inoue, Photoregulation of permeability across a membrane from a graft copolymer containing a photoresponsive polypeptide branch, *J. Am. Chem. Soc.,* **1990**, 112, 5542-5545.
6. T. Sata, Y. Shimokawa, K. Matsusaki, Preparation of ion-permeable membranes having an azobenzene moiety and their transport properties in electrodialysis, *J. Membr. Sci.*, **2000**, 171, 31-43.
7. Yu. Yampolskii, I. Pinnau, B.D. Freeman, (Eds.), Materials science of membranes for gas and vapor separation, John Wiley & Sons, Chichester, **2006**.
8. P. Pandey, R.S. Chauhan, Membranes for gas separation, *Prog. Polym. Sci*., **2001**, 26, 853-893.
9. W.J. Koros, G.K. Fleming, Membrane-based gas separation, *J. Membr. Sci*., **1993**, 83, 1-80.
10. H. Lin, B.D. Freeman, Materials selection guidelines for membranes that remove CO_2 from gas mixtures, *J. Mol. Struct.,* **2005**, 739, 57-74.
11. W.J. Koros, R. Mahajan, Pushing the limits on possibilities for large scale gas separation: which strategies?, *J. Membr. Sci.,* **2000**, 175, 181–196.
12. S.A. Stern, Polymers for gas separations: the next decade, *J. Membr. Sci*., **1994**, 94, 1-65.
13. R.W. Baker, Future directions of membrane gas separation technology, *Ind. Eng. Chem. Res.,* **2002**, 41, 1393-1411.

14. M. Kameda, K. Sumaru, T. Kanamori, T. Shinbo, Photoresponse gas permeability of azobenzene functionalized glassy polymer films, *.J. Appl. Poyml. Sci*., **2003**, 88, 2068-2072.
15. K. Weh, M. Noack, R. Ruhmann, K. Hoffmann, P. Toussaint, J. Caro, Modification of the transport properties of a polymethacrylate-azobenzene membrane by photochemical switching, *Chem. Eng. Technol*., **1998**, 21, 408-412.
16. M. Macchione, J.C. Jansen, G. De Luca, E. Drioli, Analysis of the distribution of local free volume in Hyflon® AD membranes by photochromic probes, in preparation
17. J.C. Jansen, M. Macchione and E. Drioli, High flux asymmetric gas separation membranes of modified poly(ether ether ketone) prepared by the dry phase inversion technique, *J. Membrane Sci.,* **2005**, 255, 167-180.
18. M. Macchione, J.C. Jansen, G. De Luca, E. Tocci, M. Longeri, E. Drioli, Experimental analysis and simulation of the gas transport in dense Hyflon® AD60X membranes. Influence of residual solvent, *Polymer,* **2007**, 48, 2619-2635.
19. J. G. Victor, J. M. Torkelson, On measuring the distribution of local free volume in glassy polymers by photochromic and fluorescence techniques, *Macromolecules,* **1987**, 20, 2241-2250.
20. J. Scot Royal, J.G. Victor, J.M. Torkelson, Photochromic and fluorescent probe studies in glassy polymer matrices. 4. Effects of physical aging on poly(methyl methacrylate) as sensed by a size distribution of photochromic probes, Macromolecules 25, 729-734 (1992).
21. J. Scot Royal, J.M. Torkelson, Photochromic and fluorescent probe studies in glassy polymer matrices. 5. Effects of physical aging on bisphenol-A polycarbonate and poly(vinyl acetate) as sensed by a size distribution of photochromic probes, *Macromolecules*, **1992**, 25, 4792-4796.
22. R.A. Evans, T.L. Hanley, M.A. Skidmore, T.P. Davis, G.K. Such, L.H. Yee, G.E. Ball, D.A. Lewis, The generic enhancement of photochromic dye switching speeds in a rigid polymer matrix, *Nature Materials,* **2005**, 4, 249-253.
23. P. Colaianna, G. Brinati, and V. Arcella, , Amorphous perfluor polymers, *U.S. Patent*, *5.883.177,* **1999**.
24. L. M. Robeson, Correlation of separation factor versus permeability for polymeric membranes, *J. Membr. Sci*., **1991**, 62, 165.

25. J. Crank, G. S. Park, Diffusion in Polymers, Academic Press, London, **1986**.
26. J. Algers, P. Sperr, W. Egger, L. Liszkay, G. Kögel, J. de Baerdemaeker, F.H.J. Maurer, Free volume determination of azobenzene-PMMA copolymer by a pulsed low-energy positron lifetime beam with in-situ UV illumination, *Macromolecules,* **2004**, 37, 8035-8042.
27. T. Kinoshita, New trends in photobiology. Photoresponsive membrane systems, *J. Photochem Photobiol. B Biol*., **1998**, 42, 12-19.
28. K.G. Yager, C.J. Barrett, Novel Photo-switching using azobenzene functional materials, *J. Photochem. Photobiol. A: Chem*., **2006**, 182, 250-261.
29. T.C. Merkel, B.D. Freeman, R.J. Spontak, Z. He, I. Pinnau, P. Meakin, A.J. Hill, Ultrapermeable, Reverse-Selective Nanocomposite Membranes, *Science,* **2002**, 296, 519-522

Summary

Dense solution-cast membranes of Hyflon® AD60X seem to have an unusually high tendency to retain the solvent. This reduces the thermo-mechanical stability and may cause foaming of the solution-cast polymer films upon strong heating under vacuum. Plasticization of the polymer by the residual solvent decreases the glass transition temperature; it reduces the permselectivity of the membranes and increases the gas permeability and the diffusion coefficients of the larger gas species. In comparison, melt-pressed films have a higher selectivity, mostly due to a stronger size-sieving effect, penalizing especially the diffusion rate of the gas species with the larger kinetic diameter such as CO_2, nitrogen and methane. Complete removal of the residual solvent from solution-cast films may require conditions, which are normally prohibitive for the membrane integrity, for instance drying temperatures near or above the glass transition temperature. It was discussed how besides diffusion phenomena the unusual solvent retention could be related to the particularly high FFV, to the FV distribution of Hyflon.

The photochromic probe technique was used to determine the distribution of local free volume in Hyflon® AD membranes. For this purpose, stilbenes and azobenzenes molecules are dispersed homogenously into the polymer matrix. Upon irradiation with UV or visible light with the proper wavelength the photochromic molecules undergo trans-cis isomerization and back. The crucial hypothesis, at the basis of this technique, is that photoisomerization in the glassy state requires a minimum, critical size of local free volume in the vicinity of the chromophore. This isomerization requires a certain amount of extra volume during the rotation of the molecule from the trans to the cis configuration. This procedure thus allowed the qualitative determination of the free volume distribution in Hyflon® AD60X and Hyflon® AD80X membranes by using a series of photochromic molecules requiring a different volume for the trans-cis isomerization reaction. Results reveal that in Hyflon® AD60X the size of free volume elements ranges from about 250-520 $Å^3$ and in Hyflon® AD80X from ca. 380-600 $Å^3$. This can explain the higher gas permeability of Hyflon® AD80X, otherwise hardly to understand since the two grade of Hyflon AD have equal Fractional Free Volume (FFV) and density.

Doping of Hyflon AD with azobenzene (AZB) yields phototunable gas separation membranes with an extraordinary photoresponse of the permeability. The difficulty to effectively dissolve the normally incompatible hydrocarbon AZB into the perfluorpolymer matrix can be circumvented by the clever use of different solvents with partial miscibility, and by the use of very low AZB concentrations. The use of a photoisomerizable dye molecule offers the unique possibility to introduce molecules with a very strong dipole moment in the polymer matrix without significant aggregation: the molecule is dissolved in the trans-isomeric form with low dipole moment and then converted into the cis-isomer with strong dipole moment. Only after UV irradiation the dipole moment increases from 0.5 to 3.1 Debye.

UV-induced trans-cis isomerization of the AZB molecules in the membrane produces a reproducible and completely reversible five-fold increase in CO_2 permeability in a membrane containing 0.06 wt.-% of azobenzene and a two-fold increase in CO_2/CH_4 selectivity, thus moving significantly above the Robeson upper bound. Also for the O_2/N_2 gas pair the permeability and selectivity increase simultaneously for about 300% and 20%, respectively, up to exactly the Robeson upper bound. These new membranes offer interesting perspectives for application in industrially important processes such as O_2/N_2 separation or natural gas processing. The higher permeability of these membranes for CO_2 and N_2 compared to CH_4 allows their removal from CO_2 and N_2 rich natural gas reserves while the methane stream remains at high pressure. This constitutes an enormous economic advantage, because it eliminates the necessity to re-pressurize the methane stream. This application will further benefit from the unique chemical stability and resistance to swelling of perfluorpolymers. It is surprising and not yet fully understood how the isomerization of a tiny amount of AZB may cause such dramatic changes in the gas permeability. The effect seems entirely due to an increase of the gas solubility for CO_2 and O_2, which is most likely related to the strong increase in dipole moment of AZB, from 0.5 Debye in the trans-isomer to 3.1 Debye in the cis-isomer. On the other hand, nanoscale channels seem to determine the transport of N_2 and CH_4. A better understanding of the underlying principle might lead to a breakthrough in the development of new membranes with performances systematically beyond the Robeson upper bound. To the best of my knowledge no materials with a similar combination of permeability, selectivity, fototunability and chemical and physical resistance are presently known in the literature.All observed phenomena are highly reproducible. They

are observed in membranes prepared at different moments. The effect of photoisomerization on the gas transport is reversible over various cycles by alternating irradiation at 350 nm and 440 nm, even if repeated after several months.

Further studies are currently in progress to find theoretical and experimental support for the physical origin of the observed effects.

In conclusion the present thesis has shown how Hyflon membranes present more interesting properties than other polymer membranes. Indeed, Hyflon AD has high chemical stability and resistance to most organic solvent and vapours as well as very good compromise between high permeability and still relatively high selectivity. These properties of Hyflon AD offer great perspective for the application in high-flux gas separation membranes, especially where gas streams may contain chemically aggressive species or condensable vapours.

Symbols and abbreviations

Abbreviations

AZB	azobenzene
BEV	perfluoro-butenylvinylether
CFC	chlorofluorocarbon
cmc	critical micelle concentration
CTFE	chlorotrifluoroethylene
DCM	dicloromethane
DO3	disperse orange 3
DO25	disperse orange 25
DNstil	4,4' dinitrostilbene
DR1	disperse red 1
DSC	differential scanning calorimetry
FAU	faujasite
FEP	fluoroelastomer polymers
FFV	fractional free volume
FV	free volume
FVEs	free volume elements
HRMAS	high resolution magic angle spinning
HFP	hexafluoropropylene
IGC	inverse gas chromatography
IR	infrared
MD	molecular dynamic
MFI	silicalite zeolitic membrane
MSD	mean squared displacement
NLO	non-linear optic
NMR	nuclear magnetic resonance
NPT-MD	number of particles, pressure, temperature-molecular dynamic
NVT-MD	number of particles, volume, temperature-molecular dynamic
PALS	positron annihilation lifetime spectroscopy

PC	polycarbonate; personal computer
PCMI	photochromic micro image
PCTFE	polychlorotrifluoroethylene
PDD	perfluoro- 2,2 dimethyldioxole
PE	polyethylene
PFPs	perfluoropolymers
PMMA	polymethylmethacrilate
PTFE	polytetrafluorothylene
PVC	polyvinylcloride
PVDF	polyvilinidenfluoruro
RIS	rotational isomeric state
SCF	self-consistent field
SPEEK	sulphonated polyether ether ketone
Stil	stilbene
SSC	short-side-chain
TEMPO	2,2,6,6,-tetramethylpiperidine-1-oxyl
TFE	tetrafluoroethylene
TGA	thermal gravimetric analysis
TST	transition state theory
TTD	2,2,4-trifluoromethoxy-1,3-dioxole
UV	ultraviolet
VDF	vinylidenefluoride

Symbols

a_1	activity coefficient
A	exposed membrane area
A_{dark}	absorbance with only trans isomer present
b	hole affinity constant.
B_{11}	second virial coefficient
c_0	concentration at upstream side

c_l	concentration at downstream side
c'_h	capacity of saturation
c_i	concentration of component *i*
d	average pore diameter
D	diffusion coefficient
D_c	diameter of a cylindrical cavity
D_{sp}	diameter of a spherical cavity
Ep	photon irradiance
F_c	rate of the carrier gas
G_{vis}	Poiseuille flow
G_{mol}	Knudsen flow
J_n^m	correction for pressure drop in the column
J_i (g/cm^{2}s)	flux
ΔH_m	partial molar enthalpy of mixing
k_{jum}	rate constant of jump
K_d	Henry's coefficient
K	thermal relaxation rate constant
l	membrane thickness
M_i	molecular mass of gas *i*
M_j	molecular mass of gas *j*
n_i	mole fraction of component *i*
N_a	number of diffusing molecules
o-Ps	triplet state of electron-positron pair
p	pressure
P	permeability coefficient
Ps	electron-positron pair
p-Ps	singlet state of electron-positron pair
p_F	feed pressure
p_0	pressure at t=0
$p_{P(t)}$	pressure at t=t
p_i°	reference pressure
Q_t,	total amount of penetrant

r	pore radius
r($\boldsymbol{r}$)	time independent single-particle distribution function
R_3	average radius of a spherical FVE in a polymer
S	solubility coefficient
T	temperature
Tg	glassy transition temperature
t_r	retention time
t_a	retention time of the "non-sorbable" component
U_i	coefficient of proportionality
V_g	specific retention volume
v_1	partial molar volume of component *i*.
V_1	molar volume of the sorbate
V_m	molar volume of gas
V_n	net retention volume of a sorbate
V_{occ}	occupied volume
V_P	permeate volume
V_{sp}	specific volume of polymers
V_w	van der Waals volume
w_1	weight fraction of the component with Tg_1
w_2	weight fraction of the component with Tg_2
Y	cis isomer fraction

Greek symbols

α_{ij}	selectivity
γ_1	activity coefficient
δ	chemical shift
$<\Delta^2>$	smearing factor
ε (kcal/mol)	Lennard-Jones energy
ε	membrane porosity
ε_{cis}	molar absorption coefficient of the cis isomer

ε_{trans}	molar absorption coefficient of the trans isomer
η	viscosity
Θ	time lag
λ	mean free path; wavelength of irradiation
μ_i.	chemical potential of gas *i*
μ_i°	chemical potential of pure *i*
v_i	velocity of component *i*
ν_{cor}	rotational frequency of the spin probe
ρ_{solv}	density of solvent
$\rho(\vec{\tau})$	time-independent single particle distribution function
σ (Å)	Lennard-Jones radius
$\vec{\tau}$	location
τ	tortuosity of the membrane
τ_3	lifetime of *o*-Ps
Φ	quantum yield
ω_L	mass of the polymer in the column

APPENDIX

Enclosed papers